T.C.
REPUBLIC OF TURKEY
HACETTEPE UNIVERSITY
GRADUATE SCHOOL OF HEALTH SCIENCES

THE INVESTIGATION OF THE ROLE OF REDUCED FOLATE CARRIER 1 IN THE MODELS OF ISCHEMIC STROKE AND RETINAL ISCHEMIA

Gökçe GÜRLER, M.D.

Neuroscience Program
DOCTOR OF PHILOSOPHY THESIS

ANKARA
2023

T.C.
REPUBLIC OF TURKEY
HACETTEPE UNIVERSITY
GRADUATE SCHOOL OF HEALTH SCIENCES

THE INVESTIGATION OF THE ROLE OF REDUCED FOLATE CARRIER 1 IN THE MODELS OF ISCHEMIC STROKE AND RETINAL ISCHEMIA

Gökçe GÜRLER, M.D.

Neuroscience Program
DOCTOR OF PHILOSOPHY THESIS

ADVISOR OF THE THESIS
Prof. Dr. Müge YEMİŞCİ ÖZKAN

ANKARA
2023

APPROVAL PAGE

PhD Dissertation Title: THE INVESTIGATION OF THE ROLE OF REDUCED FOLATE CARRIER 1 IN MODELS OF ISCHEMİC STROKE AND RETİNAL ISCHEMIA

Gökçe Gürler

Supervisor: Prof. Dr. Müge Yemişci Özkan

This thesis study has been approved and accepted as a PhD dissertation in "Neurosciences-Doctor of Philosophy (PhD) Program " by the assesment committee, whose members are listed below, on 16.08.2023.

Chairman of the Committee :	*Prof. Dr. Hülya Karataş Kurşun* *The Institute of Neurological Sciences and Psychiatry,* *Hacettepe University*
Member :	*Prof. Dr. Meltem Bahçelioğlu* *Department of Anatomy, Faculty of Medicine,* *Gazi University*
Member :	*Doç Dr. Banu Cahide Tel* *Department of Pharmacology, Faculty of Pharmacy,* *Hacettepe University*
Member :	Prof. Dr. *Aygün Ertuğrul* *Department of Psychiatry, Faculty of Medicine,* *Hacettepe University*
Member :	*Prof. Dr. Ertuğrul Kılıç* *Science and Advanced Technologies Research Center,* *İstanbul Medeniyet University*

This dissertation has been approved by the above committee in conformity to the related issues of Hacettepe University Graduate Education and Examination Regulation.

Prof. Müge YEMİŞCİ ÖZKAN, MD, PhD

Director

YAYIMLAMA VE FİKRİ MÜLKİYET HAKLARI BEYANI

Enstitü tarafından onaylanan lisansüstü tezimin/raporumun tamamını veya herhangi bir kısmını, basılı (kağıt) ve elektronik formatta arşivleme ve aşağıda verilen koşullarla kullanıma açma iznini Hacettepe Üniversitesine verdiğimi bildiririm. Bu izinle Üniversiteye verilen kullanım hakları dışındaki tüm fikri mülkiyet haklarım bende kalacak, tezimin tamamının ya da bir bölümünün gelecekteki çalışmalarda (makale, kitap, lisans ve patent vb.) kullanım hakları bana ait olacaktır.

Tezin kendi orijinal çalışmam olduğunu, başkalarının haklarını ihlal etmediğimi ve tezimin tek yetkili sahibi olduğumu beyan ve taahhüt ederim. Tezimde yer alan telif hakkı bulunan ve sahiplerinden yazılı izin alınarak kullanılması zorunlu metinlerin yazılı izin alınarak kullandığımı ve istenildiğinde suretlerini Üniversiteye teslim etmeyi taahhüt ederim.

Yükseköğretim Kurulu tarafından yayınlanan ***"Lisansüstü Tezlerin Elektronik Ortamda Toplanması, Düzenlenmesi ve Erişime Açılmasına İlişkin Yönerge"*** kapsamında tezim aşağıda belirtilen koşullar haricince YÖK Ulusal Tez Merkezi / H.Ü. Kütüphaneleri Açık Erişim Sisteminde erişime açılır.

- ○ Enstitü / Fakülte yönetim kurulu kararı ile tezimin erişime açılması mezuniyet tarihimden itibaren 2 yıl ertelenmiştir. (1)
- ☒ Enstitü / Fakülte yönetim kurulunun gerekçeli kararı ile tezimin erişime açılması mezuniyet tarihimden itibaren 6 ay ertelenmiştir. (2)
- ○ Tezimle ilgili gizlilik kararı verilmiştir. (3)

16./09./2023

Gökçe GÜRLER

---

i "Lisansüstü Tezlerin Elektronik Ortamda Toplanması, Düzenlenmesi ve Erişime Açılmasına İlişkin Yönerge"

(1) *Madde 6. 1. Lisansüstü tezle ilgili patent başvurusu yapılması veya patent alma sürecinin devam etmesi durumunda, tez **danışmanının** önerisi ve **enstitü anabilim dalının** uygun görüşü üzerine **enstitü** veya **fakülte yönetim kurulu** iki yıl süre ile tezin erişime açılmasının ertelenmesine karar verebilir.*

(2) *Madde 6. 2. Yeni teknik, materyal ve metotların kullanıldığı, henüz makaleye dönüşmemiş veya patent gibi yöntemlerle korunmamış ve internetten paylaşılması durumunda 3. şahıslara veya kurumlara haksız kazanç imkanı oluşturabilecek bilgi ve bulguları içeren tezler hakkında tez **danışmanının** önerisi ve **enstitü anabilim dalının** uygun görüşü üzerine **enstitü** veya **fakülte yönetim kurulunun** gerekçeli kararı ile altı ayı aşmamak üzere tezin erişime açılması engellenebilir.*

(3) *Madde 7. 1. Ulusal çıkarları veya güvenliği ilgilendiren, emniyet, istihbarat, savunma ve güvenlik, sağlık vb. konulara ilişkin lisansüstü tezlerle ilgili gizlilik kararı, **tezin yapıldığı kurum** tarafından verilir *. Kurum ve kuruluşlarla yapılan işbirliği protokolü çerçevesinde hazırlanan lisansüstü tezlere ilişkin gizlilik kararı ise, **ilgili kurum ve kuruluşun önerisi** ile **enstitü** veya **fakültenin** uygun görüşü üzerine **üniversite yönetim kurulu** tarafından verilir. Gizlilik kararı verilen tezler Yükseköğretim Kuruluna bildirilir.*
Madde 7.2. Gizlilik kararı verilen tezler gizlilik süresince enstitü veya fakülte tarafından gizlilik kuralları çerçevesinde muhafaza edilir, gizlilik kararının kaldırılması halinde Tez Otomasyon Sistemine yüklenir.

** Tez **danışmanının** önerisi ve **enstitü anabilim dalının** uygun görüşü üzerine **enstitü** veya **fakülte yönetim kurulu tarafından karar verilir.***

ETHICAL DECLARATION

In this thesis study, I declare that all the information and documents have been obtained in the base of the academic rules and all audio-visual and written information and results have been presented according to the rules of scientific ethics. I did not do any distortion in data set. In case of using other works, related studies have been fully cited in accordance with the scientific standards. I also declare that my thesis study is original except cited references. It was produced by me in consultation with supervisor (Prof. Dr. Müge Yemişci Özkan) and written according to the rules of thesis writing of Hacettepe University Institute of Health Sciences.

Gökçe GÜRLER, M.D.

ACKNOWLEDGEMENTS

Many thanks to,

My parents Sibel and Tanju Aydın, who have been supporting my goals and dreams about science, for buying my first microscope in elementary school, for supporting me in hardships during my PhD; my sister Duygu for loving me and making me stronger;

All the idealist professors that I met during medical school, Prof. Dr. Banu Anlar for giving me opportunity for research early on; Prof. Dr. Çağla Eroğlu and Prof. Dr. Donna Ferriero for giving me opportunities to learn my first basic science skills;

Dr. Gökhan Uruk for sharing all his research skills with me and supporting me through challenges in life, Dr. Nevin Belder for working in some experiments like her own and guiding me kindly; Dr. Melike Sever-Bahçekapılı for performing PCR experiments meticulously, Dr. Ümit Can Erim for developing and performing the retinal folate measurement method; Dr. Mustafa Beker for producing the lentiviral vector; Dr. Canan Çakır Aktaş for supporting financial coordination of our project, Kadir and Dilan for helping me in my busiest times; Aslıhan, Gülce, Doğa, Eda for being fun and engaging emotional supporters; Buket, Mesut, Taha, Emre Cem, Tuğçe, Dilek, Ecehan, Beyza, Onur, Bilge for walking with me alongside and making lab more fun;

All the professors supporting my PhD, Prof. Dr. Hülya Karataş Kurşun for guiding me with right questions and supporting the next steps of my career, Prof. Dr. Ertuğrul Kılıç for contributing to my paper through his valuable perspectives and encouraging my future career; Prof. Dr. Turgay Dalkara for being the founder of our department, Prof. Dr. Bülent Elibol, Prof. Dr. Emine Eren Koçak, Doç. Dr. Evren Erdener for creating a positive and friendly work environment, TÜBİTAK-2211 program for their generous support;

One before last, to my advisor, Prof. Dr. Müge Yemişci Özkan for making this thesis possible, for being the biggest supporter with her time and effort, for being a kind, generous and cheerful teacher who encourages my independence and giving me the opportunities to explore my scientific curiosity, and for supporting my success as a scientist;

Lastly, to all the broad-minded and courageous people, especially Gazi Mustafa Kemal Atatürk, who once carried out the democratic and secular revolutions which have given women the right to pursue their goals freely and have given me the chance to say I become an M.D., Ph.D. today.

ABSTRACT

Gurler, G., The Investigation the Role of Reduced Folate Carrier 1 in the Models of Ischemic Stroke and Retinal Ischemia, Hacettepe University, Graduate School of Health Sciences, Neuroscience Program, Doctor of Philosophy Thesis, Ankara, 2023. Reduced Folate Carrier 1 (RFC1, SLC19A1) is the folate transporter in the brain located at the blood-brain barrier (BBB). Polymorphisms of RFC1 in humans are linked to an increased risk of ischemic stroke. Transcriptomic studies have shown an abundant presence of RFC1 mRNA in cerebral microvascular mural cells; however, RFC1 protein had not been demonstrated yet. Our previous studies revealed the importance of microcirculation in stroke pathophysiology. The presence of RFC1 protein and its probable role in ischemic stroke, and retinal ischemia from the perspective of microvessels, remain enigmatic. In this thesis, RFC1 protein in the brain and retinal pericytes as well as in the inner blood-retina barrier (BRB) was characterized in adult mice. RFC1 protein was evaluated by the immunohistochemistry of the whole mount retinas, cerebral sections, isolated microvessels, Western blotting, and cerebral 7 Tesla MRI in separate experiments that include knock down by short interfering RNA (siRNA), and overexpression by Lentiviral Vector (LV), and pharmacological modification by methotrexate. Knocking down retinal RFC1 led to structural abnormalities in microvessels, and decreased in the expression of barrier proteins occludin, claudin-5, ZO-1, and collagen-4, resulting in the functional failure of inner BRB, as seen by an extensive IgG leakage. This failure in the brain was also detected by contrast agent leakage in MRI. Additionally, the detrimental effects of ischemia on the barriers were exacerbated. Pre-treatment with RFC1-LV partially restored collagen-4 and occludin levels in retinal ischemia. In essence, this thesis clarifies the presence of RFC1 protein in the cerebral pericytes and the inner BRB, offering a novel perspective on RFC1 as a dynamic regulator of the BBB and inner BRB under physiologic states, and emphasizes its critical role during ischemia.

Key Words: blood-brain barrier, blood-retina barrier, neurovascular unit, cerebral ischemia, retinal ischemia, RFC1, SLC19A1

This study is supported by The Scientific and Technological Research Institution of Turkey (TÜBİTAK; Grant No: 120N690) and Hacettepe University Scientific Research Coordination Unit (Project No: TDK-2020-18590)

ÖZET

Gürler, G., İndirgenmiş Folat Taşıyıcısı 1'in Rolünün İskemik İnme ve Retinal İskemi Modellerinde Araştırılması, Hacettepe Üniversitesi Sağlık Bilimleri Enstitüsü, Temel Nörolojik Bilimler Doktora Tezi, Ankara, 2023. Beyin parankimine folat taşınması iki şekilde olmaktadır. Bunlardan birincisi koroid pleksus üzerinden folat reseptör alfa (FOLRα) aracılığıyladır diğeri ise indirgenmiş folat taşıyıcısı 1 (RFC1, SLC19A1) ile kan-beyin bariyeri (KBB) üzerindendir. RFC1 literatürde özellikle koroid pleksustan folat taşınmasının bozulduğu durumlarda KBB üzerinden folat taşınmasını artırıcı alternatif bir yol olarak çalışılmıştır. Ancak güncel literatürde RFC1'in potansiyel yeni rolleri tanımlanmaya başlanmıştır. Yakın zamanda RFC1, Gen Seti Zenginleştirme Analizi (*Gene Set Enrichment Analysis*) sonucunda hipoksi-immün ilişkili bir gen olarak tanımlanmıştır. Geniş bir insan popülasyonunun değerlendirildiği bir klinik çalışmada, RFC1 polimorfizmleri iskemik inme, küçük damar oklüzyonu ve sessiz beyin enfarktına yatkınlıkla ilişkilendirilmiştir. Ayrıca beyin mikrodamarlarını sararak mikrodolaşımın ve KBB'nin kontrolünü sağlayan ve iskemide önemli görevleri bulunan heterojen gen ifade profilli mural hücrelerde (perisitler ve vasküler düz kas hücreleri) ortak genleri araştıran bir meta-analiz çalışmasında RFC1 üç ortak genden biri olarak öne çıkmıştır. Güncel literatürde iskemideki potansiyel rolüne yapılan dolaylı atfa rağmen RFC1'in iskemik inme ile direkt bağlantısına yönelik bir çalışma yapılmamıştır. Ayrıca, iskemik inme patofizyolojisinde önemli rolü bulunan perisitlerde protein düzeyinde varlığı gösterilmemiştir ve mikrodamarlardaki potansiyel rolü de çalışılmamıştır. Retina, beynin uzantısı olarak benzer anatomik ve fizyolojik özelliktedir ancak vücutta en yüksek perisit yoğunluğuna sahip olan dokudur. İç kan-retina bariyeri (KRB), KBB'ye benzer niteliktedir ve retinal iskemi ile iskemik inme arasında da önemli benzerlikler bulunmaktadır. Ancak, RFC1 proteini literatürde iç KRB'yi oluşturan perisit ve endotel hücrelerinde gösterilmemiş, retinal iskemideki potansiyel rolü çalışılmamıştır. Bu tez çalışmasında, erişkin erkek ve dişi Swiss albino fareler kullanılarak öncelikle RFC1 proteininin beyin perisitlerinde varlığının beyin kesitlerinde ve izole mikrodamar preparatlarında; retinada ise iç KRB'deki varlığının tüm retinada ve retinanın tripsin ile sindirilerek elde edilmiş mikrodamarlarında, immunohistokimyasal olarak gösterilmesi hedeflenmiştir. Ardından proteinin

fonksiyonu ve seviyeleri; RFC1'in gen susturumu için özel olarak tasarlanmış small interfering RNA (siRNA), gen ifadesinin artırılması için RFC1 geninin aşırı eksprese edilmesini sağlayan Lentiviral Vektör ve uygun kontrolleri kullanılmıştır. Bunlar beyne intrakortikal, göze intravitreal enjeksiyonlar ile tatbik edilmiştir. Ayrıca RFC1'in kompetetif inhibitörü olan metotreksat sistemik olarak verilerek taşıyıcı farmakolojik olarak modifiye edilmiştir. Fokal serebral iskemi/rekanalizasyon intraluminal model, retinal iskemi $FeCl_3$ modeli ile oluşturulmuştur. Bu patolojik durumların RFC1 proteini üzerindeki etkileri ve RFC1 proteini modifikasyonlarının patofizyolojideki rolleri immünohistokimya, histokimyasal yöntemler, Western blotlama ve diğer tamamlayıcı yöntemler ile incelenmiştir. Ayrıca başka bir grup farenin beynine RFC1-siRNA verildikten sonra iskemi/rekanalizasyon uygulanarak enfarkt hacminin değişimi ve KBB'den kontrast ajanı -gadolinyum- sızması *in vivo* yüksek çözünürlüklü (7 Tesla) manyetik rezonans görüntüleme (MRG) ile araştırılmıştır. Bu tezden elde edilen sonuçlardan ilki RFC1 proteininin beyin perisitlerinde bulunduğudur. Literatürde ilk kez iç KRB'de hem perisitlerde hem de endotel hücrelerinde RFC1 proteinin varlığı retina dokusunda ve tripsin ile izole edilen mikrodamarlarda gösterilmiştir. Intravitreal veya intrakortikal verilen RFC1-siRNA ile RFC1 protein ifadesinin susturulmasıyla 24 saat içinde KBB ve iç KRB fonksiyonel bütünlüğü bozulmuş ve endojen IgG damar dışına sızmıştır. RFC1-siRNA'nın bariyerde yol açtığı fonksiyonel yıkıma sıkı bileşke ve bazal membran proteinlerinin azalmasının eşlik ettiği retina damarlarında gösterilmiştir. Retina damarlarında bir saat retinal iskeminin RFC1 proteinini artırdığı saptanmıştır. Ancak beyin iskemisi sonrası farklı rekanalizasyon sürelerinde iskemik enfarkt, periinfarkt ve kontralateral bölgede RFC1 proteini değişmiştir. RFC1 proteinin beyin veya retina iskemisinden önce RFC1-siRNA ile azaltılması, iskeminin bariyerler üzerindeki yıkıcı etkilerini şiddetlendirmiş ve daha fazla IgG sızmasına sebep olmuştur. Ayrıca, RFC1-LV'nin intravitreal olarak retinal iskemi öncesi uygulanması ile yapılan ön tedavi, iskemiden sonra azaldığı gösterilen kollajen-4 ve okludin seviyelerini kurtararak iskeminin bariyer proteinleri üzerindeki etkisinin şiddetini azaltmıştır. Tek doz metotreksatın sistemik uygulanmasından bir saat sonra RFC1 seviyelerinde artış, 48 saat sonra ise azalış gözlemlenmiş ve metotreksatın RFC1 ifadesi üzerindeki modifiye edici etkisi gösterilmiştir. RFC1-siRNA enjeksiyonu yapılan retinalarda kontrole göre aktif folat

seviyeleri karşılaştırılmış ve RFC1 substratı folat ile ve RFC1'in bariyer üzerindeki kontrolü arasındaki ilişki araştırılmıştır. RFC1-siRNA uygulanan retinalarda kontrole göre istatistiksel anlamlı bir değişim gözlenmemiştir. Sonuç olarak, bu tez RFC1'in folat taşınması dışında fizyolojik durumda ve iskemide iç KRB ve KBB'de rolü olduğunu göstermiştir. Beyinde perisitlerde ve retinada iç KRB'de RFC1 proteininin varlığını göstermiş ve RFC1'in KBB ve KRB'nin bütünlüğünü sağlamaktaki önemini ortaya koyarak yeni bir bakış açısı sunmuştur. Erişkin farelerde bölgesel (intravitreal veya intrakortikal) RFC1 susturulması ile bariyerlerde 24 saat içinde meydana gelen yıkım RFC1'in bariyer özelliklerinin akut düzenleyicisi olduğunu göstermiştir. Bir saatlik retinal iskemide düzeyinin artışı, beyin iskemisinde ise farklı rekanalizasyon sürelerinde düzeyinin değişmesi, RFC1 proteininin gen bankalarının analizi ile elde edilen hipoksi-immun ilişkili gen tanımına uyduğunu ve iskemik inme ve retinal iskemi patofizyolojilerinde rolü olabileceğini desteklemektedir. İskemi öncesi RFC1-LV tedavisi ile iskeminin bariyer proteinlerinde meydana getirdiği azalmanın iyileşmesi, RFC1'e yönelik müdahalelerin retinal iskemi ve iskemik inme patofizyolojilerinde bariyer koruyucu işlev görebileceğini göstermiştir. RFC1 susturumu ile retina dokusunda aktif folat seviyesinde istatistiksel anlamlı bir değişim olmaması dokunun RFC1 susturulmasına karşılık folat seviyelerini kısmen telafi ettiği ve bariyerlerde meydana gelen değişimin dokunun veya organizmanın aktif folat düzeyleri ile ilişkisiz olabileceğini önermiştir. Tüm bu sonuçlar RFC1'in, beyin ve retina parankimine folat taşıma fonksiyonun yanı sıra sağlıkta ve iskemide KBB ve KRB'nin dinamik bir düzenleyicisi olduğuna ve RFC1 polimorfizmlerinin yatkınlık yarattığı iskemi ilişkili durumların altta yatan patogenezinin bu açıdan araştırılması gerektiğine işaret etmektedir. Bu tez, RFC1 proteinin yeni işlevlerini ortaya koymakla beraber varlığı ve önemi bilinmeyen ancak gen veri bankalarının matematiksel analizi veya -omik yaklaşımları ile yapılan araştırmalarda adı ön plana çıkan proteinler için kavramsal bir çalışma modeli önermektedir. Günümüzde bu yaklaşımlar her ne kadar ileri ve gelişmiş olsalar bile beyin araştırmalarında *in vivo* modellerin ve 'gözle görme'nin önemini, proteinlerin rollerinin anlaşılmasında şaşırtıcı sonuçlar ortaya koyabileceğini göstermektedir. RFC1'in KBB ve iç KRB üzerinde sahip olduğu etkinin mekanizmasının anlaşılmaya çalışılması bu tezden sonra bir odak noktası olmaya

devam edecektir. İleri araştırmalar, RFC1'in özelliklerini, protein-protein etkileşimlerini ve patofizyolojide üstlendiği rolleri aydınlatmayı amaçlamaktadır.

Anahtar Kelimeler: kan-beyin bariyeri, kan-retina bariyeri, nörovasküler ünite, serebral iskemi, retina iskemisi, RFC1, SLC19A1

Bu çalışma Türkiye Bilimsel ve Teknolojik Araştırma Kurumu (TÜBİTAK Proje No: 120N690) ve Hacettepe Üniversitesi Bilimsel Araştırma Koordinasyon Birimi (Proje No: TDK-2020-18590) tarafından desteklenmiştir.

TABLE OF CONTENTS

SYMBOLS AND ABBREVIATIONS

°C	Celsius degree
µL	Microliter
µM	Micromolar
g	Gram
h	Hour
kDa	Kilodalton
kg	Kilogram
mg	Milligram
min	Minutes
mL	Milliliter
mm	Millimeter
5-MTHF	5-methyltetrahydrofolate
BBB	Blood-brain barrier
BCA	Bicinchoninic acid
BRB	Blood-retina barrier
CD13	Aminopeptidase N
cGAS	Cyclic GMP-AMP synthase
CNS	Central Nervous System
CSF	Cerebrospinal fluid
dH2O	Distilled water
ERG	Electroretinography
FACS	Fluorescence activated cell sorting

$FeCl_3$	Ferric chloride
FRα/FOLR1	folate receptor alpha
GCL	Ganglion cell layer
Gd	Gadolinium
HBSS	Hank's Balanced Salt Solution
HIF1α	Hypoxia-inducible factor 1-alpha
i.p.	Intraperitoneally
IgG	Immunoglobulin G
INL	Inner nuclear layer
LC3	Microtubule-associated protein light chain
LSCI	Laser speckle contrast imaging
LV	Lentiviral vectors
MCA	Middle Cerebral Artery
MCAo	Middle Cerebral Artery occlusion
MRI	Magnetic Resonance Imaging
mRNA	Messenger RNA
MTX	Methotrexate
NG2	Neural/glial antigen 2
NGS	Normal Goat Serum
NRF-1	Nuclear respiratory factor 1
ONL	Outer nuclear layer
PBS	Phosphate buffered saline
PCFT	Proton-coupled folate transporter

PDGFR-β	Platelet-derived growth factor receptor beta
PFA	Paraformaldehyde
pMCAo	Permanent middle cerebral artery occlusion
PMX	Pemetrexed
qRT-PCR	Polymerase Chain Reaction
rCBF	Regional Cerebral Blood Flow
RFC1	Reduced Folate Carrier 1
RIPA	Radioimmunoprecipitation assay
RNAseq	RNA sequencing
ROI	Region of interest
RPE	Retinal Pigment Epithelium
siRNA	Short interfering RNA
SLC19a1	Solute carrier family 19 (folate transporter), member 1
SNPs	Single nucleotide polymorphisms
STING	Stimulator of interferon genes
TBS	Tris-buffered saline
tMCAo	Transient middle cerebral artery occlusion
UV	Ultraviolet
ZO-1	Zonula occludens 1

LIST OF FIGURES AND TABLES

1. INTRODUCTION

The Reduced Folate Carrier 1 (RFC1), also called solute carrier family 19 member 1 (SLC19A1/SLC19a1), is known to be responsible for transporting folates via blood-brain barrier (BBB) to the brain parenchyma (1, 2). RFC1 polymorphisms in human studies were associated with ischemic stroke and silent brain infarcts. Furthermore, the recent cerebral microvessel transcriptome data showed prominent RFC1 presence in mural cells (pericytes and vascular smooth muscle cells), the cells crucial with various roles in the regulation of microvascular blood flow and barrier integrity (3). However, the roles of RFC1 neither in the microvasculature nor in ischemia have been clarified.

In ischemic stroke, the interruption or reduction of blood supply to the parts of the brain prevents the brain tissue from getting the vital oxygen and nutrients and leads to tissue damage. The only treatments for acute ischemic stroke are the tissue plasminogen activator (tPA) that should be given within the first 4.5 h from the onset, and endovascular treatment strategies that can be employed within 6-8 h in patients with large vessel occlusions (4). It is crucial to develop new treatment strategies, and find new target molecules for stroke treatment, hence understanding the pathophysiology is a necessity. RFC1 is recently defined as the hypoxia–immune-related gene, and was shown to change during insults like hyperglycemia, nitric oxide exposure, hyperhomocysteinemia and oxidative stress (5-8). Having associated with ischemic stroke and silent brain infarcts in a human clinical study, the role of RFC1 in the pathophysiology of ischemic stroke has never been investigated before.

Retina is the extension of the brain, displaying similarities in terms of anatomy, function, and response to insults (9). Also, retinal ischemia shows similarities to cerebral ischemia. The inner BRB is found within in the inner retinal microvessels and comprises specialized endothelial cells secured by tight junctions, enclosed by basal lamina, pericytes, and perivascular astrocytes; hence it is similar to BBB essential for the maintenance of homeostasis through its selective properties such as harboring specialized nutrient carriers (10). The retinal microvessels have similar features to the brain and are unique for having the highest pericyte cell ratio in the body (11-13). Thus, retina is an excellent model for investigating the role of RFC1, whose presence

is plenty in mural cells, in health and in ischemia. Moreover, the presence of RFC1 protein in inner BRB and retinal mural cells has never been shown in the literature, although there is only one study that investigated the mechanisms and kinetics of folate transport *in vitro* at the inner BRB and indicated that RFC1 as a candidate protein there.

The initial hypothesis of this thesis is to elucidate the presence of RFC1 in the cerebral pericytes and cells of the inner BRB, retinal endothelial cells and pericytes using immunohistochemistry and confocal microscopy. Subsequently, the study aims to clarify the potential functions of RFC1 in the pathophysiology of cerebral and retinal ischemia in the mouse surgical models of permanent retinal ischemia and focal cerebral ischemia/recanalization induced via intraluminal monofilament technique. Moreover, this thesis seeks to understand the role of RFC1 in the BBB and inner BRB by targeting its function and levels *in vivo* genetically through a custom designed short interfering RNA (RFC1-siRNA), an overexpressing Lentiviral Vector (LV), or pharmacologically by methotrexate. The resulting effects of modification of RFC1 levels on cerebral and retinal ischemia along with microvascular changes is meticulously evaluated by immunohistochemistry, histochemical techniques, Western blotting, confocal microscopy, and other complementary methods.

2. GENERAL INFORMATION

2.1 The Basic Molecular and Pharmacological Properties of Reduced Folate Carrier 1

Reduced Folate Carrier 1 (RFC1 also named as solute carrier family 19 member 1 (SLC19a1) is a transporter protein of 12 transmembrane domains with internally oriented N and C termini. It is a member of SLC19 family of transporters (14, 15). Although SLC19A1 is the approved name for the human gene by HUGO Gene Nomenclature Committee (HGNC), RFC1 (the nomenclature used here) and RFC1 are both also used as synonyms for the gene which encodes the reduced folate transporter protein. SLC19a1 is used for Mus musculus gene (16, 17). Although it is 64-66% conserved between humans and rodents, N and C termini and the connecting loop between TMDs 6 and 7 shows species-specific differences (14). Species homologies for RFC proteins GenBank accession numbers are: Homo sapiens (human) NP 001069921; Pan troglodytes (chimpanzee) XP 001157360; Gallus gallus (chicken) NP 001006513; Danio rerio (zebrafish) XP 687261; Bos taurus (cow) NP 001069921; Rattus norvegicus (Norway rat) NP 001030309; Cricetulus griseus (Chinese hamster) U17566; Mus musculus (mouse) NP 112473; Xenopus laevis (African clawed frog) NM 001092530 (Figure 2.1.).

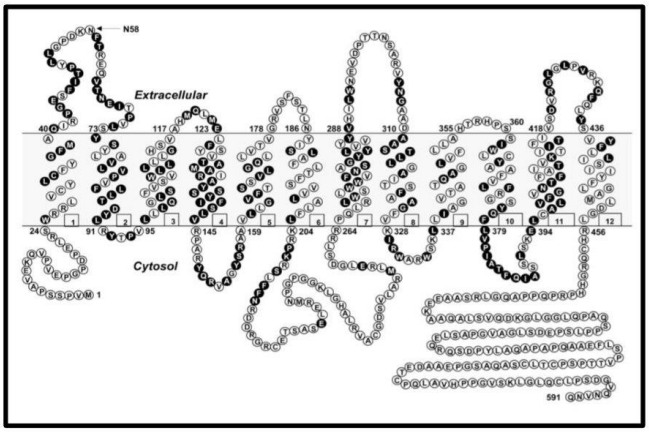

Figure 2.1. Topology representation of the Reduced Folate Carrier 1. The model showcases 12 transmembrane domains, with the N and C termini oriented internally, an outwardly positioned N-glycosylation site (Asn-58), and a cytosolic loop linking

6^{th} and 7^{th} transmembrane domains. Conserved amino acids across RFCs from diverse species are symbolized as black circles (Figure Source: 14).

RFC1 is an anion antiporter with a weight of 57-65 kDa, which works effectively at a neutral pH of 7.4 and exchanges folate with organic/inorganic anions. Documented in 1968 by Goldman et al. in the murine leukemia cells for the first time, the sequence and structure of the transporter of human and rodent RFC1 had been extensively studied by cloning over decades especially in the context of transporting of folates, folate derivatives, and antifolates (18-20).

As the name implies, RFC1 is best known for transporting reduced folates (14, 15). Folate is the overarching term for B9 family of vitamins, of which the common chemical element is the pteroyl group. Physiologically active form of folates are naturally found as reduced (protonated) forms such as formyltetrahydrofolates in the cells or methyltetrahydrofolate (MTHF) as the dominant form in plasma (21). Upon entering cells, reduced folates acquire glutamate moieties resulting in polyanionic character that reduces decrease their affinity to efflux pump. Folic acid, on the other hand, commonly referred as folate, indeed is a manufactured synthetic molecule used in food fortification and is a poor substrate of RFC1. Other than reduced folates (e.g., formyltetrahydrofolates and methyltetrahydrofolates), there are other substrates (agonists) for RFC1. These substrates share a common trait of having anionic character and include ring systems with varying aromaticity (15).

RFC1 is clinically important for the treatment of diseases due to its role in transporting the anti-tumoral and anti-rheumatic drugs such as methotrexate (MTX), pemetrexed (PMX), raltitrexed, and pralatrexate, which are high-affinity substrates of RFC1. These exogenously administrated drugs are named as antifolates due to their binding affinities showing micromolar range as reduced folates, and therefore, in fierce competition for binding to RFC1 and passing into the cell with folates (14, 22).

Furthermore, RFC1 has recently been demonstrated in the cell lines to serve as an importer of immunotransmitter of 2′3′-Cyclic GMP-AMP (cGAMP) and other cyclic dinucleotides which are activators of the cyclic GMP-AMP synthase and stimulator of interferon genes (cGAS-STING) pathway which has antitumoral and antiviral effects (23, 24). It was shown that cGAMP, the potent activator of the STING protein, is transported into the cells by RFC1 (25, 26). Additionally, STING activation

was associated with neuroinflammation in senescence and neurodegenerative diseases, causing BBB deterioration.

2.2 Reduced Folate Carrier 1 In the Central Nervous System

2.2.1 Reduced Folate Carrier 1 in the Brain

RFC1 is ubiquitously expressed in mammalian tissues abundantly where folate absorption, and reabsorption take place such as the small intestine, colon and kidneys. Additionally, it is prominently expressed in cells with high metabolic demand for folate, driven by rapid proliferation rates as observed in hematopoietic stem cells and cancer cells (27). At the protein level, RFC1 localization in human brain was reported in choroid plexus epithelial cells, neurons, and endothelial cells earlier (27, 28). A recent study characterizing RFC1 expression in brain cells exhaustively revealed its presence in arachnoid barrier epithelial cells, astrocytes, and microglial cells in addition to its abundant and canonical expression in neurons and endothelial cells. Strikingly, even within this detailed characterization study, RFC1 expression in mural cells was overlooked (28).

The roles of RFC1 in the brain have been mentioned within various context including its role in transporting folate from choroid plexus epithelial cells, its relevance to neurodevelopmental disorders or neural tube defects, and its involvement in delivering of chemotherapeutics to the brain tumors. Besides, as elaborated below, its variants were found to carry a potential risk for ischemic stroke or silent brain infarctions.

Folate is delivered via two ways in the brain: One is via the choroid plexus comprising the blood-cerebrospinal fluid (CSF) barrier, and the other is via BBB. Choroid plexus is majorly responsible for folate delivery to the CSF where folate is typically concentrated four times than the plasma (29). Three major transporters act in concert to transport folate in the choroid plexus: i) reduced folate carrier 1 (RFC1; RFC; SLC19A1), ii) proton-coupled folate transporter (PCFT; SLC46A1), and iii) folate receptor alpha (FRα; FOLR1). It was shown that FRα and PCFT function together at the choroid plexus epithelial cells for the passage of folate to the brain. Folate is taken by receptor-mediated endocytosis to the choroid plexus epithelium via

FRα with high affinity, and subsequently delivered to CSF in exosomes (Figure 2.2.). PCFT is proposed as responsible for folate transport from exosomes to cytosol, thus supporting the survival of choroid plexus epithelial cells (30).

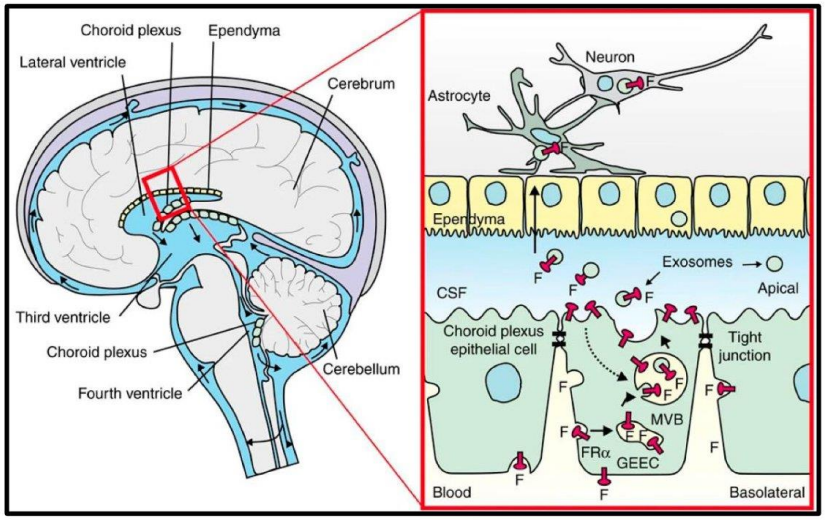

Figure 2.2. Proposed model of folate transport in choroid plexus. The illustration depicts the circulation of the CSF through the ventricles and subarachnoid space. The inset provides a closer view of folate (F) transport from blood to CSF via choroid plexus epithelial cells. Within these cells, FRα is primarily responsible for internalizing folate via receptor-mediated endocytosis subsequently creating FRα-positive folate-containing endosomes. These endosomes are later released into the CSF to cross the ependyma to reach neurons and glial cells (Figure Source: 30).

Dysfunctions of either FRα or PCFT have been shown to result in low folate levels in CSF leading to some childhood neurodegenerative disorders such as cerebral folate deficiency and hereditary folate malabsorption, respectively (31, 32). Nevertheless, mutations in RFC1 have not been identified as the leading cause of any specific childhood neurological disorders. In experimental models, its knockout was lethal, as evident from RFC1 knockout embryos (33). Some studies linked the polymorphisms of RFC1 to neural tube defects; however, the association remains unclear and might be ethnicity specific (34-36). Additionally, variants in RFC1 have been mentioned in autism spectrum disorder in Asian population, but causal connection has not been examined (37). Another brain-related disease that RFC1 mentioned for was Wernicke-Korsakoff syndrome, a neurological disorder stemmed

from chronic alcohol misuse, where a variation of Slc19a1 (rs1051266) was identified as a risk gene (38).

In adults, antifolates, such as MTX and PMX, which are competitive inhibitors and high affinity substrates for RFC1, are used for the treatment of brain tumors such as glioblastomas. A study showed substantial RFC1 expression in glioblastoma stem cells; however, the expression level reduced as the cellular differentiation advanced. Therefore, stem cells displayed sensitive to MTX treatment, suggesting a potential role of RFC1 in enhancing efficacy of chemotherapy (39).

In a recent clinical meta-analysis, RFC1 polymorphisms were associated with risk factors for ischemic stroke, small artery occlusion, and silent brain infarcts (40). However, pathophysiological aspect of the interplay between ischemic stroke and RFC1 has never been studied in the literature, and hence we aimed to explore in this thesis.

2.2.2. Reduced Folate Carrier 1 in the Blood-Brain Barrier

The BBB acting as a dynamic barrier separating the CNS from the peripheral blood flow. It is comprised of specialized endothelial cells sealed with high-density tight junctions and serves to maintain a stable environment for optimal CNS function. The BBB possesses distinct anatomical characteristics, including specialized tight junctions, minimal pinocytic activity, polarized expression of transporters, carriers, and receptors, which regulate the entry and exit of molecular substances and nutrients. The integrity of the barrier is preserved and supported by surrounding cells like astrocytes, microglia and pericytes (Figure 2.3.). These cells act like a regulators, influencing the orientation and abundance of tight- and adherent-junction proteins in endothelial cells, as well as basal membrane proteins.

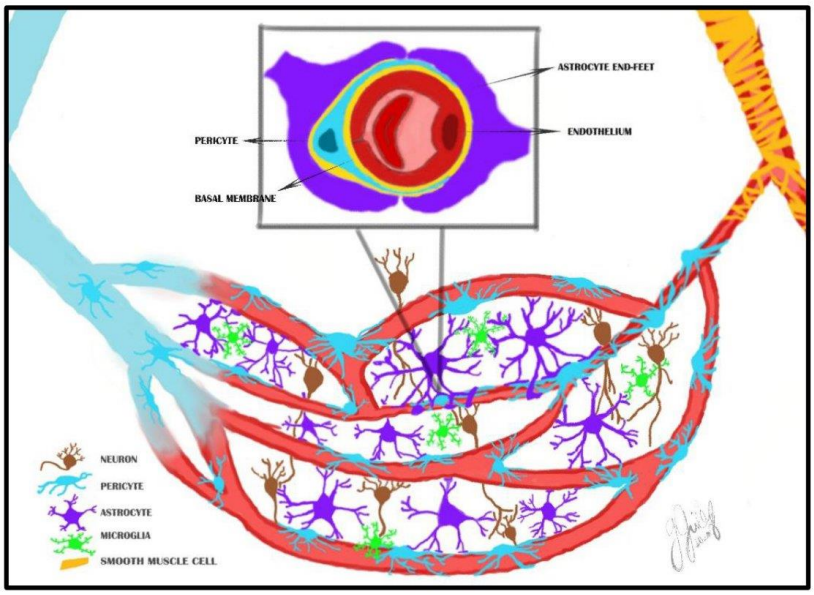

Figure 2.3. Schematic view of the brain microvasculature and blood-brain barrier (BBB). An arteriole illustrated is (red-yellow) branching into capillaries (red) and rejoining to veins (blue). Schematic cross section of the blood vessel at the capillary level where the BBB is positioned in the center. The BBB is composed of a monolayer of endothelial cells sealed with tight junctions. Pericytes have a ‘‘bump-on-a-log’’ appearance and are embedded in a basement membrane. Capillary vessel wall is covered by astrocytic end feet. The microvasculature is composed of microvascular cells involving endothelial cells and pericytes on brain capillaries, vascular smooth muscle cells on arterioles and veins, supported by glial cells like astrocytes, microglia, oligodendrocytes, and neurons.

The BBB regulates the exchange of nutrients between the blood and the brain parenchyma creating a microenvironment that supports neurological functions (41). The presence of RFC1 protein in cerebral capillary endothelial cells is defined previously in several studies (1, 2, 27, 42). However, folate delivery via the BBB is generally appreciated as having secondary importance compared to the choroid plexus. Clinical reports showed that Frα and PCFT deficiency led to compromised folate delivery via choroid plexus; however, folate is still delivered to the brain via BBB, albeit in suboptimal amounts, thereby alleviating the severity of neurological symptoms (43). Augmentation of the folate transporters in the BBB was presented as an alternative strategy to provide folate delivery to the brain (1, 2).

The impact of RFC1 localized in the cerebral endothelial cells on the brain folate homeostasis is yet unclear. Several nuclear receptors, which are DNA-binding transcription factors, were discussed as the regulators of RFC1 and PCFT levels, which can be modified to upregulate folate levels when needed. Particularly, the activation of Vitamin-D receptor (VDR) through its ligand 1,25-dihydroxyvitamin-D was shown to upregulate RFC1 levels in endothelial cell lines and in isolated mouse brain microvessels comprising the BBB (2). Furthermore, in FRα knockout mouse model, Vitamin-D supplementation resulted in nearly wildtype level folate levels in CSF, suggesting that the regulation of RFC1 at the BBB can serve as an alternative pathway for folate transport (1).

A recent single-cell RNA sequencing study unveiled that the expression of RFC1 was present in the mural cells (pericytes and vascular smooth muscle cells). Moreover, when the transcriptome analysis of the brain mural cells was combined with previous data in a meta-analysis, it was found that the cerebral mural cells had three common enriched genes, one of which was surprisingly RFC1 (3). Interestingly, this was the first study that imply RFC1 expression in mural cells and had mentioned that this transporter is neither characterized nor studied in the context of mural cells before. Although the protein expression was determined in the endothelium, RFC1 protein level in cerebral mural cells, where its mRNA was abundant, was not studied yet. Furthermore, there are only a few studies that searched for its probable functions in the endothelial and mural cells (27, 42, 44).

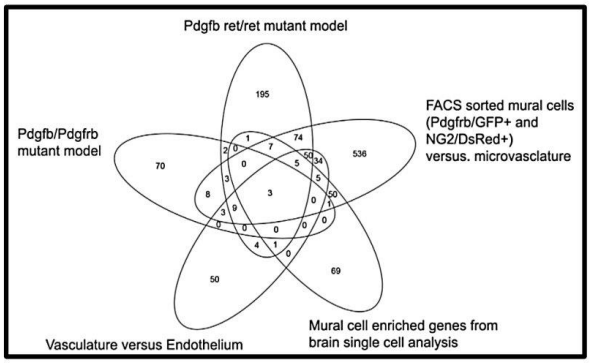

Figure 2.4. Venn diagram depicting the overlap of detected mural cell genes between five different transcriptomics studies. Three genes, one of which was surprisingly RFC1, were explored as common. (Figure Source: 3).

Therefore, in this thesis, one of our objectives is to detect RFC1 protein expression in the pericytes and endothelial cells cerebral microvessels, and to investigate its probable roles in the BBB.

2.2.3. Reduced Folate Carrier 1 in the Retina

Retina is considered as the extension of the brain with its similar anatomical and physiological features including its barrier properties, separating it from the systemic circulation. The retina has two blood barriers: outer and inner. The retinal pigment epithelium (RPE) is a specialized epithelium between the neural retina and the choriocapillaris and constitutes the outer blood-retinal barrier (oBRB). The oBRB is responsible for nourishment of outer 1/3 of retina. The remaining 2/3 of retinal tissue is nourished by branches of central retinal artery creating a layered elaborate microvascular network. Those microvessels comprises the inner blood-retinal barrier (inner BRB). Hence the inner BRB resembles the BBB.

The role of RFC1 in the retina was discussed in terms of its presence in the apical membrane of the RPE to transport folate from the choroidal blood to the retina. Folate enters RPE via FRα from the basal membrane of the RPE and exits the cell via RFC1 from the apex (45). Experimental findings determined that in RPE, RFC1 activity and expression was modified with oxidative stress, hyperglycemia, nitric oxide and hyperhomocysteinemia (6-8). However, the RFC1 was not associated with a specific retinal disorder.

2.2.4. Reduced Folate Carrier 1 in the inner Blood-Retinal Barrier

The inner BRB is found in the inner retinal microvessels and comprises specialized endothelial cells secured by tight junctions, enclosed by basal lamina, pericytes, and perivascular astrocytes; hence it is essential for the maintenance of homeostasis through its selective properties like harboring specialized nutrient carriers (9, 10). Pericytes are a crucial element of the inner BRB and have various roles including the regulation of microvascular blood flow, immunity, and barrier integrity in health and pathologic states such as ischemia. Also, the retina is unique for having the highest pericyte: endothelia ratio in the body, probably due to its high metabolic activity and need for controlled blood flow.

Although RFC1 protein expression was shown in RPE, there was no known study about RFC1 protein expression in the inner BRB, hence the retinal microvessels, and mural cells. Only one study investigated the mechanisms and kinetics of folate transport at the inner BRB and elucidated that RFC1 should be the primary responsible element in the BRB, but this study was an *in vitro* study done on rat inner BRB model by using isolated rat retinal endothelial cells, hence TR-inner BRB2 cells. Besides, the manuscript did not include RFC1 at the protein level neither in the endothelial cells nor in pericytes, but mRNA expression of RFC1 was assessed by reverse transcription-polymerase chain reaction (RT-PCR) analysis and quantitative real-time PCR.

The expression of RFC1 in other types of retinal cells was presented in a transcriptomics study of adult neural retina characterized by using single cell RNAseq in a recent study. This study included photoreceptor cells (rod and cone), glial cells (Müller and astrocytes), and the retinal neurons (bipolar cells, amacrine cells, retinal ganglion cells, horizontal cells) (46). In this study, while only bipolar cells showed considerable amount of RFC1 expression, retinal ganglion cells and rod photoreceptors showed no RFC1 expression, yet the other cell types showed no or minimal RFC1 expression. Also, this study ignored the cell types constituting the microvessels.

The recent cerebral microvessel transcriptome data showing prominent RFC1 presence in cerebral pericytes and that the retinal microvessels having similar features to the brain and are unique for having the highest pericyte ratio in the makes it an excellent candidate to investigate the presence and the role of the RFC1. Therefore, our other aim in this thesis was to investigate the presence of RFC1 protein in the inner BRB, and especially at the pericytes and endothelial cells.

2.3. Cerebral Ischemia and Retinal Ischemia

2.3.1. Pathophysiology of Cerebral Ischemia and Retinal Ischemia

Stroke is the second leading cause of mortality worldwide. Around 80% of strokes are ischemic, where interruption or reduction of blood supply to part of the brain prevents the brain tissue from getting the vital oxygen and nutrients and leads to tissue damage. The global burden of stroke is vast; approximately 15 million people worldwide suffer from stroke each year (47, 48). One in three stroke patients die, and survivors have serious neurological deficits, which are both emotionally and financially an issue for the patients, families, and countries. The only treatments for acute ischemic stroke are the tissue plasminogen activator (tPA) that should be given within the first 4.5 hours from the onset, and endovascular treatment strategies that can be employed within 6-8 hours in patients with large vessel occlusions (4). It is crucial to develop new treatment strategies, and find new target molecules for stroke treatment, hence understanding the pathophysiology is a necessity. Animal stroke models in rodents are frequently used to study innovative therapeutic agents. The widely used replicable one is the focal cerebral ischemia model, where typically middle cerebral artery is occluded, and pathophysiological or neuroprotection studies are performed.

The pericytes -ignored for a long time- on the cerebral microvessels, begin to contract approximately one hour after the onset of ischemia and this contraction increased with time, causing the constriction of the microvessels, and impeding the reperfusion of tissue despite recanalization of the occluded large cerebral arteries (11). Hence, the main cause of this phenomenon known as ‘no reflow’, which negatively affects tissue survival, was pericytes at the level of microcirculation (11, 49-51). Besides, in our laboratories we showed that if microvascular reperfusion were promoted, it could provide neuroprotection, and increase tissue survival (52, 53). Pericytes, nonetheless, are vastly susceptible to injury. Ischemia unfavorably impacts pericytes on cerebral microcirculation, leading to the stroke-induced tissue damage by disrupting microvascular blood flow and BBB integrity (11, 49, 54-56). Briefly, our studies and literature showed that pericytes are critical in cerebral blood flow regulation, ischemic stroke, development and maintenance of the BBB, angiogenesis,

and neurovascular function (55). Also, pericytes have an important role in neurodegenerative disorders like Alzheimer's disease (57, 58).

Retinal ischemia, a common cause of visual impairment and blindness, occurs when the retinal circulation is ceased leading to unmet retinal metabolic needs. Retinal ischemia may be caused by two reasons one is systemic circulatory failure such as heart failure or hypovolemic shock, the other is, more often, local circulatory failure. The central retinal artery occlusion is relatively common reason for retinal ischemia and leads to ischemia of the inner retinal layers (59).

The branches of central retinal artery give rise to elaborate vascular network organized in inner layers of retina. The superficial microvascular layer lays on the nerve fiber layer. Three deeper microvascular layers (sublaminar, intermediate, and deep) are located in between neuronal synapses in the inner and outer plexiform layers). In healthy retina, deeper microvasculature is organized in specialized endothelial cells, sealed with tight junctions, and surrounded with pericytes. Due to the similar microcirculation characteristics, retinal ischemia is comparable to cerebral ischemia (11-13). Yet, retinal ischemia models is widely used for ischemic pathophysiology studies since it is the easily accessible extension of central nervous system with a well-known anatomy (60).

2.3.2. The Potential Relevance of Reduced Folate Carrier 1 in Ischemic Stroke and Retinal Ischemia

RFC1 might have a role in cerebral ischemia, as indicated by a human clinical study showing that RFC1 single nucleotide polymorphisms (SNPs) were associated with ischemic stroke especially small vessel artery occlusion and silent brain infarctions (cerebral infarcts seen on Magnetic Resonance Imaging without any corresponding stroke episodes) (40). In this study, -43C>T, 80A>G, and 696T>C polymorphisms were shown indirectly affecting plasma homocysteine and folate levels leading to homocysteine and folate levels in the blood of those patients to be mildly inversely correlated in control, stroke, or silent brain infarction patients. However, they emphasized that the polymorphisms that they studied did not have a direct relationship with plasma homocysteine and folate levels implying that the patients having those polymorphisms did not necessarily have hyperhomocysteinemia

that can result in ischemic complications. Among the three polymorphisms, two were missense (-43C>T, 80A>G), and the other one was a synonymous variant (696T>C) in which the single nucleotid change in the coding region of RFC1 does not result in an amino acid substitution. These mean that the two of them had an amino acid substitution which may lead to protein alteration/malfunction, while the other was expected to produce the same protein. In particular, missense variant (80A>G) leading to an arginine to histidine conversion, was associated with a higher affinity for folate in the literature. However, this polymorphism was not individually associated with the change in plasma folate or homocysteine levels, but it is only associated with hyperhomocyteinemia when combined with polymorphisms in other folate pathway genes (e.g., MTHFR 677TT genotype) (61-63). Moreover, although synonymous variants (in this case 696T>C) produce same protein without any aminoacid changes, they can have a significant effect on the DNA level affecting transcription factor binding, resulting in changes in the level of transcription levels and eventually translation of RFC1 gene (64). Therefore, although variants of RFC1 was linked to ischemic stroke, silent brain infarction and small vessel occlusions, the mechanistic explanation was still missing.

Although, a recent human clinical study implied the importance of RFC1 in ischemic stroke, there is no pre-clinical study examining its precise role in ischemia. Therefore, we investigated -omics studies reporting the transcript or protein alterations after ischemic stroke, and the details are reported in the Table 2.1. As one can perceive from the table, 3 out of 13 studies reported no change in the RFC1 mRNA levels in microvessel fragments, astrocytes, or cerebellar cortex after transient middle cerebral artery occlusion (tMCAo) model in rodents. Besides, 8 of 13 studies did not even mention RFC1/Slc19a1 gene in their datasets. Finally, only 2 studies reported that RFC1 levels was affected by ischemic stroke. One of them was performed on mice to decipher the effect of aging on the expression profile of microglial cells, and yet reported in the supplemental dataset that RFC1 was upregulated in microglia in the young whereas downregulated in the old mice, but this difference was not statistically significant. In the other study, endothelial cells isolated from the infarct region showed no difference in RFC1 expression in the acute (24 h) or subacute (72 h) timeframe but showed upregulation chronically (1 month).

In the -omics literature of retinal ischemia, on the other hand, there are two studies showing change in RFC1 levels after ischemia. RFC1 mRNA was shown to be significantly higher after 24 h when compared to controls in the rat model of ischemia/recanalization induced by intraocular pressure (65, 66). There is no study investigating the changes of RFC1 at the protein level or investigating the pathophysiology determining the importance of RFC1 in retinal ischemia. However, RFC1 activity and expression is found to be modified by pathologic states such as oxidative stress, hyperglycemia, nitric oxide and hyperhomocysteinemia in RPE suggesting that retinal ischemia can also modify RFC1 protein level (6-8).

Although the inconsistent results from previous -omics studies spark controversy over the possible role of the RFC1 in ischemia, the aforementioned clinical study, which showed polymorphisms of RFC1 was associated with ischemic stroke and silent brain infarcts, raise the possibility that RFC1 might have contribute the ischemic pathophysiology of stroke as well as retinal ischemia which serves a proxy of ischemic stroke due to similarities in anatomy and physiology.

Another aspect of the potential role of RFC1 in cerebral ischemia could be derived from a meta-analysis pointing to elevated RFC1 mRNA levels in cerebral mural cells, suggesting RFC1 could be important for mural cell physiology. Our previous findings and relevant literature showed that pericytes play a crucial role in the pathophysiology of ischemic stroke. Therefore, RFC1 might be important in ischemic pathophysiology particularly by affecting the mural cells (63). The retina due to having the highest pericyte number, and inner BRB being similar to BBB, and cerebral microcirculation to the retinal; it is also possible that RFC1 could be affected in the retinal ischemia in addition to cerebral ischemia. Therefore, in this thesis, the potential contribution, and roles of RFC1 in the retinal and cerebral ischemia models were investigated.

Table 2.1. -omics studies reporting the changes in genes after ischemic stroke.

	ORGANISM	TISSUE/CELL TYPE	MODEL	DURATION OF I/R	RFC1 ALTERATION	DATA	REF.
1	Mouse	Microvessel Fragments	tMCAo	60 min+24h 60 min+7 days	No change	RNAseq	(67)
2	Mouse	Astrocytes	tMCAo	60 min+72 h	No change	RNAseq	(68)
3	Rat	Cerebellar Cortex	tMCAo	90 min+48 h	No change	Microarray	(69)
4	Mouse	Isolated Microglia from ischemic hemisphere	pMCAo	Sacrification: 14 days	Increase in ischemic microglia in the young; decrease in ischemic microglia in aged mice, not significant	RNAseq	(70)
5	Mouse	Infarct region, Endothelial cells	pMCAo	24 h (acute) 72 h (subacute) 1 month (chronic)	24 h (acute): No change 72 h (subacute): No change 1 month (chronic): increased	RNAseq	(71)
6	Rat	Ischemic Hemisphere	tMCAo	2h+24h	N/A	Proteomics	(72)
7	Rat	Periinfarct region	tMCAo	60min+4days	N/A	Transcriptomics&proteomics	(73)
8	Mouse	Cortex	pMCAo	Sacrification: 1, 3, 7, 14, or 28 days	N/A	Proteomics	(74)
9	Rat	Brain, NA	tMCAo,	NA	N/A	Multiomics	(75)
10	Mouse	Periinfarct & cortex regions	tMCAo,	90min+24h 90min+48h	N/A	Proteomics	(76)
11	Human	Blood & post-mortem brain samples from six stroke patients	-	Comparing the infarct core with the contralateral brain region	N/A	Transcriptomics&proteomics	(77)
12	Rat	Periinfarct & core regions	pMCAo	24h 3days	N/A	Microarray	(78)
13	Rat	N/A	pMCAo	1week 4weeks 8weeks	N/A	RNAseq	(79)

N/A: Not available; pMCAo: permanent middle cerebral artery occlusion; REF.:reference; tMCAo: transient middle cerebral artery occlusion; RNAseq: RNA sequencing

3. MATERIALS AND METHODS

3.1. Methods Used Both for the Brain and Retina Experiments

3.1.1. Animals

All experiments were approved by Hacettepe University Animal Experimentations Local Ethics Board (No: 2019/13-06 and 2021/03-19). Animal housing, care, and the experimental procedures were done in accordance with institutional and ARRIVE guidelines. Same sex littermates of adult male and female Swiss albino mice (25-35 g) were kept together in conventional cages in rooms with a 12-h light–dark cycle, controlled temperature (22 ± 2 °C) and humidity (50-60%). All mice were provided with ad libitum standardized mouse diet and drinking water. The experimental groups, and the number of mice is given in Table 3.1. All the *in vivo* experiments were performed in a blinded and randomized manner. For all the surgical procedures for brain experiments mentioned below, mice were anesthetized with isoflurane (4-5% induction dose, followed by 1.5-2% maintenance). Corneal reflex and hind-paw nociceptive reflex sensitivity were assessed periodically for depth of anesthesia. O_2 flow rate was maintained around 2 L/min via a facemask. Body temperature was monitored with a rectal probe and maintained at 37.0 ± 0.2°C by a homeothermic blanket control unit (Harvard Apparatus, USA). Pulse rate and oxygen saturation was be monitored with an oximeter (The LifeSense® VET Pulse Oximeter, Nonin Medical Inc., USA) from the right lower limb.

For all the retinal surgical procedures such as intravitreal injections and retinal ischemia, the animals were anesthetized with ketamine (80 mg/kg, intraperitoneal injection, Ketalar®, Pfizer, Cambridge, United Kingdom) and xylazine (8 mg/kg, intraperitoneal injection, Alfazyne® 2%, Alfasan International, Woerden, the Netherlands). A rectal probe connected to the homeothermic blanket with a control unit (Harvard Apparatus, U.S.A.) was utilized to control the body temperature (37.0 ± 0.5°C). Pulse rate and oxygen saturation were monitored from the right lower limb via an oximeter (The LifeSense® VET Pulse Oximeter, Nonin Medical Inc., USA).

Table 3.1. Table of groups and number of mice for the experiments.

	Groups	**n**
BRAIN ***In Vivo*** **Experiments**	Naive	12
	Ischemia/Recanalization (1h, 24h, 48h)	30
	RFC1-siRNA	6
	Scrambled-siRNA	6
	MTX i.p.	12
	MTX + Ischemia/Recanalization (1h, 24h, 48h)	14
In Vivo **7T-MRI**	RFC1-siRNA+ Sham	1
	Scrambled-siRNA + Ischemia/Recanalization (24h)	7
	RFC1-siRNA + Ischemia/Recanalization (24h)	6
RETINA ***In Vivo*** **Experiments**	Naive	20
	Ischemia (1h)	6
	RFC1-siRNA	32
	Scrambled-siRNA	28
	RFC1-siRNA + Ischemia (1h)	3
	Scrambled-siRNA + Ischemia (1h)	3
	RFC1-LV	6
	Control-LV	6
	RFC1-LV + Ischemia (1h)	3
	Control-LV + Ischemia (1h)	3
	5-MTHF Intravitreal	12
TOTAL	**Total number of animals**	216

5-MTHF: 5-methyltetrahydrofolate; 7T-MRI: 7 Tesla Magnetic Resonance Imaging; LV: i.p.;intraperitoneal; LV:Lentiviral Vector; RFC1: Reduced Folate Carrier 1; siRNA: short interfering RNA.

3.1.2. Immunohistochemical Studies

Following brain experiments, mice were sacrificed via transcardial perfusion with 4% paraformaldehyde (PFA) solution, and the brains were immersed in 4% PFA for 24 h and then in 30% sucrose (in PBS [Phosphate Buffered Saline]) for 2 days to obtain tissue cryopreservation. Brain sections of 20 µm thick were used. For

immunohistochemical studies of the retina, whole mount retinas, 20 µm thick radial sections and isolated retinal microvessels were used. PFA fixed whole mount retinas were kept in in 0.5% PBS-Triton-X, freezed 15 min at -80°C and thawed for 15 min at room temperature following overnight incubation in 2% TritonX-100 (Merck Millipore, 1086031000) PBS for permeabilization.

In general, tissues incubated in TBS (Tris-buffered saline) containing 0.3% Triton-X for 30 minutes at room temperature, then blocked in 10% normal goat serum (NGS) for 1 h at room temperature, and then incubated overnight (or three overnights for whole mount retinas) at +4°C with primary antibodies against RFC1 (SLC19A1, MyBioSource MBS9134642 and Sigma-Aldrich V44167; produced in rabbit). For mural cells against PDGFR-β (R&D Systems, AF1042), NG2 (Sigma AB5320A4), CD13 (Acris Antibodies, AM26636AF-N). For endothelium CD31 (BD Bioscience, 550274), tight junctions ZO-1 (Sigma, MAB1520), Claudin-5 (Invitrogen, 35-2500). For basal membrane collagen-4 (Abcam, ab6586). For autophagy Microtubule-associated protein light chain LC3-II (ab192890; Doç. Dr. Banu Cahide Tel provided), for folate receptor alpha FOLRα (908303, BioLegend) markers are used. We used two commercial polyclonal antibodies developed against different non-overlapping epitopes of RFC1. RFC1/SLC19a1 antibody from MyBioSource (MBS9134642) was produced against a recombinant fusion protein containing a sequence related to amino acids 452-591 of human SLC19A1 (NP_919231.1), while RFC1/SLC19a1antibody from Sigma-Aldrich (AV44167) was produced against Synthetic peptide directed towards the N terminal region of human SLC19A1 (NP_919231). BBB leakage was determined by Cy3-conjugated anti-mouse IgG (Thermo Scientific™, A10522). After rinsing, the sections were incubated with appropriate secondary antibodies (Alexa Fluor 488, 555 or Cy3, Cy2 conjugated) for 60 min at room temperature. To visualize vessels, sections were incubated with 'Fluorescein' or 'Texas Red' labeled Lectin (Vector Laboratories, Burlingame, CA). Negative control stainings for all the antibodies were done without using the primary antibody. Positive control stainings for RFC1 was be done by labelling choroid plexus, kidney, and RPE where the staining of RFC1 had already been established in literature (27, 42). The sections were covered with Hoechst 33258 (Molecular Probes, ThermoFisher Scientific) that label cellular nuclei. Images of the stained sections were obtained by laser-scanning confocal

microscope (Leica SP8 or Zeiss LSM 980 with Airyscan 2) with appropriate objectives and lasers.

3.1.3. Western Blotting

Whole brain tissue from sham, core, peri-infarct area, and contralateral hemispheres or whole retinas were lysed in RIPA buffer, homogenized on ice, centrifugated in 10000xg for 20 min at 4°C. Pellets were dissolved in ddH_20, protein concentration of the lysates was quantified using BCA protein assay kit. After loading proteins, 120 V was applied on the gel for 1.5 h, by applying 120 mAmp for each membrane for 2 h in room temperature, were transferred onto PVDF membrane. Membranes were blocked with 5% BSA in 0.1% TBS-Tween for 1 h at room temperature. Membranes were incubated with primary antibody against RFC1 (Sigma-Aldrich V44167) at +4°C overnight. After washing in 0.1% TBS-Tween, they were incubated in goat anti-rabbit HRP conjugate (Invitrogen, 31460) solution in 2 h at room temperature. For detection, the membranes were treated with enhanced chemiluminescent (ECL) substrate (34094, Thermo Scientific™). Imaging was done by Kodak 4000M Image Station. β-tubulin III was used as an internal standard, and densitometric measurements were made by ImageJ 1.52 version (NIH, Bethesda, and Maryland). Data was expressed as ratios to β-tubulin III values.

3.1.4. Quantitative Reverse Transcriptase-Polymerase Chain Reaction (qRT-PCR)

To ensure the success of siRNA-mediated gene silencing method, RFC1 gene expression was analyzed by the qRT-PCR method as described previously (80). Wedge shaped brain tissue from the injection site was obtained freshly. For the retinas, eyeballs were freshly dissected in ice-cold sterile PBS under a surgical microscope to get the retina intact. RNA isolation was done with RNA isolation kit (Invitrogen™) according to manufacturer's instructions. The RNA was reverse transcribed to cDNA using a high-capacity reverse transcription cDNA kit (Applied Biosystems). Primer pairs specific to mouse RFC1/SLC19a1 (Mm00446220_m1) and Tubb4a (Mm00726185_s1, beta 4A class IVA as a housekeeping gene) were constructed and verified by Life Technologies to use with TaqMan qPCR chemistry (TaqMan™ Gene

Expression Assay, Applied Biosystems™, 4331182). Amplicon context sequences for RFC1/SLC19a1 and beta 4A class IVA are shown in Table 3.2. All assays were done in triplicates with the housekeeping gene beta-tubulin 4a as internal control. The difference in CT values (ΔCT) between the RFC1 (SLC19A1) gene and the housekeeping gene was then normalized to the corresponding ΔCT of the vehicle control (ΔΔCT) and expressed as fold expression ($2^{-\Delta\Delta CT}$) to assess the relative difference in mRNA expression.

Table 3.2. Gene symbols, the full names of the genes, accession number of transcripts and amplicon context sequences of RFC1/SLC19a1 and beta 4A class IVA.

Symbols	The full names of genes	Accession numbers of transcripts	Amplicon context sequences
RFC1/SLC19a1	Mus musculus solute carrier family 19 (folate transporter), member 1 [Mus musculus (house mouse)]	NM_031196.3:1240-1390	CGGGACATCTGGGTGTGCTACGTGACCTTTGTGCTTTTCCGTGGGGCCTACCAGTTCCTTGTGCCCATTGCCACTTTTCAGATTGCGTCTTCCCTGTCTAAAGAGCTCTGTGCATTGGTCTTTGGGATCAACACTTTCCTAGCTACTGCGC
Tubb4a	Mus musculus tubulin, beta 4A class IVA (Tubb4a)	NM_009451.3:1852-2030	CCACCTTCTTAGATCTTGAAAATCCTTTCCTTTATGCCCTGTCCCTTCCCCAGCACTCCTGAACCATTCTCCTCCACCTCTGACATGCCCAGATATTTCTCTAGATCTTAACATTTTCCCCAGCCTCCAAGTCCTCTCACCTTGCCTTACCTCTGACCTCACAGCTACCCACTCCTGAC

3.1.5. Gene Silencing *in vivo* by Short Interfering RNA (siRNA)

To silence RFC1 gene, we used two custom-designed mouse RFC1 (Slc19a1) Accell siRNAs targeted to two different regions of RFC1 mRNA and two Accell scrambled (control) siRNAs (Horizon Discovery, Waterbeach, United Kingdom). Accell siRNA has several advantages as it does not need any transfection reagents which may have unwanted effects when applied in vivo. Furthermore, they could be internalized by any type of mammalian cells (81). Accell siRNAs have been previously proven to be uniformly distributed across rat retinal tissue and successfully inhibit various genes following intravitreal delivery (82). Product codes of siRNAs with sequences are given in Table 3.3. RFC1-siRNA-1 and RFC1-siRNA-2 or scrambled (control) siRNA-1 and 2 were pooled in equal volumes for administration to improve the potency and specificity.

For brain studies, mice were placed in a stereotaxic frame and, via 27 G syringe (80308, Hamilton, U.S.A.), double injection of 100 µM pooled siRNA solutions (RFC1-siRNAs or Scrambled-siRNAs) were made 1 mm deep intracortically into the area of the brain supplied via middle cerebral artery under surgical stereomicroscope. After 24 h, we either proceeded to cerebral ischemia or sacrificed mice, and determined the levels of mRNA or protein.

We delivered 100 µM pooled RFC1-siRNAs or Scrambled-siRNAs intravitreally to the eyes (2.3 µL/ eye) of animals via 33 G Neuros Syringe (1701 RN, Hamilton). We did not utilize contralateral eyes as controls to avoid the possible transfer of siRNAs to the opposite side (83, 84). After 24 h, we either proceeded to retinal ischemia or sacrificed mice, and determined the levels of mRNA or protein.

Table 3.3. The product codes and the sequences of sense strands of RFC1 siRNA and scrambled (control) siRNAs.

	PRODUCT CODES	**SEQUENCES OF SENSE STRAND**
RFC1-siRNA-1	A-044248-13	C.C.A.G.C.C.U.A.C.U.U.C.A.U.G.C.U.U.U.U.U
RFC1-siRNA-2	A-044248-15	C.C.A.G.G.A.A.A.C.U.A.G.A.U.C.G.C.A.U.U.U
Scrambled siRNA-1	D-001910-01	U.G.G.U.U.U.A.C.A.U.G.U.C.G.A.C.U.A.A.U.U
Scrambled siRNA-2	D-001910-03	U.G.G.U.U.U.A.C.A.U.G.U.U.U.U.C.C.U.A.U.U

3.1.6. Imaging and Analysis

The images of the stained whole mount retinas, retinal microvessels, and retinal radial sections were obtained with Leica TCS SP8 confocal laser scanning microscope (Leica, Wetzlar, Germany) with a diode laser 405, 638 and OPSL 488, 552 nm, with a X, Y, and Z-movement controller, and a high-resolution PMT (Zeiss, Oberkochen, Germany) and HyD (Leica) detectors. Images were either acquired in a single focal plane while keeping settings constant between experimental or control groups for analysis or Z-stack mode with 0.80 µm wide steps along the Z axis. For analysis of immunostained retinal microvessels, 1024x1024 pixels and 276.79x276.79 µm sized, middle of the Z axis level images was used. Acquired images were exported as 8-bit grayscale .tiff formats from Leica Application Suite X (LAS X; version 3.5.5.19976)

and opened in ImageJ 1.52 version. First, the lectin frame of each image was filtered by Gaussian blur (sigma=4) to reduce the random noise, and Huang Thresholding was applied to mask the lectin-positive microvessel areas of the images. After de-speckling (Process tab>Noise>Despeckle) and eroding (Process tab>Binary>Erode), the binary image was divided by 255 using Math function (Process tab>Math>Divide) to convert microvessel pixels to "1" and background pixels to "0". Later, either "RAW" lectin image or the overlapping grayscale image belonging to tight junctions or collagen-4 was divided by the binary of the lectin image. This created 32-bit grayscale images in which microvessels had singular intensity and the background had infinity. Finally, the mean grey value (RFU, range between 0-255) was obtained which corresponded to the mean intensity of the pixels occupying the microvessel area. Number of pericytes were quantified from Lectin and Hoechst labelled microvessel preparations by researchers blinded to the experimental or control groups. As pericytes are well known to have protruding nuclei, they were easy to distinguish morphologically and spatially from endothelial cells having flat nuclei. The total microvessel length was measured with AngioTool (version 0.6a (64 bits), October 2014) software, and pericyte number per mm of microvessel length was calculated (85). IgG extravasation was calculated from the 150x150 µm sized ROIs of 8-bit grayscale .tiff format images of wholemount retinas labeled with Cy3-conjugated anti-mouse IgG and lectin. The IgG and lectin frames were applied Huang Thresholding to detect the IgG and lectin-positive pixel counts. After thresholding, the binary images were divided by 255 to convert IgG positive and lectin positive pixels to "1" and background pixels to "0". Next, the IgG positive pixel counts are divided into lectin positive pixel counts (Figure 3.1.).

To further explore localization of RFC1, we performed double immunostainings with endothelial marker CD31 which is distributed over the entire endothelial cell surface, luminal, abluminal, and lateral allowing us to label the whole endothelial cell surface (86). We employed radial cryo-sections of retinas from PFA fixated eyeballs which allows us to visualize the luminal surface of retinal microvessels. We also performed immunostainings with two types of antibodies which were targeted to two different regions of RFC1 protein to eliminate the possibility of antibody-related variations in distribution. Imaging was performed by confocal laser

scanning microscope (Zeiss LSM 980 with Airyscan 2) with 40x magnification (W-Plan Apochromat 40x/1.0 DIC VIS-IR M27) that allowed us to perform super-resolution confocal imaging with Airyscan detector technology.

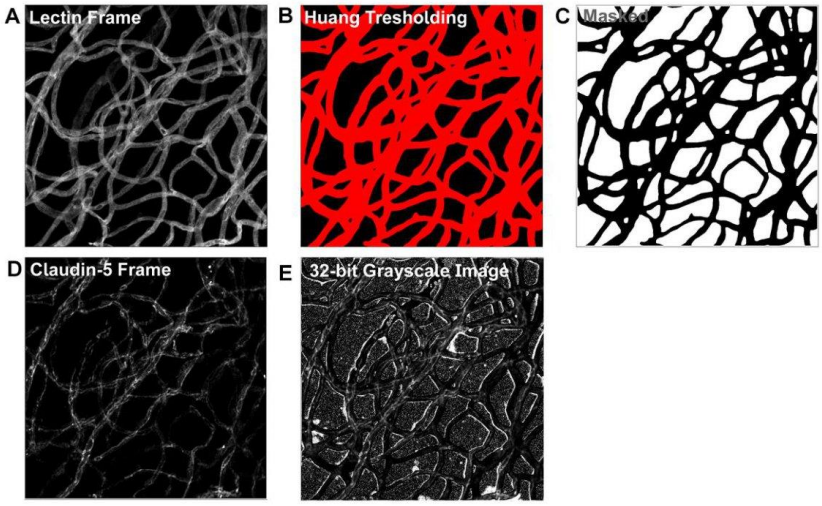

Figure 3.1. Steps involved in the Image J analysis of the double stained retinal microvessels. A) Double stained images were exported as 8-bit grayscale .tiff formats and opened in ImageJ. First, lectin frame belonging to each image filtered by Gaussian blur (sigma=4) to reduce the random noise were overlapped with microvessel signal. B) After, Huang Thresholding was applied to mask lectin positive microvessel area of the image. C) Next, masked image was de-speckled (Process tab>Noise>Despeckle) and eroded (Process tab>Binary>Erode), the resulting binary image divided by 255 using Math function (Process tab>Math>Divide) to convert microvessel pixels to "1" and background pixels to "0". D) Later," RAW" overlapping grayscale image belonging to tight junctions (for this example Claudin-5) were divided by the binary. E) This created 32-bit grayscale images which microvessels had original intensity while the background had infinity. After, mean grey value (RFU, range between 0-255) was obtained which gave the mean intensity of the pixels occupying the microvessel area. To express relative changes in percent the mean grey values obtained from experimental groups divided by averaged value of control groups and multiplied by 100.

To measure the potential microvessel diameter changes in retinal microvessels, images from lectin-labelled retinal trypsin digest preparations were used. Pericyte-associated vascular diameter of individual pericytes per microvessel branch was measured as described before. Briefly, to account for changes in pericyte position relative to the vessel wall, the measurements were taken at juxtanuclear sections

perpendicular to the vessel axis. The mean of each juxtanuclear section per pericyte was calculated and divided by the initial diameter of each vascular segment to provide an intrinsic baseline correction. This resulting value was defined as the "juxtanuclear diameter ratio" (87).

To structurally assess retinas, we labeled radial cryo-sections of 20-µm thick retinas from PFA fixated eyeballs with β-Tubulin III (as a ganglion cell marker), lectin and Hoechst 33258. To standardize, four individual sections that included optic nerve were chosen and ROI were determined from either side of the optic nerve in every section. We determined the number of ganglion cells (GC), total thickness of retinal sections, inner nuclear layer thickness (INL thickness; which predominantly includes bipolar cells), and outer nuclear layer thickness (ONL thickness; which predominantly includes photoreceptors) in retinal sections. To evaluate GC survival, the number of β-Tubulin III positive, lectin negative cells were counted manually in four sections in ROIs which were placed to cover 250 µm retinal section length (Figure 4.20.)

Brain microvessels were imaged via by Leica TCS SP8 confocal laser scanning microscope with 40x magnification (HCX APO L U-V-I 40x/0.80 WATER). Tile scan images to capture the whole section were acquired by scanning multiple partial images 10x magnification (HC APO L U-V-I 10x/0.30 WATER) and these were auto-stitched by Leica Application Suite Software (version 3.7.4.23463).

3.1.7. Statistical analysis

Data were analyzed using IBM SPSS 23 statistical analysis program, and were expressed as mean ± S.E.M. All data sets were tested for normality using the Shapiro-Wilk normality test. The groups containing normally distributed data were tested using a two-way Student's t test or analysis of variance (ANOVA). Non-normally distributed data such as microvessel constriction and cell counts, ischemic volumes, protein expressions were compared using the Mann-Whitney U test (for two groups), and Kruskal Wallis (for more than two groups). Gene expression ratio in the RFC1-siRNA group were expressed as a percentage of the ratio of the housekeeping gene.

3.2. Methods Used for the Brain Experiments

3.2.1. Focal Cerebral Ischemia/Recanalization Model

Focal cerebral ischemia/recanalization model was employed by proximal middle cerebral artery occlusion (MCAo) with intraluminal monofilament technique as described previously (11, 53). Briefly, mouse was placed supine position under anesthesia, and a midline neck incision was made under a surgical microscope. The right common, external, and internal carotid arteries were exposed, common and external carotid arteries were ligated with 6-0 nylon suture proximally. A small incision was made through common carotid artery 1 mm proximal to carotid bifurcation. Silicon rubber-coated monofilament (8-0) was introduced into the internal carotid artery. The regional cerebral blood flow (rCBF) was measured by laser-Doppler flowmetry (PeriFlux 6000, PERIMED, Sweden). A flexible probe (PF-318 of PeriFlux PF 2B, Perimed Jarfalla, Sweden) was placed over the skull (2 mm posterior, 6mm lateral to the bregma), away from large pial vessels to monitor blood flow in middle cerebral artery (MCA) territory. After obtaining a stable preischemic rCBF for 10 min, the MCA was occluded by advancing the filament 10 mm distal to the carotid bifurcation. rCBF was continuously monitored during ischemia (90 mins) and the first 10 mins of reperfusion. Reperfusion was accomplished by pulling the filament back. Systolic blood pressure was measured non-invasively from the tail via Laser Speckle Contrast imaging (88), two times 10 minutes before, and three times within 30 minutes after MCAo. Ischemia was done for 90 minutes, then filament was drawn for recanalization for 1 h, 24 h , and 48 h. Sham surgery was performed with all the surgical steps except introduction of the filament. Mice were placed on a heating blanket until they fully recover from anesthesia. The animals that showed hemodynamic instability or subarachnoid hemorrhage or died during surgery were excluded. The sample size required for infarct volume determination was calculated with the program G Power 3.1.9.4 (89). Neurological motor examination was performed 24 h after the MCAo according to the Modified Bederson score as grade 0: no observable neurologic deficit (normal), grade 1: forelimb flexion, grade 2: forelimb flexion and decreased resistance to lateral push, grade 3: circling, grade 4: circling and

spinning around the cranial-caudal axis, grade 5: no spontaneous movement contralateral side at rest or no spontaneous motor activity (severe) (90).

3.2.2. Systemic Methotrexate (MTX) Administration

One hour before the brain ischemia, 400 mg/kg MTX (Koçak Farma, Ankara, TURKEY) was injected intraperitoneally (i.p.). Maximally tolerated dose of MTX for systemic injections is 760 mg/kg in mice (91). 400 mg/kg was chosen because it is a high dose that we expect to see the changes less than 24 h (92). Also, this dose used in a study which investigated the relationship between circadian rhythm and MTX toxicity in mice. In support of this study we have pharmacokinetic properties of this dose of the drug in a time-dependent manner (93).

3.2.3. Isolation of the Brain Microvessels

The brain was placed in ice cold HBSS and HEPES solution mixture in a petri dish. Under a stereomicroscope (Nikon SMZ745T) pineal gland, meninx and choroid plexus were removed, and the tissue was homogenized, then centrifugated at 2.000 g for 10 min at 4°C, supernatant was discarded. Then, 18% 70.000 kDa Dextran was added on the pellet, centrifugated at 4.400 g for 15 min at 4°C to separate the non-vascular brain tissue. The pellet with vessels was filtered through 100 µm and 40 µm filters to obtain microvessel fragments, and centrifugated (94). The immunohistochemical and Western blotting studies were performed as stated above, from the isolated vessels of naive, sham, treated and ischemic mice.

3.2.4. Magnetic Resonance Imaging (MRI)

In vivo MRI was performed at the CERMEP imaging platform (Lyon, France), as previously described (95-99). In brief, MRI was performed by a 7 Tesla (7T) horizontal-bore Bruker Avance II rodent imaging system (Bruker Biospin, Ettlingen, Germany), using a 50-mm inner diameter birdcage coil for transmission and a 15-mm diameter surface coil for reception. The *in vivo* MRI protocol comprised a diffusion-, perfusion-weighted, spin-echo, T1- and T2- image axial sequences. Figure 3.1. shows the design of the experiments for MRI. First, siRNAs (RFC1-siRNA, n=7, and Scrambled-siRNA, n=7; Table 3.1.) were injected to mice intracortically. After 24 h

MCAo was induced. An acute high resolution (7 T) MRI was acquired straightaway. Following 90 min ischemia, animals were recanalized and at 24 h post-ischemia, a follow-up MRI was obtained using the same sequences as the first MRI.

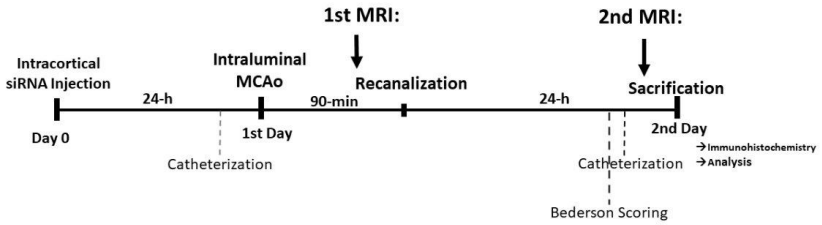

Figure 3.2. Experimental timeline of MRI experiments. Mice were intracortically injected with 100 μM of siRNA at day 0 (D0). At day 1 (D1) animals were catheterized to administer Gadolinium (Gd; 550 Da) intravenously during MRI, and then MCAo was induced, and imaged immediately by MRI. After 90 min of ischemia, mice were recanalized. At day 2 (D2) they were re-catheterized for Gd intervention and re-imaged with MRI. Then mice were sacrificed for post-mortem immunohistochemical studies and other analyses.

For the MRI procedure, anesthesia was induced with a mixture of air and 3.5% isoflurane, maintained at 2% isoflurane (ISO-VET, Piramal Healthcare, Morpeth, UK). Then animals were placed in MRI-compatible mouse cradle. The respiratory rhythm was cautiously monitored by a pressure sensor linked to a monitoring system (ECG Trigger Unit HR V2.0, RAPID Biomedical, Rimpar, Germany), as well as the body temperature to maintain within the physiological boundaries.

3.3. Methods Used for Retina Experiments

3.3.1. Retinal Ischemia Model

The retinal ischemia model used here was previously developed in our laboratory (100). In brief, anesthetized mice were put in a prone position under a stereoscope (SMZ1000, Nikon Instruments Inc., Amsterdam, The Netherlands) and their heads were immobilized with a nosepiece. Central retinal arteries located in the central optic nerve were exposed via cautious retroorbital dissection. A small strip (0.3 × 1 mm) of 30% $FeCl_3$–soaked filter paper was placed on the optic nerve for 3 min to trigger clot formation and occlude the central retinal artery (Figure 3.2). Based on our previous observations, we used 1 h of ischemia, as it was sufficient to induce ischemic

changes in the microcirculation such as mural cell contractions (11, 13). One h later, eyeballs were collected under anesthesia, and animals were sacrificed.

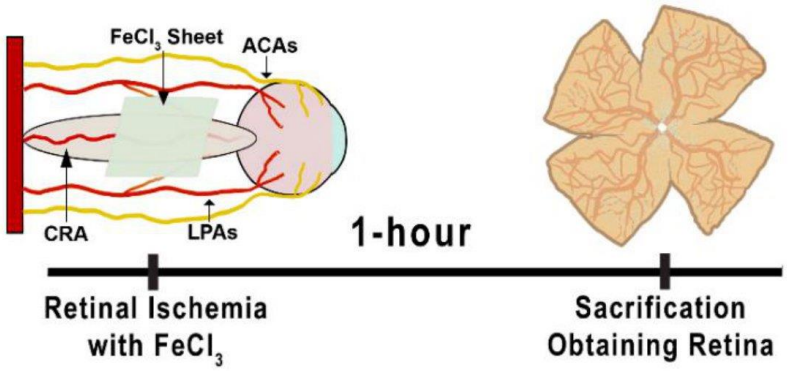

Figure 3.3. Timeline of retinal ischemia experiments. Schematic drawing of permanent FeCl3 retinal ischemia model which is performed by placing a small piece of (0.3 × 1 mm) filter paper saturated by 30% $FeCl_3$ on optic nerve for 3 min to occlude CRA. 1 h later animals were sacrificed, and the retinas were obtained. ACA: anterior cilliary artery, CRA: central retinal artery, LPCA: long posterior cilliary artery. Duygu Gürler prepared the figure.

3.3.2. Retinal Whole Mount Preparation

The eyeballs harvested were immersed in 4% PFA for 1 h, and under a stereomicroscope, a puncture was made at the corneal border with an insulin needle while eyeballs were resting in one drop of PBS at room temperature. A circular cut along the limbus was made with the help of a micro-dissector. Following the extraction of the lens and vitreous body, the intact retina was detached from the sclera via a 45-degrees thick curved tip tweezer by going around the edges. Then, the flattened retina was placed into a centrifuge tube consisting of 200 µL PBS for immunohistochemistry.

3.3.3. Retinal Radial Section Preparations

Obtained eyeballs were immersed in 4% PFA for 24 h followed by incubation in 30% sucrose for 2 days. Next, 20 µm sections were obtained by cryostat.

3.3.4. Retinal Trypsin Digest Preparation

We used modified retinal trypsin digestion protocol to isolate retinal microvessels from the surrounding tissue (101). Retinas were separated in cold PBS, then immersed in 250 µL filtered ddH_20, and, at room temperature, kept on a shaker until they disintegrated. Then kept in 0.3% trypsin (PAN Biotech 1:250) 0.1 M Tris buffer (pH 7.8) in the incubator adjusted to 37°C. The separation of microvessels were seen clearly, tissue was washed with dH_2O, and the procedure was repeated until no debris remained. Isolated retinal microvessels were transferred to poly-L-lysine coated slides without disrupting their integrity, and air-dried. This method allowed isolation of the retinal vessels containing endothelial cells, basal lamina, pericytes, the attached perivascular astrocyte processes, without the other cell types like photoreceptor cells.

3.3.5. Gene Overexpression *in vivo* by Lentiviral Vector (LV)

Lentiviral vectors (LV) that express either green fluorescent protein (GFP) (Control-LV) or GFP with RFC1 (RFC1-LV) driven by EF-1 alpha promoter were used to overexpress RFC1 gene in the retina. The lentiviral packaging system used for RFC1-LV or control-LV was second-generation and was an effective and safe technique in production. Total RNA from cultured mouse neuro 2a cells was extracted using AllPrep DNA/RNA/Protein Mini Kit (80004, Qiagen, Hilden, Germany) following the manufacturer's instructions. Transcriptor First Strand cDNA Synthesis Kit (04896866001, Roche, Basel, Switzerland) was used to obtain complementary DNA (cDNA). The coding region of Mus musculus SLC19a1 variant 1/RFC1 (NCBI Reference Sequence: NM_031196.3) was amplified with specific primers (forward 5'-agtcagaattcatggtgcccactggccag-3'and reverse 5'-AGTCAGGATCCTCAAGCCTTGGCTTCGACTCTT -3') with fast digest restriction enzymes EcoRl (FD0274, Thermo Fisher Scientific, Massachusetts, USA) and BamHI (FD0054, Thermo Fisher Scientific). Restriction enzymes BamHI and EcoRI were used to digest the PCR product of SLC19a1 and expression plasmids (pLenti-EF1α-GFP-2A-Puro; Applied Biological Materials, Richmond, Canada). Subsequently, ligation was realized with T4 DNA ligase (EL0014, Thermo Fisher Scientific). Sequencing pMD2.G and psPAX plasmids, kindly provided by Dr. Didier Trono (Ecole Polytechnique Federale, Lausanne, Switzerland), were used to confirm

the insert. They were employed as complementary vectors of the packaging of the lentiviral system (12259; 12260, Addgene, United Kingdom). HEK293T cell line (6×10^6 cells) was chosen to be seeded on 10 cm plates (CLS3294, Corning, New York, USA). The following day, the vector transfection Lipofectamine 3000 (L3000015, Thermo Fisher Scientific) was applied according to the manufacturer's instructions. Shortly, 7 µg lentiviral vector, 3.5 µg pMD2.G, and 7 µg psPAX were used to prepare DNA-lipid complexes. The DNA-lipid complex was added slowly after 10 min of incubation at room temperature. Six hours after transfection, the medium was changed with fresh DMEM (P04–01158, Pan Biotech, Bavaria Germany) and was incubated at 37°C in a humid atmosphere consisting of 5% CO_2. Twenty-four and fifty-two hours following the transfection, the medium was harvested, centrifuged for 10 min at 2000 rpm, and filtered with a low binding filter with a 0.45 µm pore size. After ultra-centrifuging at 120,000 g for 2 h, viral particles were dissolved in Dulbecco's Phosphate Buffered Saline (DPBS) without calcium and magnesium (P04–3650, Pan Biotech). The plasmid with no DNA inserted was packaged with the same procedures to use as a control. The viral titer (1×10^8 lentivirus particles in 1 µl 0.1 M PBS) was measured by a previously published protocol (102).

LV (1×10^8 lentivirus particles in 1 µl 0.1 M PBS) were intravitreally delivered to the retina (2 µL/eye) via 33 G Neuros Syringe (1701 RN, Hamilton). Ten days after the delivery, we either proceeded to retinal ischemia or sacrificed mice to obtain eyeballs.

3.3.6. Electroretinography (ERG)

A modified scotopic ERG protocol (103) was performed on mice that were kept in complete darkness for 24 h before ERG. Anesthetized mice were placed on a heating pad in prone position. To record the electrical activity in the eye, three electrodes were used. The ground electrode was a needle electrode was inserted beneath the skin at the base of the tail, the reference electrode was inserted in the mouth, and the measuring electrode was placed in contact with the cornea of the eye being measured. Pupils were dilated with topical administration of 2.5% phenylephrine. The eyeballs were protruded by tightening a loop of a simple knot that was circumferentially slipped over the eyeball. After moistening the cornea with saline (0.9% NaCl), the eye was

presented with blue LED flashes in 5V potential, with repeat rate 0.2 Hz and pulse width 0.01 second. The band pass filters were set to 1-1000 Hz. The signals were recorded and analyzed by PowerLab 16/35 data acquisition system and displayed by LabChart Reader 8 (AD Instruments).

3.3.7. 5-MTHF analysis via HPLC in retinal samples

We treated animals either with 100 nM RFC1-siRNA (n=3), Scrambled-siRNA (n=5), low dose 5-MTHF (1.5 µl 5-MTHF dissolved in DMSO (0.2 mg/ml) and high dose 5-MTHF (1.5 µl 5-MTHF dissolved in DMSO (10 mg/ml) intravitreally via 33 g Hamilton. We obtained eyeballs 24-hours later and immediately placed them in sterile ice-cold PBS. Eyes were collected 3 hours later. Under surgical microscope we dissected retinas from eyeballs with sterile surgical tools. Retinas were snap-frozen in 2 ml tubes in liquid nitrogen, stored at -80°C. Then retinas were weighed and homogenized with Tissuelyser LT (QUIAGEN) with 50 mM Hepes pH 8.0 buffer and 100 µL of solvent containing 1% ascorbic acid at +4°C for 10 min at 50 1/s. The homogenized retinas were centrifuged at 14000 rpm for 10 min at +4°C and the homogeneous part was taken. Homogenates were taken in 10 kDa filters and centrifuged again for 30 minutes under the same conditions. After centrifugation, the filtered portion was aliquoted. Prepared samples were analyzed by HPLC (Waters Alliance, 2690 HPLC and W2475 FLD) system with fluorescence detector at 280 nm excitation and 360 nm emission wavelengths. The results are expressed in mean of 5-MTHF in ng/g ±SEM (104).

3.3.8. 5-MTHF analysis via LC MS/MS in plasma samples

After obtaining eyeballs under deep urethane anesthesia, whole blood was collected via 1 ml heparinized insulin needles from a cardiac puncture. 100-600 ul blood was collected from each animal before cardiac arrest. Blood was stored immediately in EDTA-treated tubes on ice protected from light. Tubes were centrifugated 2000 g for 15 minutes at +4°C. Plasma was taken to the 2 ml tubes which were snap-frozen in liquid nitrogen. Next, plasma samples stored at -80°C were thawed at room conditions. 50 µL of solvent containing 50 mM Hepes pH 8.0 buffer and 1% ascorbic acid was added onto 50 µl of plasma and vortexed for 10 s. 100 µl of

acetonitrile was added to the mixture and vortexed for another 10 s. It was kept at +4°C for 30 min to complete the protein precipitation. It was then centrifuged at 14000 rpm for 20 minutes at 4°C. The supernatant was taken. Prepared plasma samples were analyzed in LC-MS/MS (Agilent Technologies, 1290 LC and 6460 TripleQuad) in +MRM mode (460.0 -> 313.0) (105).

4. RESULTS

4.1. Results of the Brain Experiments

4.1.1. RFC1 protein is abundantly expressed in the endothelial cells and pericytes of the brain

The scarcity of antibodies for RFC1 immunohistochemistry until recently was a challenge for studies; hence, most former studies used RFC1 antiserum or homemade antibodies to mark RFC1 protein in the tissues (26, 27, 106). The availability of commercial RFC1 antibodies that were confirmed by immunohistochemistry and by Western blotting facilitated the research in the field(1, 2).

We first immunohistochemically examined RFC1 in the frozen brain sections. We observed that RFC1 was distributed continuously and diffusely throughout the brain microvessels. RFC1 was immunohistochemically co-labeled with the endothelial marker, cluster of differentiation 31 (CD31), and as expected, determined that CD31+ microvessels were immunopositive for RFC1 (Figure 4.1.A.). The RFC1 immunopositivity was also confirmed in a-SMA positive microvessels (Figure 4.1.B.). We then labeled the microvessels with well-defined pericyte markers including, platelet-derived growth factor receptor beta (PDGFR-β) and aminopeptidase-N (CD13) and all of which showed colocalization with RFC1 (Figure 4.1.C.). These indicated that RFC1 protein was present both in the endothelial cells and pericytes. We also confirmed from Human Protein Atlas that human brain microvessels were RFC1 immunopositive in human post-mortem cerebral cortex (107). Additionally, even the atlas mentioned endothelial cells and neuronal cells were immunopositive, and glial cells were negative, it omitted that the pericytes, which were deciphered by their bump-on-a log shape, being immunopositive for RFC1 (108).

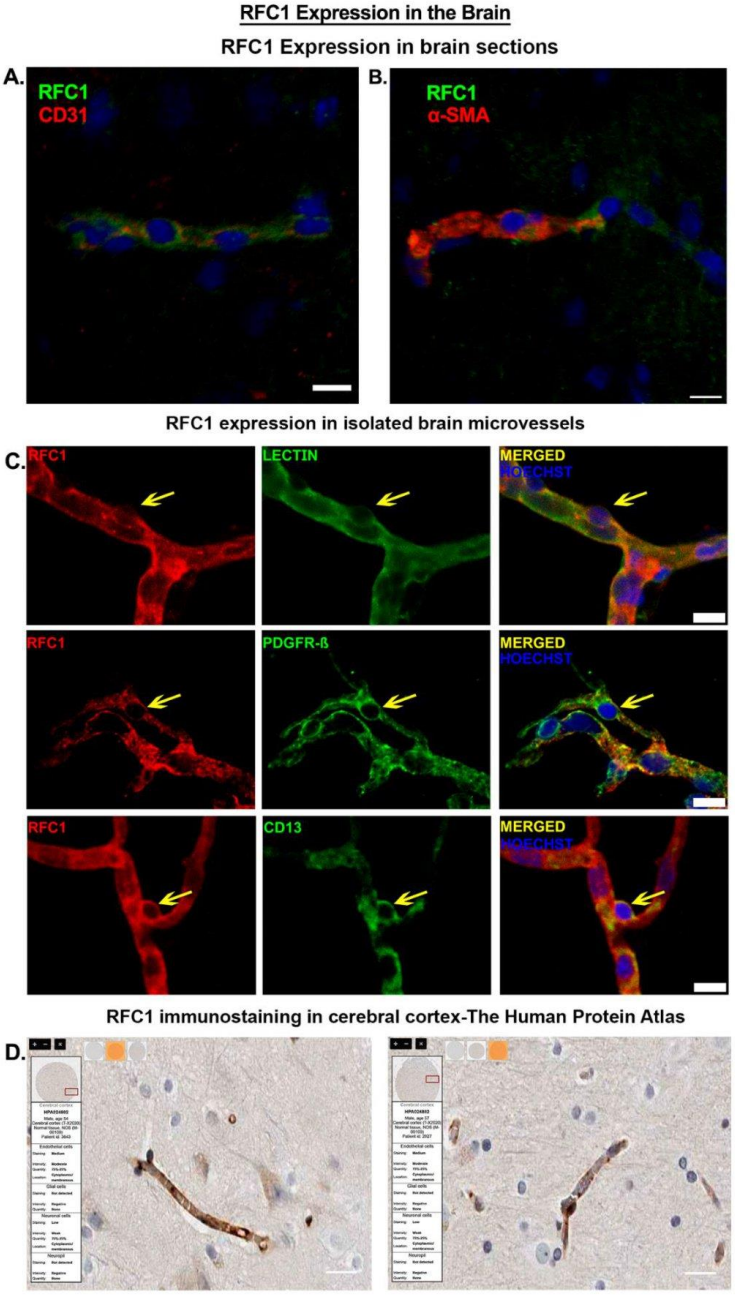

Figure 4.1. RFC1 protein was present in endothelial cells and pericytes of the microvessels of the mouse brain. A) Ex vivo labeling of 20 µm cryo-section from PFA

fixated brains of naive Swiss Albino mice with anti-RFC1 antibody (green), and endothelial marker CD31 (red). Abundant RFC1 immunopositivity was observed along CD31-positive microvessels. B) RFC1 is expressed in α-SMA positive (red) microvessels as well. C) The microvessels (< 9 μm diameter) isolated from fresh brains were immunohistochemically labelled with anti-RFC1 antibody (red). RFC1 (red) colocalized with the vessel marker Lectin (green) and the accepted pericyte markers PDGFR-β and CD13 (green) (n=3/marker). Scale bars: 10 μm D) RFC1/SLC19A1 expression localized to human brain microvasculature in the Human Protein Atlas (107). Nuclei were labeled with Hoechst 33258 (blue).

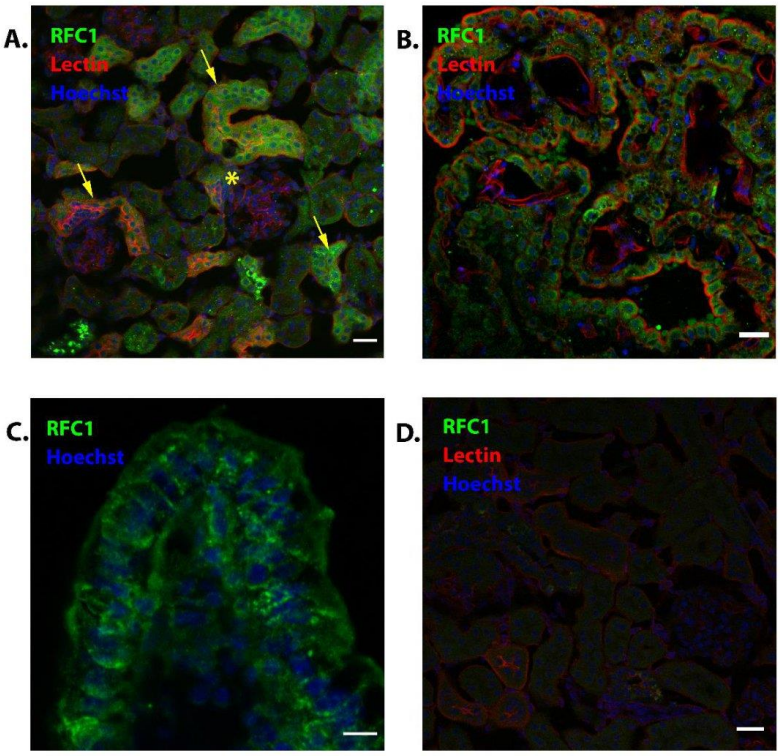

Figure 4.2. Immunofluorescent labeling of positive control tissues with anti-RFC1 antibody. A) Anti-RFC1 antibody (green) is marked (yellow arrows) in the kidney proximal tubules where folate reabsorption takes place. Texas Red Lectin (red) marked the glomeruli and tubule walls. The fact that the glomeruli (yellow stars) consisting of capillaries lined by specialized endothelial cells do not stain with RFC1 as expected, showed that the staining we obtained in brain capillaries was specific. B, C) RFC1 protein was immunopositive in untreated mice tissue sections of brain choroid plexus, and intestinal mucosa, respectively. D) Negative control staining with anti-RFC1 antibody. No fluorescent signal was detected in the negative immunohistochemical control examination of the untreated mouse kidney section without treatment with

using anti-RFC1 antibody and adding the secondary antibody. Nuclei are marked with Hoechst 33258 (blue). Scale bars: 25 μm.

The RFC1 immunolabeling was confirmed by positive immunolabeling of the tissues that are known to have abundant RFC1 protein in the literature and demonstrated immunohistochemically. The first one is the kidney tissue. The kidneys play an important role in maintaining folate homeostasis in the body through the process of glomerular filtration and tubular reabsorption. Circulating folate is freely filtered in the glomeruli, mainly in the form of 5-methyltetrahydrofolate (5-MTHF). Most of the filtered folate is reabsorbed in the proximal tubules. This reabsorption process is an important mechanism to prevent urinary folate loss. RFC1 is located on the basolateral membrane of proximal tubular cells. In immunolabeling, the RFC1 protein was marked in the kidney proximal tubules (Figure 4.2., yellow arrows). In addition, glomerular cells composed of specialized endothelial cells but known not to express RFC1 were not labeled with anti-RFC1 antibody (Figure 4.2., asterisk). This also served as an intra-tissue control. The choroid plexus was used as the second positive control. The choroid plexus separates the systemic blood flow from the CSF. Folate in CSF is approximately 4 times the concentration found in plasma, and RFC1 is located on the choroid plexus epithelium, contributing to the concentration of folate in CSF. The mucosa of the jejunum is the third positive control tissue containing RFC1, which contributes to the absorption of folate from food (27). To confirm that the stainings were not non-specific, control stainings in the absence of primary antibody was also performed (Figure 4.2.).

4.1.2. Cerebral Ischemia Alters RFC1 Protein Level

It was aimed to investigate the expression of RFC1 in the brains that underwent recanalization for 1 h, 24 h and 48 h following 90 min of MCAo. The RFC1 immunoreactivity was apparent and diffuse throughout the contralateral brain regions such as the cortex, striatum, hippocampus, and subcortical white matter. However, in the ipsilateral hemisphere, we observed a decreased immunofluorescence at each time point in the core region (Figure 4.3.). The core and periinfarct regions were confirmed by the corresponding pale regions in Nissl staining of the subsequent sections (40 μm separate). In addition, Western blotting validated that RFC1 expression dropped

dramatically in the core region at all timepoints, and this result suggested that RFC1 decrease in immunohistochemistry was not accounted for loss of immunoreactivity due to ischemia causing antigen hindering (109).

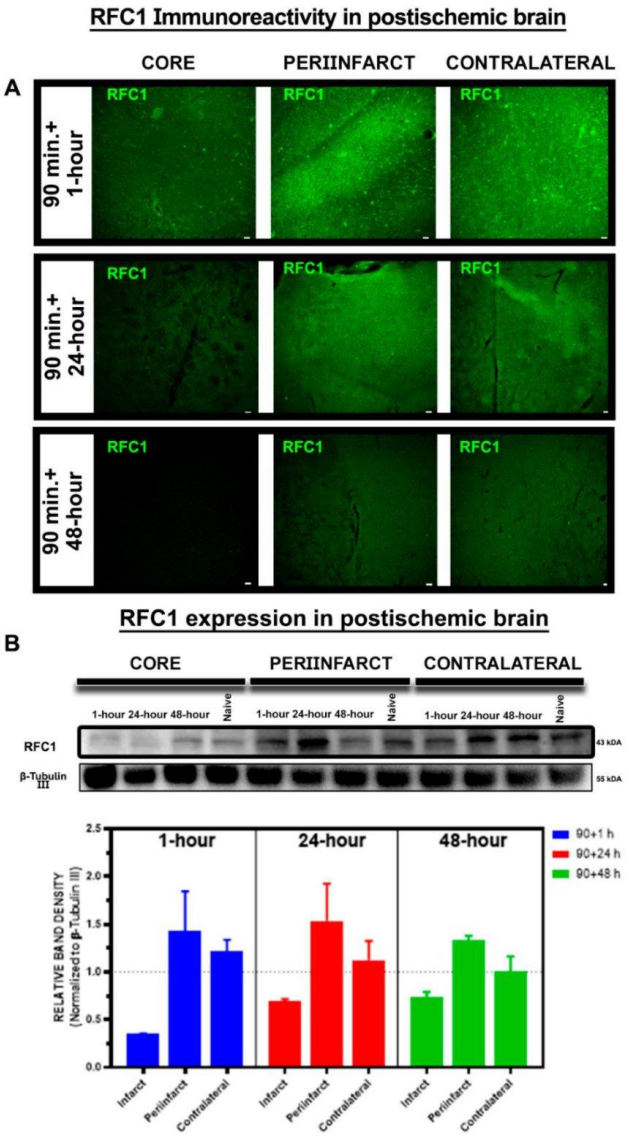

Figure 4.3. Changes in RFC1 protein expression. A) Representative photomicrographs acquired from core (i), periinfarct (ii), and contralateral (iii) regions

of the ischemic brains immunohistochemically labelled by anti-RFC1 after 90 min MCAo followed by different recanalization durations (1 h, 24 h, 48 h; n=3/recanalization duration). The images were obtained 10x objective (HC APO L U-V-I 10x/0.30 WATER). B) Representative results of Western blot analysis for RFC1 protein expression in the core (i), periinfarct (ii), and contralateral (iii) hemisphere extracts from naive and mice sacrificed at 1 h, 24 h, and 48 h after recanalization (n=3/recanalization duration). Note that a band of about 43 kDa corresponding to RFC1 protein was observed higher in the periinfarct of ischemic hemisphere at 24 h; however, that was not statistically significant. C) Quantification of RFC1 protein expression. Data were obtained relative density measurements of bands which were normalized to β-tubulin III as the loading control. Results were expressed in relative optical density and represented as mean ± S.E.M. The intensity of RFC1 protein expression in periinfarct region significantly increased at 1 h, stayed increased at 24 h, and decreased at 48 h. Scale bar=25 micron.

4.1.3. Ischemia Changes the Distribution of RFC1 Protein at the Microvessel Level

After detecting ischemia caused changes in the expression of RFC1 protein at the brain parenchyma, the distribution of RFC1 at the microvessels was made by isolating microvessels from ischemic brains. As a result, while non-ischemic microvessels showed diffuse and homogenous RFC1 staining, ischemic microvessels showed interrupted and punctate pattern (Figure 4.4).

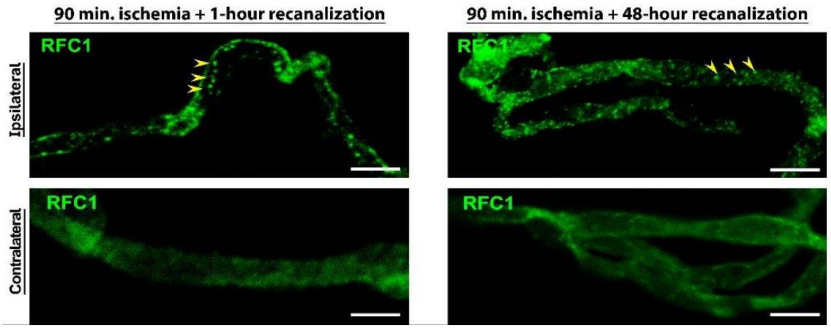

Figure 4.4. RFC1 immunopositivity in microvessels obtained from the ischemic brains. RFC1 labeling with anti-RFC1 antibody in isolated microvessels according to ischemic regions was examined. RFC1 were observed to be more punctate and interrupted (green) isolated from the ischemic region. Whereas microvessels isolated from the contralateral hemisphere showed diffuse and homogenous RFC1 staining. Scale bars: 25 μm.

4.1.4. Pharmacological Intervention to Alter RFC1 Protein Expression

RFC1 does not have specific pharmacological modifier in the literature. Thus, MTX, a high affinity substate of RFC1 and competitive inhibitor of folate transport via RFC1 was chosen to investigate to modify the RFC1 level in the brain. The pharmacological intervention was achieved by systemic MTX treatment and was expected to block the function of the protein for a limited period of time, as its half-life was found to be 33.8±6.5 minutes in mouse (91). Even if it had limited half-life, *in vitro* studies showed 30% decrease in mRNA levels of RFC1 24 h after exposure to MTX, and a decrease in RFC1 protein level following a single dose of MTX (110). Therefore, we examined RFC1 levels in the brain after the 1, 24, and 48 h of single dose i.p. MTX injection.

Immunofluorescent labelling and Western blotting (Figure 4.5.) of whole brain homogenates were performed from brains sacrificed at 1 h, 24 h and 48 h after administration of MTX (400 mg/kg). Confocal microscopy images were obtained from the cortex of middle cerebral artery territory of the brains (Figure 4.5.). It was observed that MTX increased the level of RFC1 acutely even after a single dose i.p. administration. RFC1 levels 24 h after MTX were not consistent in our Western blotting, probably due to technical reasons. Conversely, 48 h after MTX, a decreased RFC1 level was determined which is in line with the literature.

The increase might be due to the fact that, as MTX is a competitive substrate of RFC1, it may reduce the intracellular transport of folate causing an increased need of RFC1 levels for cells to transport adequate folate. However, because of some further technical issues, and our other primary aims, we did not do further studies.

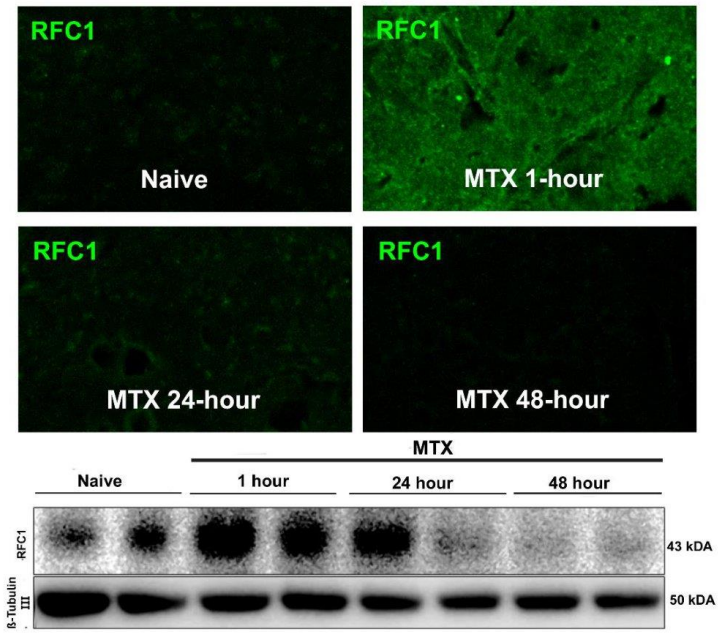

Figure 4.5. The effect of single dose systemic MTX. After single dose MTX (i.p.) mice sacrificed at 1, 24 and 48 h. Immunofluorescent images and Western blotting of the brains of each mouse suggest that single dose of systemic MTX increased RFC1 protein levels at 1 h, and RFC1 protein was lowest at 48 h in the brain.

4.1.5. Pharmacological Intervention to Alter RFC1 Before Acute Ischemia Rescues RFC1 Protein Expression

Since upregulation RFC1 protein 1 h after MTX treatment was determined, it was tried as a pre-treatment to rescue ischemia induced RFC1 protein changes after ischemia.

The intensity of the RFC1 signal appears to be increased in both the core, periinfarct and contralateral regions of the brains of the ischemia/recanalized animals following single dose MTX (400 mg/kg) administration (Figure 4.6.).

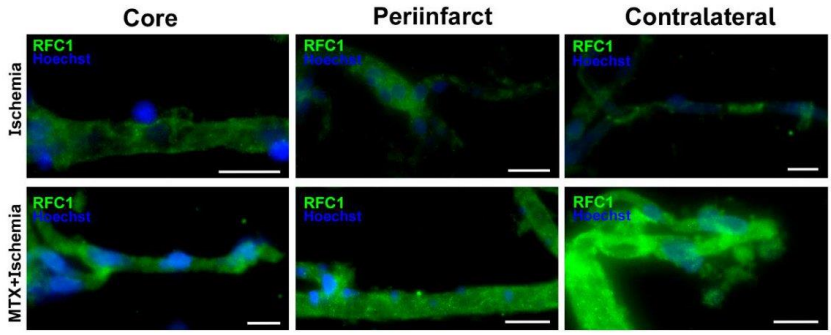

Figure 4.6. RFC1 immunofluorescence in the microvessels changing via pharmacological intervention before ischemia/recanalization. Animals were treated with i.p. MTX or vehicle 1 h before 90 min MCAo and 1 h recanalization (n=3). The core, periinfarct and contralateral regions of the brains were dissected and microvessels were freshly isolated. Immunohistochemistry with anti-RFC1 antibody (green) revealed an increase in ischemia induced RFC1 decrease. Nuclei were marked with Hoechst 33258. Scale bars: 10 μm.

4.1.6. Pharmacological Intervention Altering RFC1 Protein Expression Leads to Alteration in Infarct Size 48 h after ischemia

The evaluation of infarct size was made from 12 standard sections of 20-micron thickness covering the MCA territory. After Nissl (Cresyl Violet) staining application to these sections (Figure 4.7.), standard images were taken at 1x magnification under the light microscope. The researcher who took the images were blinded to recanalization periods and/or MTX application and, the images measurements from the images were done by another researcher in a randomized manner. Adjusted infarct area that is corrected for edema was calculated by subtracting the non-infarcted area of ipsilateral hemisphere from contralateral hemisphere in mm^2 using the ImageJ program (111). This procedure was repeated for 12 slices taken from each brain, and the total infarct area obtained from each brain was multiplied by the standard antero-posterior distance between the first and last slice, 0.96 mm, to obtain the infarct volume. To compensate for the variation that may be caused by inter-animal brain size differences, the infarct volume of each brain was plotted as a percentage of the calculated contralateral hemisphere volume.

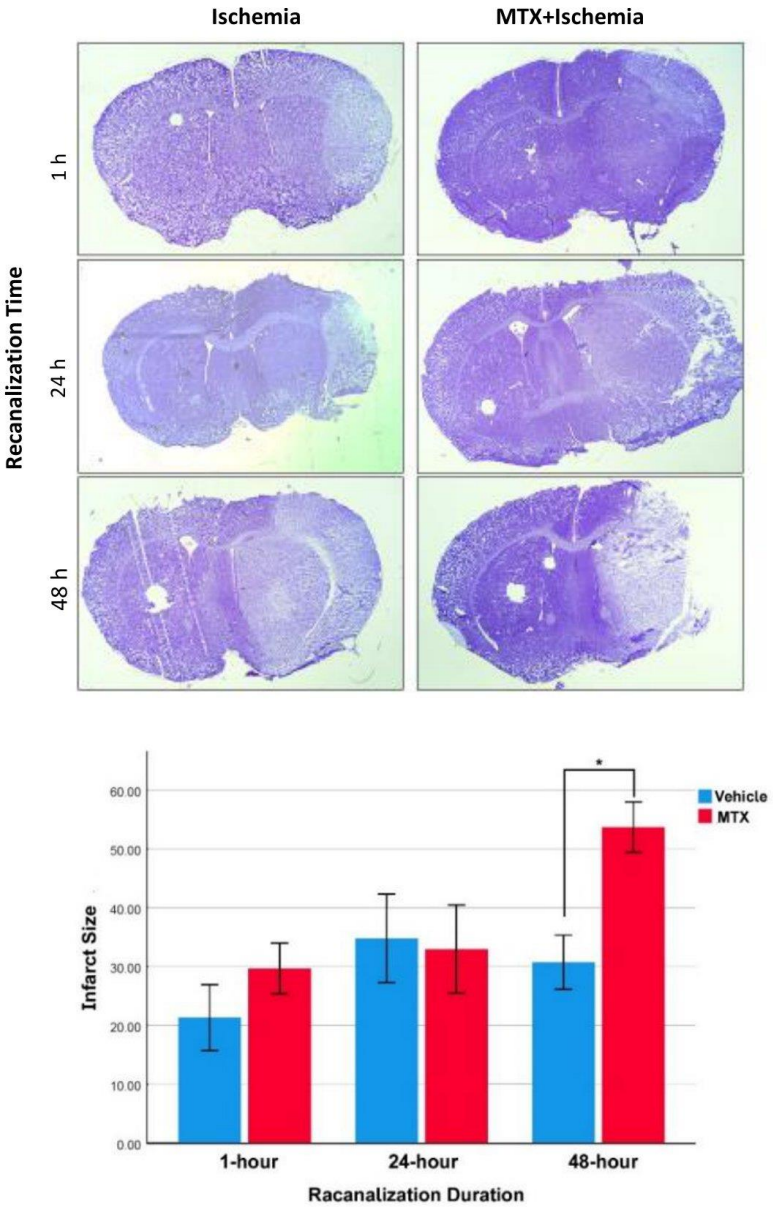

Figure 4.7. The infarct volume decreased with MTX pretreatment in 90 min MCAo ischemia and 48 h recanalization. The representative images of Nissl stainings from brain sections of the animals that were recanalizated for 1, 24 or 48 h after 90 min MCAo, or pretreated with MTX ones are shown at 1x magnification under the light

microscope. Intact areas appear purple, where infarction appear light purple or white (left). Infarct sizes were obtained from Nissl staining and comparisons were made between groups (right). Data are expressed as mean ± S.E.M. (*p=0.009, Bonferroni correction applied after comparison between means. n=4-6 for each ischemia group; n=3-4 for MTX+Ischemia groups).

After ischemia following MTX administration, no significant change in infarct volume was observed in 1-h recanalization group compared to control ischemia (Figure 4.7., bar graph). This might be attributed to the low sensitivity of infarct volume assessment using Nissl staining within 1 h of recanalization after 90 min of ischemia. Besides, this can be interpreted that despite the increase in total RFC1 protein induced by MTX, this elevation could not provide neuroprotection. However, the statistical significance might have changed if the number of mice in this group was increased.

It was observed that animals pretreated with MTX before ischemia had a larger infarct volume than non-treated ones only in the 48-h recanalization group not in other recanalization groups. It is important to note that 48 h recanalization time corresponds to approximately 48 h after MTX administration (Figure 4.7., bar graph). Although a decreased RFC1 level was determined after 48 h MTX, it is challenging to infer that the decrease in RFC1 level was associated with an increase in infarct volume at that timepoint. Since MTX, apart from being a competitive inhibitor of RFC1, is known to change the transcription of various genes that affect the folate cycle in a cell. Moreover, in one study, the half-life of systemic MTX in mice was found to be 33.8±6.5 minutes (91). Therefore, since it is accepted that the drugs are cleared from the systemic circulation after 4 or 5 half-lives, only the 1-h recanalization group is in the interval where we can observe the competitive inhibitor effect of folate transport of MTX. The difference in infarct volume in the 48-h recanalization group suggests that the impact of MTX could be mediated by affecting intracellular pathways and gene transcriptions in this late timepoint. However, the detection of a larger infarct in the 48-h recanalization group following 90 minutes of ischemia with a single dose of systemic MTX administration is a first in the literature. Therefore, this result indicates that the potential harm of MTX in ischemic stroke should be investigated more closely clinically, considering that it is a widely used drug in rheumatic diseases and as a chemotherapeutic in humans.

In addition, MTX administration before early ischemia/recanalization increased RFC1 expression at the microvessel level. It is planned to be investigated if MTX application changes the microvessel level at different recanalization times.

4.1.7. Brain RFC1 is downregulated *in vivo* by RFC1 targeted Accell siRNA

RFC1-siRNA (50 μM) or Scrambled siRNA (50 μM) were injected to mice intracerebroventricularly and and their middle cerebral artery territories were removed 48 h later. Next, tissue RNA was isolated, and qRT-PCR was performed. The relative mRNA level determined by qRT-PCR between groups were not statistically significant. The mean ± S.E.M for the Scrambled-siRNA and RFC1-siRNA group were 1.11± 0.15 and 1.05±0.18, respectively.

Since no success was achieved in silencing RFC1 mRNA expression in the brain with intracerebroventricular siRNA application it was planned to inject siRNA directly into the middle cerebral artery territory. Since the mouse cortex is thin and superficial (≈1 um), large amounts of fluid cannot be injected, and overflow appears. For this reason, it was planned to double to concentration of siRNA to 100 μM and to give 1 μl of siRNA via each injection. A double burr hole was opened to target the middle cerebral artery territory and the stereotaxic frame was angled, and the cut end of the Hamilton injector was aimed to enter the cortex in accordance with the curved cerebral surface (Figure 4.8.A, B.).

We delivered a combination containing the same amount of specifically designed two RFC1 targeted Accell siRNAs (RFC1-siRNA) or two Scrambled siRNAs intracortically and sacrificed the mice 24 h later. To confirm the knockdown of RFC1, we obtained fresh brains and determined a pronounced decrease in RFC1 mRNA by *30.1%* compared to Scrambled siRNA (p=0.0286, Figure 4.9.A.). In line with these, RFC1 immunosignal intensity decreased on the injection site both in microvessels and neurons of RFC1-siRNA injected brains (Fig 4.9.B.). Moreover, the radius of the circle defined by dashed lines where the RFC1 gene appears to be markedly reduced is 500 microns. This, indeed, was evidence of the effect that intracortically injected RFC1-siRNA reached at a distance of 500 microns at minimum.

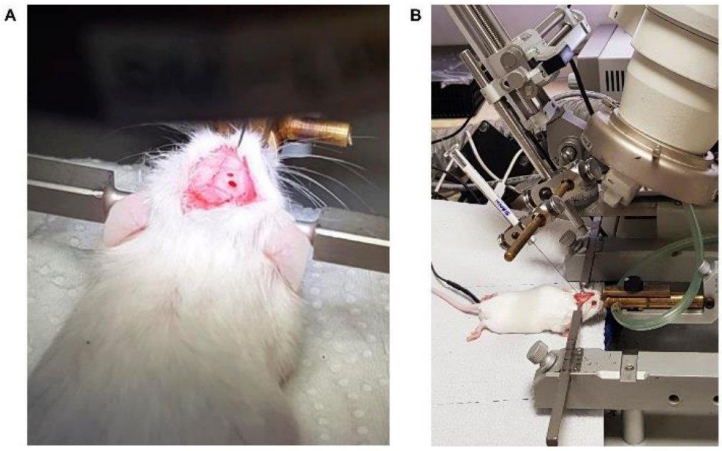

Figure 4.8. Intracerebral siRNA injection position in stereotaxic frame. A) Mice were placed in a stereotaxic frame under isoflurane anesthesia. The double burr hole opened to the skull, B) and the intracortical injection is seen.

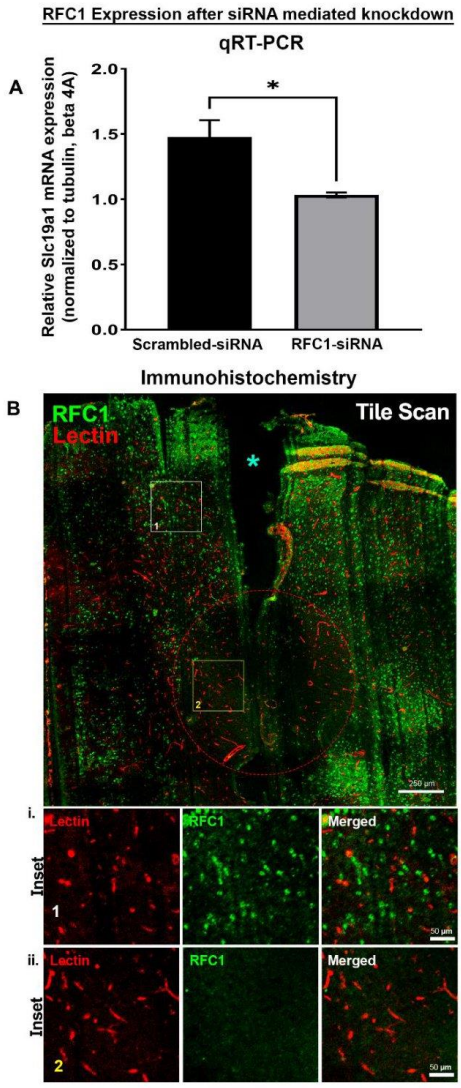

Figure 4.9. RFC1 knockdown is done in vivo by Accell siRNA in the brain. A) The graph shows that intracortical RFC1-siRNA delivery reduced RFC1 mRNA levels by *30.1%* when compared to Scrambled-siRNA (*p=0.0286). B) In fresh brain sections, RFC1 immunoreactivity was seen as decreased locally indicated by circular region demarcated by a red dashed line. Injection trace shown by cyan asterisk. Scale bar=250 micron. C i,ii) In magnification, both neuronal cell bodies and lectin positive microvessels seemed to lack of RFC1 immunopositivity. Scale bar=50 micron.

4.1.8. siRNA mediated RFC1 knockdown led to BBB disruption and endogenous IgG extravasation

We determined that RFC1 is expressed abundantly on endothelial cells and the pericytes of the BBB. Besides, folate is known to be important in BBB. So, the function of RFC1 in the BBB could not be ignored also considering our findings regarding the retina (will be mentioned later). Thus, intracortical and intrastriatal injections of RFC1-siRNA and Scrambled-siRNA were done and the brain sections were stained with fluorescently labeled antibody against endogenous mouse IgG to show extravasation.

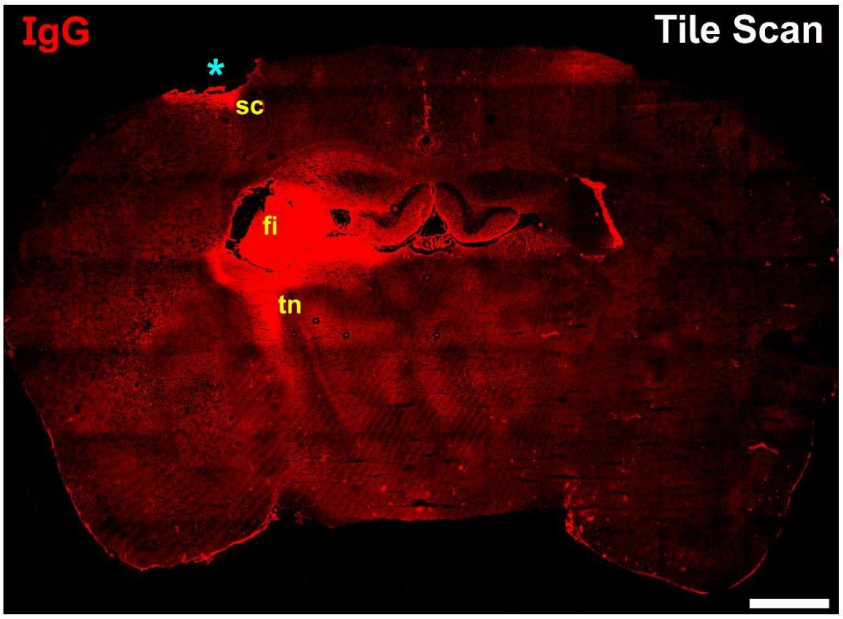

Figure 4.10. Intrathalamic siRNA injection resulted in IgG leakage along with the injection trace. The Hamilton injector was introduced 1700 micron deep into the brain in (ML:1.8, AP: -1.4, DV: 3.2). Syringe was retracted while slowly administering the siRNA over minimum of 5 minutes. Accordingly, thalamic nuclei (tn), fimbria (fi), and sensorial cortex (sc) along the trace showed IgG leakage. Scale bar=500 micron.

Due to the superficial nature of intracortical injections and to rule out the effect of meningeal leakage due to the trauma of injection we first injected siRNA deep in

the brain. The figure shows the injection of 1700 micron deep to the brain resulting in IgG leakage on the site of injection and along the injection trace (Figure 4.10.).

After confirming that the siRNA injection led to IgG leakage, intracortical injections were made, and this result was validated in the intracortical injections as well (Figure 4.11.)

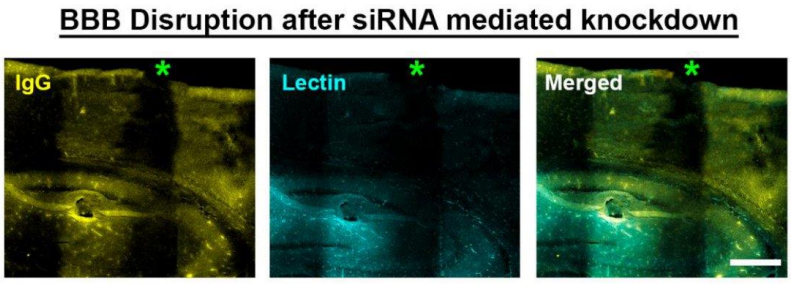

Figure 4.11. siRNA mediated RFC1 knockdown led to BBB disruption and endogenous IgG extravasation. After *in vivo* imaging same brain was obtained, sectioned, and labeled by Lectin (cyan) and incubated with Cy3 labeled goat anti-mouse antibody (yellow) to visualize the extravasated endogenous mouse IgG (155 kDa). Injection site can be seen under the asterisk. RFC1-siRNA mediated knockdown led to significant IgG extravasation in microvessels. Scale bar=50 micron.

4.1.9. RFC1 Knockdown Led to Autophagy Activation both in Neurons and Endothelial Cells

The autophagy is emphasized in maintaining BBB integrity in the recent literature (112). Furthermore, RFC1, interestingly, shows protein-protein interaction with a lysosomal protein LAMP1, and several other proteins playing role in apoptosis and autophagy pathway (KRAS, HRAS, calnexin, caveolin-1 etc.). Therefore, observing that RFC1 knockdown leading to severe barrier impairment, possible related mechanisms were also examined.

LC3 is a fine marker for activation of autophagy. Indeed, the conversion of LC3-I to LC3-II is widely used to observe autophagy activation over time. The amount of LC3-II is proportional to the amount of autophagosomes, which are double-membrane vesicles that will later fuse with lysosomes (113). Therefore, after injecting RFC1-siRNA intracortically to one hemisphere, and Scrambled-siRNA to the

contralateral one, LC3-II was immunohistochemically determined at the injection site (Figure 4.12.)

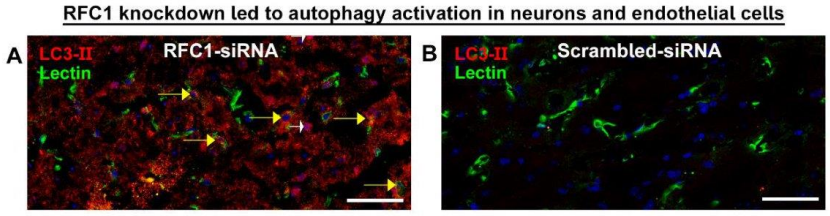

Figure 4.12. RFC1 knockdown led to activation of autophagy in neurons and endothelial cells. Representative photomicrograph from the brain injected either RFC1-siRNA or Scrambled siRNA. A) RFC1-siRNA induced autophagic marker LC3-II in neurons (white arrows) and in lectin positive endothelial cells (yellow arrows). B) Scrambled-siRNA injection did not lead induction of autophagic marker LC3-II. Nuclei were marked with Hoechst 33258. Scale bar=50 micron.

Consequently, it was determined that both neurons and endothelial cells showed autophagic activation at the injection site of RFC1-siRNA whereas Scrambled-siRNA did not lead to LC3-II expression. This result might suggest a possible relationship between RFC1 knockdown and autophagy pathway leading to BBB impairment. However, more detailed studies are needed.

4.1.10. RFC1-siRNA administration before ischemia led to Gadolinium leakage from the BBB at 24 h of ischemia

MRI is crucial in human stroke diagnosis and treatment. For translational medicine, studying physiology and pathophysiology with noninvasive methods is of utmost importance. To investigate the effects of RFC1-siRNA on infarct size and BBB, mice were imaged in vivo in acute and subacute phase of cerebral ischemia/recanalization with high resolution MRI modality (7T) at the CERMEP imaging platform (Lyon, France).

RFC1-siRNA or Scrambled-siRNA injections were performed in 14 male Swiss albino mice with the permission of the ethics committee obtained from the University of Lyon (the authorization number is: APAFIS#36695), and MCAo experiments were planned 24 h later. Ischemia was performed for 90 min followed by 24 h recanalization. MRI was planned two times for each mouse, with perfusion and

diffusion weighted imaging and generating Apparent diffusion coefficient (ADC) maps during the occlusion. T1 and T2 imaging including T1-weighted dynamic contrast-enhanced MRI by intravenous administration of the contrast agent Gd were the other sequences obtain during occlusion and next day after recanalization (Figure 4.13.). The induction of MCAo was shown in the Figure 4.14. demonstrating 9 animals that completed the first day of MRI. Next day in the morning, we found 1 animal from Scrambled-siRNA group and 1 animal from RFC1-siRNA group found dead; therefore, Bederson scoring was made in the 7 animals that were alive (Figure 4.15.). The scoring was not different statistically between groups. However, the median was higher in RFC1-siRNA group. The animal having the score 5 from RFC1-siRNA group had died during the second MRI. Therefore, the number of the animals which completed 24 h recanalization duration were only 4 animals from Scrambled-siRNA group, and 2 animals from RFC1-siRNA group. Besides, it had been decided to subject one animal out of 14 animals to sham surgery after RFC1-siRNA was injected (Figure 4.17.).

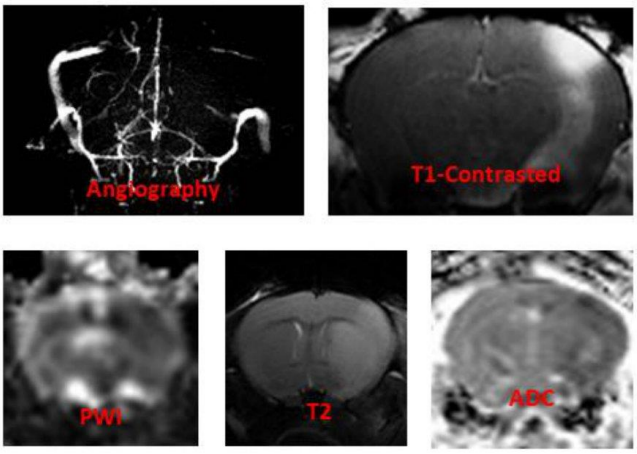

Figure 4.13. The sequences obtained by MRI. Comprehensive MRI protocol was applied using MR angiography, T1-contrasted, perfusion-weighted imaging (PWI), T2, and Apparent diffusion coefficient (ADC).

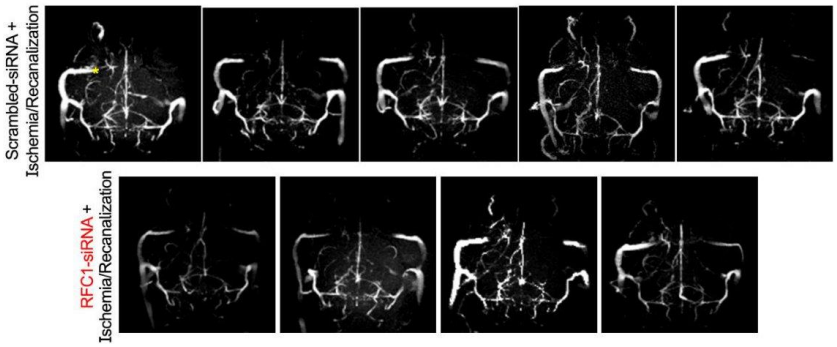

Figure 4.14. Angiography of MCAo validation. Panel shows the angiography of animals whose ischemia were successfully induced. Yellow asterisk shows contralateral middle cerebral artery. Notice that the trace of ipsilateral middle cerebral artery is missing due to successful occlusion.

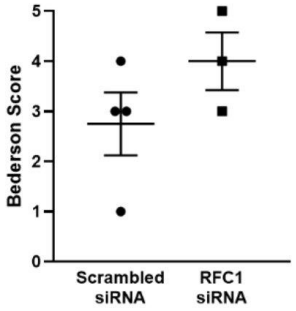

Figure 4.15. The graph showing Bederson Score. Scoring was made next day of the MCAo induction. Post-stroke Bederson Score between groups were not statistically different. Note that there were 3 animals in the RFC1-siRNA group at the time of the scoring. However, one of them, which was scored as 5 (no spontaneous movement contralateral side), died during MRI.

We first observed that RFC1-siRNA treated ischemic brains demonstrated broader Gd leakage compared to Scrambled-siRNA treated ones. We quantified in the cortex since we showed that RFC1-siRNA spreads limitedly. We decided to proportionate the cortical Gd leakage area to the cortical infarct area. The reason for choosing the infarct area as a denominator was, the fact that ischemia itself could cause Gd leakage at 24 h since it deteriorated BBB integrity. The variation in striatal infarct sizes and striatal leakage increased standard deviation leading to false negativity. Thus,

we determined that introducing RFC1-siRNA before ischemia resulted in larger leakage area.

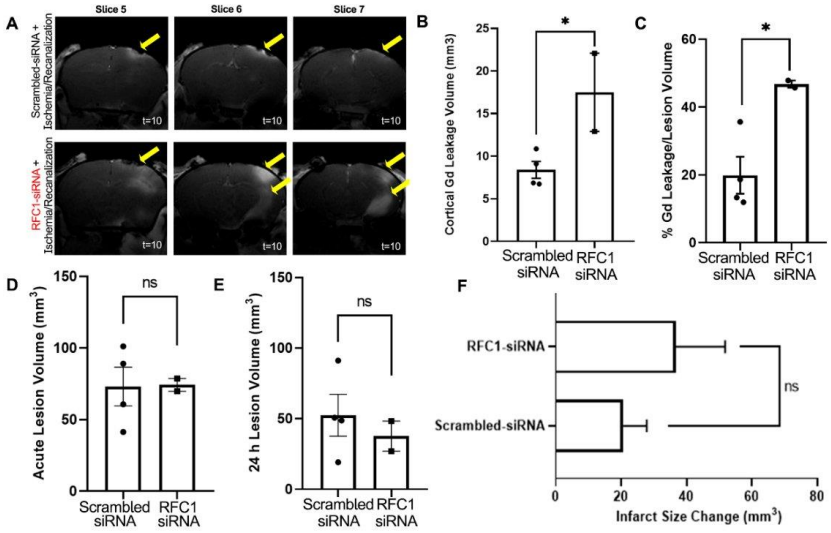

Figure 4.16. RFC1-siRNA administration before ischemia led Gadolinium leakage from the blood-brain barrier at 24 h of ischemia; however, the infarct size was not affected. A) Animals injected with RFC1-siRNA or Scrambled-siRNA were administered intravenous Gd at the end of 24 h of recanalization time and BBB permeability was examined. Accordingly, RFC1-siRNA administration before ischemia caused more Gd leakage from the BBB at the 24th h of ischemia. The upper panel shows minimal Gd leakage in the ischemic brain slices, while the panel below representing the RFC1-siRNA injected ischemic brains shows widespread Gd leakage. The leakage is especially observed in cortical areas where RFC1-siRNA injection had been made. B) The graph shows the cortical Gd leakage volume in mm3, which was found higher in RFC1-siRNA injected brains (*p=0.045). C) Cortical Gd leakage volume in ratio to cortical infarct volume was still higher in RFC1-siRNA group than Scrambled-siRNA group (*p=0.03). D, E) In those brains, neither acute cortical lesion volumes nor 24 h cortical lesion volumes were statistically different, which suggests RFC1-siRNA knockdown did not lead to brain tissue infarction although it leads significant BBB leakage. F) The change in the infarct size over 24-h was slightly higher in RFC1-siRNA group; however, not statistically different between groups.

The acute cortical ischemic lesion volumes, 24 h cortical lesion volumes, and the change in the infarct size over 24 h were not statistically different between groups, which suggests that even RFC1-siRNA knockdown that led to significant BBB breakdown, did not lead to larger infarction at least at this sample size. However, 2 out

of 4 RFC1-siRNA injected animals died within 24 h of ischemia injection whereas only 1 out of 5 animals died in the Scrambled-siRNA group.

Additionally, we verified that RFC1-siRNA led to Gd leakage without ischemia in T1-contrasted images from the mouse which underwent sham surgery and injected with RFC1-siRNA 24 h before MRI (Figure 4.17.).

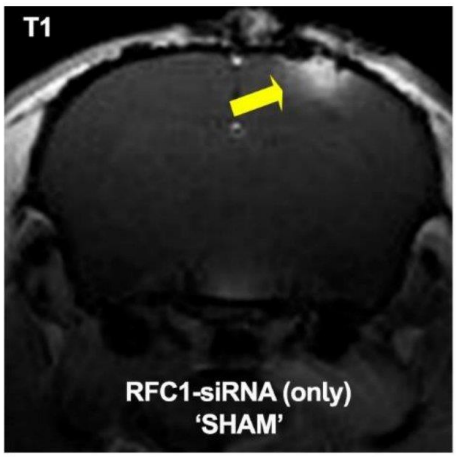

Figure 4.17. The T1-contrasted MRI of sham animal. MRI which was obtained 24 h after cortical RFC1-siRNA injection. Gd leakage is seen locally as hyperintensity in the cortex and shown by an arrow.

The acquisition of MRI and histology of the same brains allowed direct correlation between *in vivo* MRI and histological parameters. Therefore, the mice which went through MRI procedure and completed 24 h recanalization were sacrificed by cardiac perfusion under urethane anesthesia. The brains were extracted and immersed in 4% PFA and was sectioned.

Later, equally spaced 20 μm sections were taken from the brains to include the middle cerebral artery region. To correlate MRI findings to histology, morphological assessments were made via Hoechst staining of sections. Shape and size of corpus callosum, and ventricles were assessed to choose the best brain section to correspond to nine registered MRI slices for each brain.

The example of a tile scan showing RFC1 staining pattern and corresponding T2-weighted MRI slice of the was given in the Figure 4.18. In line with the previous

findings, RFC1 was decreased in the infarct region. In the periinfarct region, however; the amount of RFC1 was reduced in the RFC1-siRNA injected brains due to the knockdown. More comprehensive assessments will be made in the future.

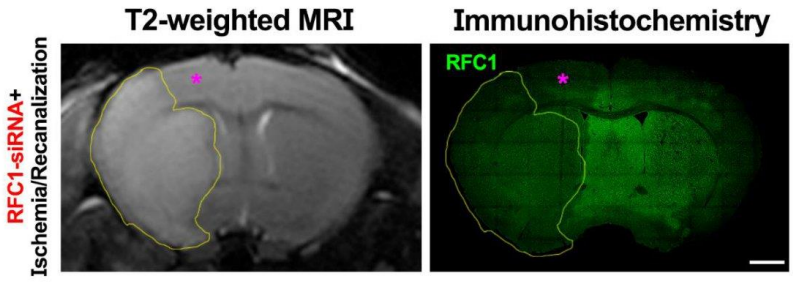

Figure 4.18. Correlation between MRI images and the immunohistochemical findings. Example shows T2-weighted image and corresponding 20-um brain section immunostained with anti-RFC1 antibody (green) obtained from RFC1-siRNA injected ischemic brain. The infarction area showed RFC1 signal decrease in the corresponding tile scan compared to contralateral. Periinfarct (asterisk) region showed diminished RFC1 signal, since RFC1-siRNA injected periinfarct region. Note that the cortex area which had diminished RFC1 signal is not infarcted.

4.2. Results of the Retina Experiments

4.2.1. RFC1 protein is abundantly expressed in the endothelial cells and pericytes of the inner BRB

In retina, RFC1 was immunohistochemically examined in the radial retina sections, and as expected, determined that RPE was immunopositive (Figure 4.19.A.). This was also confirmed in whole mount retina preparations (Figure 4.19.B.) (114). RFC1 immunopositivity was also found in the ganglion cell layer (GCL), inner and outer plexiform layers (INL and OPL) that coincided with the superficial and deep microvascular plexus. Hence, the RFC1 immunosignal was identified in the retinal layers comprising microvessels (Figure 4.19.A, C.). Two different antibodies, high concentrations, and long incubation durations like three overnights at +4°C with the primary antibody for the 200 µm thick whole mount retinal preparations were used to visualize retinal microvessels. Likewise, isolating retinal microvessels with the trypsin

digestion method provided us with an easier and more consistent preparation for immunostainings.

RFC1 was observed as distributed continuously and diffusely throughout the retinal microvessels (Figure 4.19.D.). RFC1 was immunohistochemically co-labeled with the endothelial marker, cluster of differentiation 31 (CD31), whose immunoreactivity exclusively outlined the endothelial cells. As a convincing finding that there was no crosstalk in immunoreactivity, RFC1 labeling was determined to colocalize with both the endothelial cells, and the 'bump on a log' shaped cells (Figure 4.19.E., arrows), which designates pericytes.

Microvessels were then labeled with well-defined pericyte markers including the neural/glial antigen 2 (NG2), CD13, and PDGFR-β all of which showed colocalization with RFC1 (Figure 4.19.F-H.). These indicated that RFC1 protein was present both in the endothelial cells and pericytes. Additionally, double immunostainings were performed with endothelial marker CD31 distributed over the entire endothelial cell surface, luminal, abluminal, and lateral (86). This allowed to label the whole endothelial cell surface on radial cryo-sections of retinas and to visualize the luminal surface of retinal microvessels. The immunostainings resulted in both luminal and abluminal labeling (Figure 4.20.). Abluminal staining of RFC1 could be stemmed from either abluminal plasma membrane of endothelial cells or pericytes. For now, with the resources in our hands, we are not capable to resolve such subtle differences. However, in fact, ultrastructural determination of RFC1 protein could reveal the exact localization of it in pericytes and endothelial cells. Besides, RFC1 is known to have intracytoplasmic forms which may lead to the intracytoplasmic stainings which may explain our dispersed pattern of stainings of RFC1 in our figures (such as Figure 4.19.E-H) (115-117).

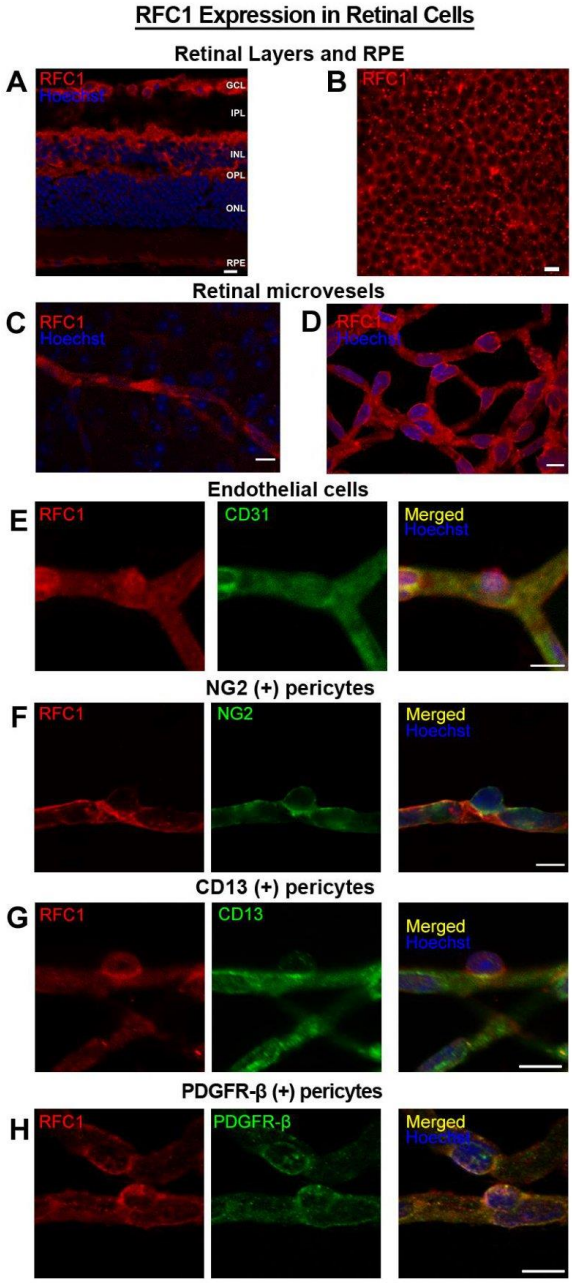

Figure 4.19. RFC1 protein is abundantly expressed in endothelial cells and pericytes of the retinal microvessels. A) Ex-vivo labeling of 20 µm radial cryo-section from PFA

fixated eyeballs of naive Swiss Albino mice with anti-RFC1 antibody (red). Abundant RFC1 immunopositivity is observed along ganglion cell layer (GCL), inner plexiform layer (IPL), outer plexiform layer (OPL) where retinal microvessels form vascular horizontal vascular beds; as well as the retinal pigment epithelium (RPE). However, this preparation limited the observation of microvessels, hence inner BRB as it commonly comprised circular microvessels rather than longitudinal ones. Scale bar = 25 μm B) RPE which is known to express RFC1 previously, and in concordance is well stained with anti-RFC1 antibody (red) that served us as positive control. C) The microvessels constituting inner BRB at the deep vascular plexus of the retina are immunohistochemically labelled with anti-RFC1 antibody in PFA fixated whole-mount retinas. D) The retinal microvessels which were obtained via retinal trypsin digestion method that allowed to get only microvessels (< 9 μm diameter) were immunofluorescently labeled with anti-RFC1 antibody (n=6 retina; red). Nuclei were labeled with Hoechst 33258 (blue). E-H) RFC1 (red) colocalizes with the endothelial marker CD31 (green), and the accepted pericyte markers NG2, CD13, PDGFR-β (green) shown respectively (n=3/marker). Nuclei were labeled with Hoechst 33258 (blue). Scale bars: 10 μm.

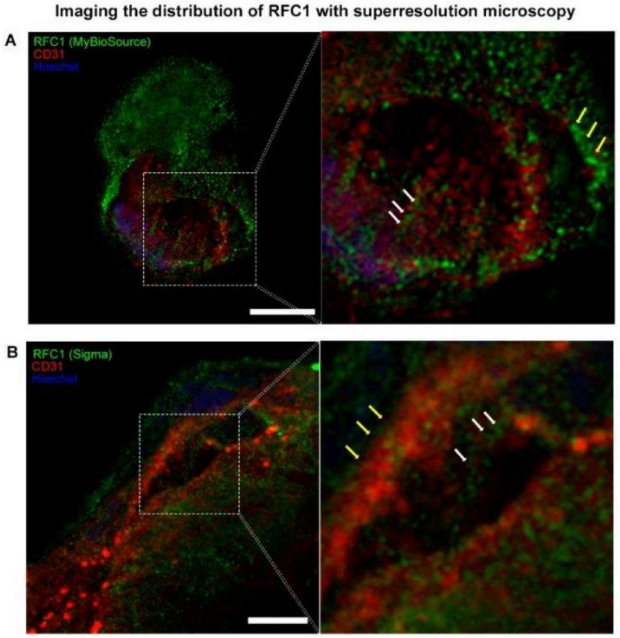

Figure 4.20. Super-resolution microscopy of retinal radial sections to reveal the distribution of RFC1 protein over the endothelial cell surface. A) 3D reconstruction of RFC1 immunostaining performed by MyBioSource antibody which is targeted to N-terminal region of protein. B) 3D reconstruction of RFC1 immunostaining performed by Sigma antibody which is targeted to C-terminal region of protein. In both stainings, RFC1 puncta are localized on the luminal endothelial cell surface stained by CD31 (white arrows). RFC1 puncta are also visible from the abluminal side (yellow arrows),

indicating abluminal endothelial cell membrane or pericyte localization of RFC1 protein. Scale bars=10 μm.

4.2.2. Retinal RFC1 is downregulated *in vivo* by RFC1 targeted Accell siRNA, and leads to disruption of the inner BRB

A combination containing the same amount of specifically designed two RFC1-siRNAs or two Scrambled siRNAs were delivered intravitreally, and the mice were sacrificed 24 h later. The knockdown of RFC1 was determined from fresh whole retinas as a pronounced decrease in RFC1 protein via Western Blotting ($p=0.028$; Figure 4.21.A, B.). Additionally, RFC1-siRNA significantly decreased RFC1 mRNA by 24.75% compared to Scrambled siRNA ($p=0.004$, Figure 4.21.C.). In line with these, RFC1 immunosignal intensity was diminished in the microvessels of RFC1-siRNA injected retinas when mean grey value of RFC1 immunosignal (i.e., fluorescence intensity) was measured (72.1%, $p<0.0001$; Figure 4.21.C, D.). We also noticed that RFC1-siRNA treated retinas were fragile, and prone to damage during the procedures.

The immunostaining of the whole mount retinas also confirmed RFC1-siRNA knockdown with diminished RFC1 immunosignal, and further showed that Lectin staining was weaker and interrupted in RFC1-siRNA treated preparations, indicating that microvessels might be structurally damaged (Figure 4.21.G.). In addition, these retinal microvessels demonstrated lower NG2 signal compared to Scrambled siRNA treated ones, which suggested that pericytes might also be damaged by RFC1-siRNA (Figure 4.21.E.). However, to address if the reduction in RFC1 immunoreactivity in siRNA treated microvessels might be associated with the change in microvascular tonus we assessed the pericyte-associated vascular diameter in each microvessel branch. No change was found in juxtanuclear diameter ratio between RFC1-siRNA and Scrambled-siRNA treated groups (Figure 4.21.F.). Next, the loss of pericytes was assessed by using pericyte density (soma per mm capillary). No significant decline in pericyte density was found in RFC1-siRNA administered retinas suggesting that RFC1 decrease may not affect pericyte maintenance, as it did not reduce pericytes in number at least at this time point (Figure 4.21.G.). However, one could not exclude disruption of pericyte functions via RFC1-siRNA since there is marked decline in the expression of pericyte marker NG2.

As it was determined that retinal microvessels express RFC1 protein abundantly, and could be efficiently knock down RFC1 *in vivo*, whether RFC1 suppression may lead to any changes in the inner BRB was elucidated.

Strikingly, knocking down retinal RFC1 diminished immunoreactivity of the tight junction-associated transmembrane proteins occludin, claudin-5, and cytoplasmic adaptor protein zonula occludens-1 (ZO-1), as well as the main basement membrane protein collagen-4 in trypsin digested microvessels (Figure 4.21.H-K.). In RFC1-siRNA treated microvessels, immunoreactivity of collagen-4 that surrounds the abluminal membrane of endothelial cells and covers pericytes residing in the basement membrane decreased by 68% (p=0.0043), occludin decreased by 57.03% (p=0.0043), and claudin-5 decreased by 76.26% (p=0.0006). ZO-1, the intracellular adaptor protein establishing a link between occludin, and intracellular actin cytoskeleton decreased by 53.22% (p=0.0012).

Moreover, the changes observed in the inner BRB were not associated with immersive structural damage. In morphological analysis of retinal radial sections, no significant difference in GC number, total retinal, INL, and ONL thickness was observed between control and RFC1-siRNA group indicating RFC1-knockdown did not lead to an overall structural and morphological damage (Fig 4.22.F.). Furthermore, The ERG showed that the scotopic a- and b-wave amplitudes of RFC1-siRNA and Scrambled-siRNA treated retinas were similar suggesting no worsening of the rod photoreceptor and the inner retina functions (Figure 4.22.A-C.). The implicit time a-wave peak remained unaltered between our experimental and control groups (Figure 4.22.D.). However, interestingly, the implicit time b-wave peak increased in RFC1-siRNA treated retinas (Figure 4.22.E., p=0.029), which suggests that there was a delay in the speed of the signal transmission through the bipolar cells in the retina.

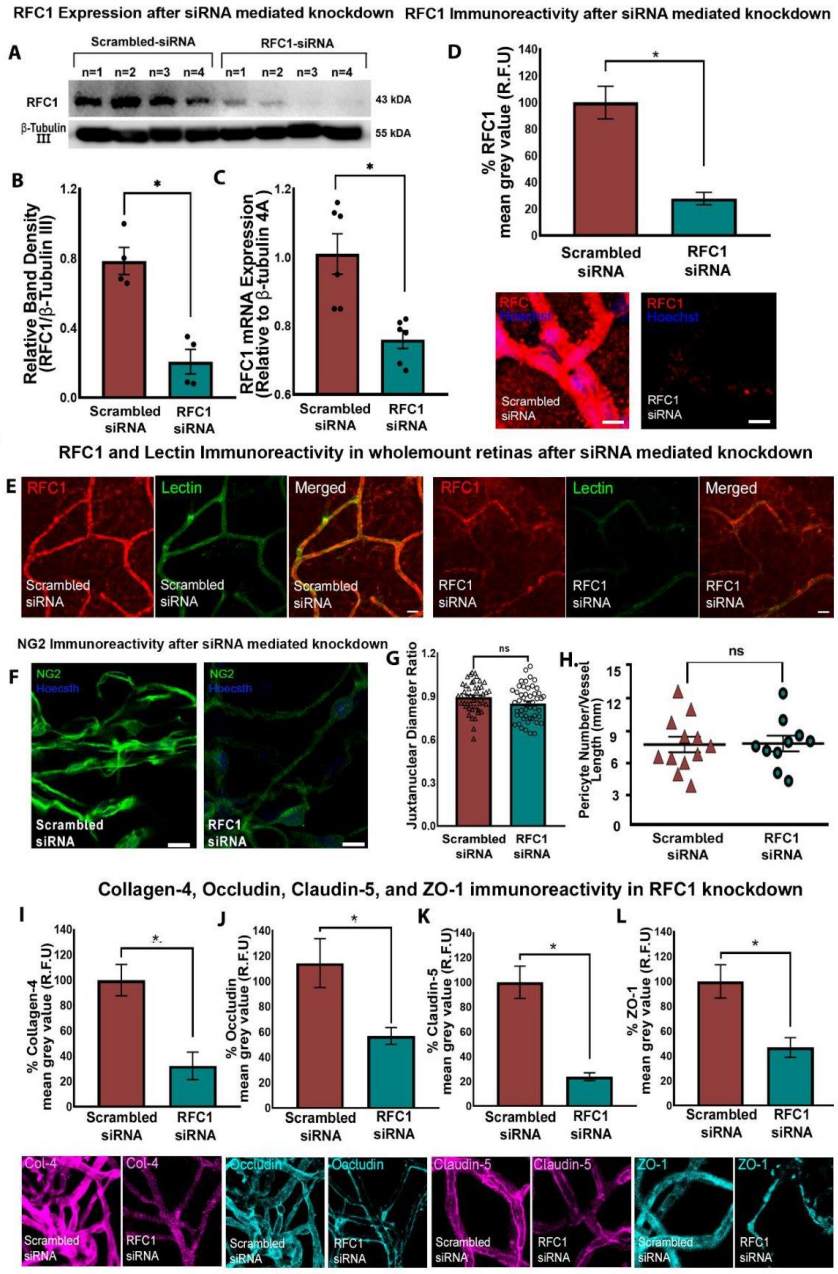

Figure 4.21. The validation of Accell siRNA mediated in vivo RFC1 knockdown, which led to a reduction in critical proteins of the inner BRB. A) Western blotting

image of retinas (n=4 mice/group) depicting the robust decrease in RFC1 protein of RFC1-siRNA delivered ones compared to Scrambled-siRNA. β-Tubulin III was loading control. 35 μg protein was loaded for each retina. B) The graph illustrates the quantification of the relative band densities of given Western blotting image which expresses RFC1 band density in proportion to β-Tubulin III, which shows decrease in relative protein levels in RFC1-siRNA treated retinas (*p=0.028). C) The graph shows that RFC1-siRNA delivery reduced retinal RFC1 mRNA levels by 24.75% when compared to Scrambled-siRNA (*p=0.004). D) The graph illustrates the percentage of mean grey value of RFC1 frame in lectin positive microvessel area in RFC1-siRNA treated group normalized to Scrambled-siRNA treated group as described in Methods section. RFC1-siRNA delivery significantly reduced the percent of the mean grey values of RFC1 by 72.10% (n=4). Representative confocal images of Scrambled-siRNA or RFC1-siRNA delivered retinal microvessels stained by anti-RFC1 antibody (red). E) Whole mount retinas were labeled by anti-RFC1 antibody (red) and Fluorescein Lectin (green). RFC1 immunosignal was decreased and interrupted along deep retinal microvessels. Also, lectin signal was weakened in RFC1-siRNA treated retinas representing the structural decomposition of microvessels. F) RFC1-siRNA treated retinal microvessels showed less NG2 immunosignal compared to Scrambled-siRNA treated ones, indicating that pericytes might also be damaged by RFC1-siRNA. G) However, juxtanuclear diameter ratio of total of 97 pericyte-associated microvessel were measured (n=3/group) and no significant changes were found. The dots represent the mean of each juxtanuclear section per pericyte and divided by the initial diameter of each vascular segment. H) Also, pericyte body counts per microvessel length (mm) were not different between the groups. n = 3 images were analyzed per animal. I-L) RFC1-siRNA delivery significantly reduced the percent of the mean grey values of Collagen-4 68% (n=4), Occludin 57.03% (n=3), Claudin-5 76.26% (n=4), and ZO-1 53.22% (n=4). The reductions that are statistically significant represented as *$p \leq 0.05$. Nuclei are labelled with Hoechst 33258 (blue), Data are mean ± S.E.M Mann-Whitney U; Scale bars: 10 μm.

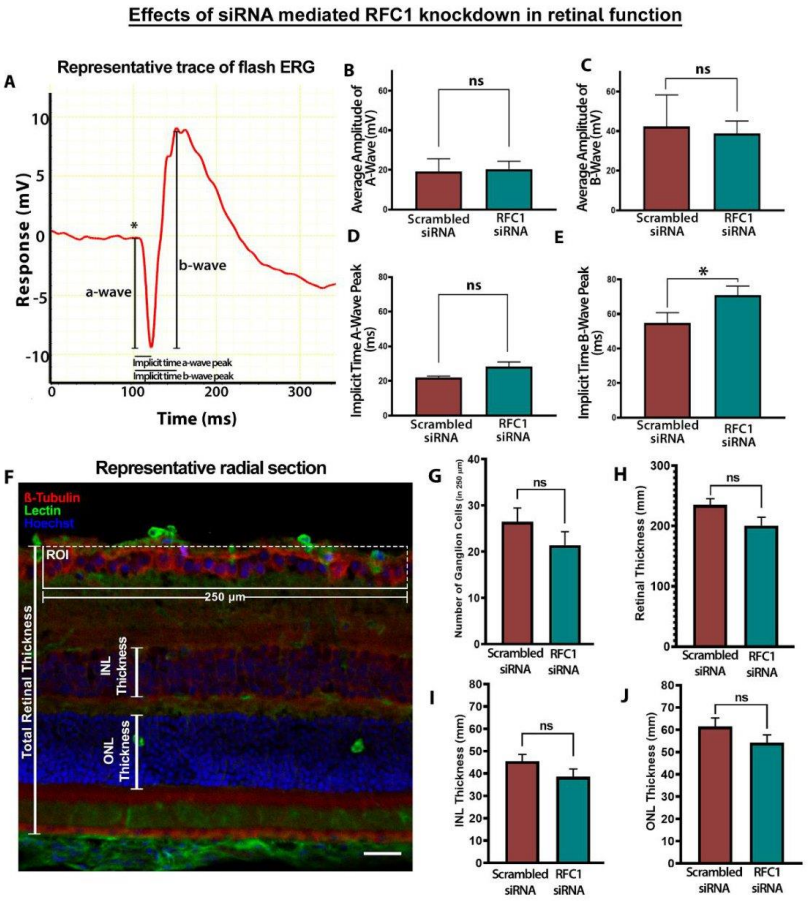

Figure 4.22. Effects of siRNA mediated RFC1 knockdown in the retina. A) Representative scotopic (dark-adapted) ERG. The ERG recordings include measurements of the a-wave, b-wave, and implicit time of a-wave peak and b-wave peak. The amplitude of the a-wave is determined by measuring the distance between the baseline and the lowest point of the negative deflection. On the other hand, the amplitude of the b-wave is calculated by measuring the distance between the maximum point of the a-wave and the peak of the positive deflection of the b-wave. 0 mV indicates baseline response. B, C) Comparison of mean amplitudes ± SEM of scotopic a-wave and b-wave between Scrambled-siRNA and RFC1-siRNA treated mice. D, E) Comparison of mean implicit time ± SEM of A-wave peak and B-wave peak between Scrambled-siRNA and RFC1-siRNA mice. Only average of the implicit time B-wave peak between Scrambled-siRNA (55±3.0 ms) and RFC1-siRNA (71±2.7 ms) was different (*p=0.029; n=4/group). F) β-Tubulin III (red), Lectin (green), and Hoechst 33258 (blue) stained central retinal cross-sections were imaged with confocal microscopy. To manually count GC number, ROIs in 250 µm length was placed on

ganglion cell layer. Total retinal thickness was determined from nerve fiber layer to retinal pigment epithelium. Width of the INL (the distance between the inner plexiform layer and the outer plexiform layer) and ONL (the distance between the outer plexiform layer and the outer limiting membrane) were determined by a fluorescent nuclear dye (Hoechst 33258). G-J) The bar graphs show that there is no statistically significant difference in abovementioned parameters between RFC1-siRNA and Scrambled-siRNA treated groups (n=3/per group). Data are mean ± S.E.M Mann-Whitney U; Scale bar: 25 μm. GCL: ganglion cell layer, INL: inner nuclear layer, ONL: outer nuclear layer, ROI: Region of interest.

4.2.3. Retinal RFC1 is upregulated *in vivo* by LV overexpressing RFC1, and this upregulation changes the inner BRB properties

Next, to increase the expression of RFC1 in mouse retinas via LV carrying RFC1 was aimed as described in detail in the methods section. LV gene delivery method was preferred due to its efficiency to induce stable gene expression, its tropism to the inner retina and the cells of retinal microvessels when delivered intravitreally (118, 119).

The efficient RFC1 protein overexpression was shown by Western Blotting in cell lysates (Figure 4.23.A.). Subsequently, to validate the *in vivo* LV-mediated transduction, mice had unilateral intravitreal LV injections. No animals developed any local infections. The eyeballs of mice (n=3) that received intravitreal Control-LV bearing GFP were harvested 10 days after. The retinal and perimicrovascular cells showed GFP expression disclosing that the cells were infected with LV (Figure 4.23.B.).

The overexpression of RFC1 by LV in the retina was also observed immunohistochemically. RFC1 immunoreactivity revealed a marked intensity increase in both the retinal whole mount and retinal microvessel preparations in RFC1-LV compared to Control-LV (Figure 4.23.C., D.) with 167.5% increase in RFC1 immunosignal ($p=0.0159$; Figure 4.23.D.).

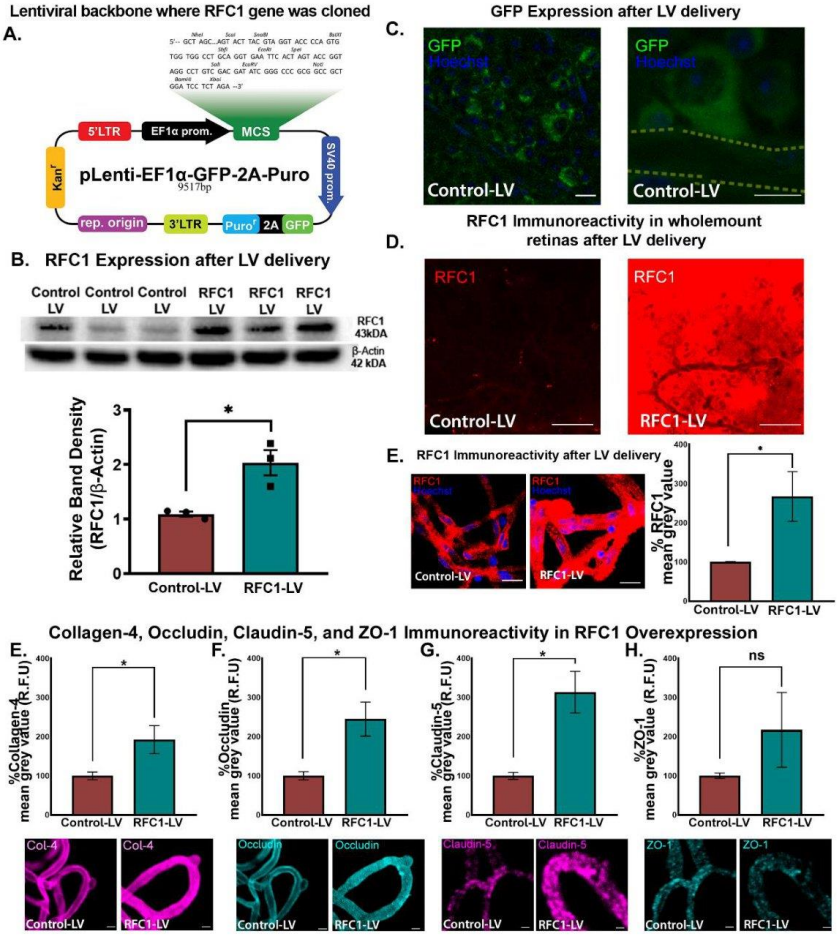

Figure 4.23. The validation of lentiviral vector-mediated overexpression of RFC1 protein in vivo, which led to an increase in the proteins of BRB. A) The Western Blotting image shows corresponding overexpression of RFC1 protein in RFC1-LV transduced neuroblastoma cells (N2a) compared to Control-LV transduced cells. For cell culture lysates, Beta-Actin was the loading control. B) The graph illustrates the quantification of the relative band densities of given Western blotting image which expresses RFC1 band density in proportion to β-Actin, which shows increase in relative protein levels in RFC1-LV treated retinas (*p= 0.016). B) The confocal images from whole mount retinas confirmed the intravitreal delivery of Control-LV into the mouse eye showing lentiviral vectors infected various retinal cells, as reporter gene GFP (green) signal indicated. Also, as magnified image showed, perivascular cells and pericytes expressed GFP protein in LV-RFC1 or Control-LV injected retinas, microvessel trace was shown by dashed line. C) The representative images of whole mount retinas which had been treated by LV-RFC1 showed increased RFC1

immunosignal (red) compared to Control-LV injected control retinas (n=3). D) The graph illustrates the percentage of mean grey value of RFC1 frame in lectin positive microvessel area in RFC1-LV treated group normalized to Control-LV treated group as described in Methods section. RFC1-LV delivery significantly increased the percent of the mean grey values of RFC1 (n=3). E-H) RFC1-LV delivery significantly increased the percent of the mean grey values of Collagen-4 (n=4), Occludin (n=3), Claudin-5 (n=3), but not ZO-1 compared to Control-LV delivered groups. (*$p \leq 0.05$). Collagen-4 (magenta), Occludin (cyan) Lectin (Yellow) immunosignal increased as well as Claudin-5 (magenta) except ZO-1 (cyan) via RFC1-LV treatment compared to Control-LV treatment. Nuclei were labelled with Hoechst 33258 (blue) Data are mean ± S.E.M. Mann-Whitney U; Scale bars: 10 μm.

As the suppression of RFC1 levels led to an extensive structural damage in retinal microvessels, whether RFC1 overexpression had any effects was further investigated. Immunohistochemistry of tight junction proteins (occludin, claudin-5), intracellular adaptor protein ZO-1, and main basement membrane protein collagen-4 in retinal microvessels (from n=3 retina/per marker, Figure 4.23.E-H.) were done ten days after administration. RFC1-LV administered retinal microvessels displayed increased immunosignal in occludin (p=0.0059), claudin-5 (p=0.0040), and collagen-4 (p=0.0159) compared to Control-LV ones (Figure 4.23.E-G.). However, the immunosignal of ZO-1 did not differ between the groups (Figure 4.23.H.).

4.2.4. Retinal ischemia alters RFC1 protein and decreases the inner BRB proteins which can be ameliorated by RFC1 overexpression

After observing the potential role of RFC1 protein in maintaining the inner BRB, whether RFC1 protein has a role in retinal ischemia was investigated. We made 1 h permanent retinal ischemia, as it is considered sufficient to observe microvessel-related changes such as capillary constrictions or protrusion of the contracted pericyte soma from the microvessel wall (Figure 4.24.C., white asterisk), and yet an early time point to allow us to minimize the effects of inflammation (11-13).

Following ischemia, the expression of RFC1 protein was enhanced significantly compared to controls detected by Western blotting (p=0.025; Figure 4.24.A., B.) and RFC1 immunopositivity ($p < 0.0001$; Figure 4.24.C.). The pronounced RFC1 signal was detected in the protruding pericytes (Figure 4.24.C., white arrows) probable of an increased signal in affected cells.

Whether retinal ischemia caused any alterations in the inner BRB proteins was investigated and observed that 1 hr retinal ischemia decreased collagen-4 and occludin immunosignal compared to controls ($p=0.0140$, $p=0.0317$ respectively; Figure 4.24.D, E.).

Finally, whether RFC1-siRNA knockdown induced disruption of the inner BRB proteins resulted in barrier dysfunction was studied. Vessels were stained with lectin and endogenous IgG extravasation was determined by fluorescently labeled anti-mouse IgG antibody (Figure 4.25.A., red arrows). RFC1-siRNA treated mice displayed endogenous IgG leakage (Figure 4.25.A., red arrows), while Scrambled-siRNA treated retinas did not show any. This indicated that RFC1 is essentially required for the structural and functional integrity of the inner BRB in health.

On the other hand, no IgG extravasation after 1 h retinal ischemia was observed, so it significantly did not compromise the integrity of inner BRB (Figure 4.25.B.). This observation was consistent with the literature since 1 h retinal ischemia causes early changes such as capillary constrictions (white arrows, Figure 4.25.B), but it does not suffice for the inner BRB disruption to the extent of allowing endogenous IgG (150 kDa) leakage through paracellular barrier even if disintegration of tight junctions commenced (120-122). Then, whether knocking-down RFC1 before ischemia would provoke disruption of the inner BRB was studied. When RFC1-siRNA was administered 24 h before retinal ischemia, a significant amount of endogenous IgG extravasation was determined (Figure 4.25.B., red arrows). As Scrambled siRNA administration 24 h before retinal ischemia led to no apparent IgG extravasation, this indicated that decreased RFC1 levels accelerated the inner BRB disruption in acute retinal ischemia. Additionally, any edema or morphological changes throughout the retinal sections were not observed.

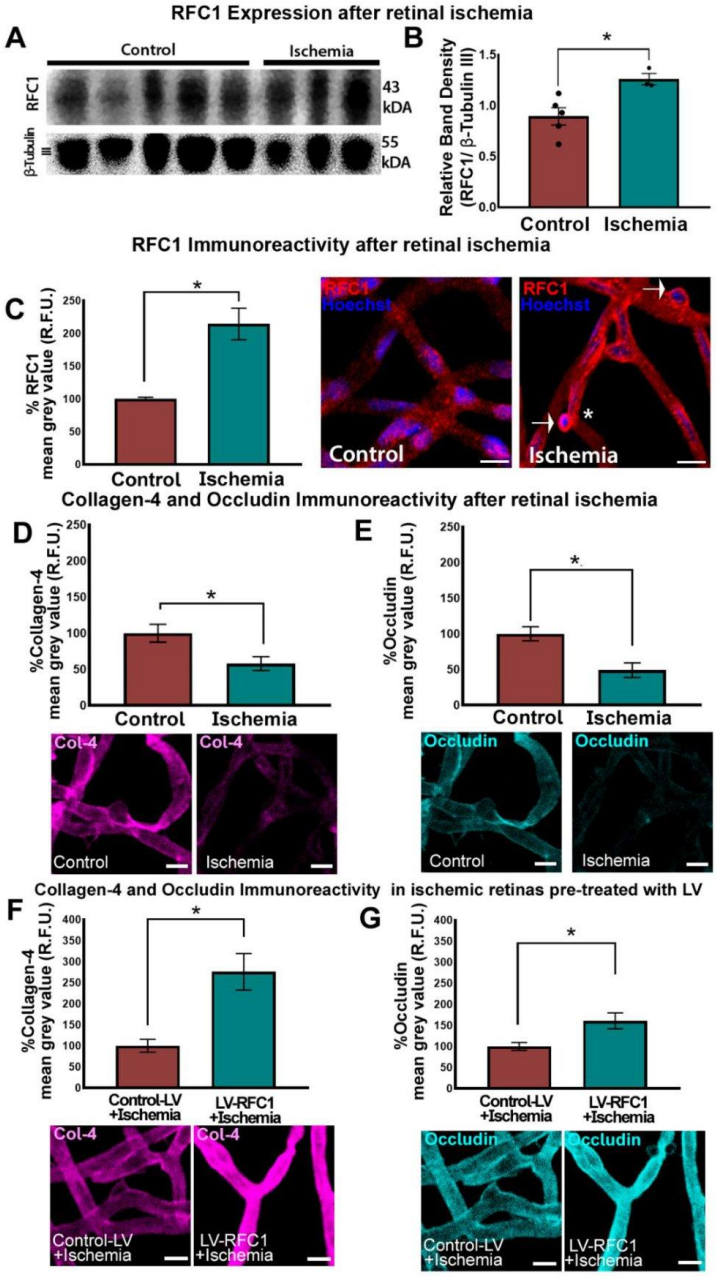

Figure 4.24. RFC1 protein increased after retinal ischemia, and the overexpression of RFC1 before ischemia by LV salvaged decreased collagen-4 and occludin levels. A)

The representative Western blotting image from Control (n=5) and ischemic (n=3) retinas. Housekeeping gene β-Tubulin III was used as loading control. B) The graph shows the relative density measurements of bands which were calculated by proportioning to loading control. One-h permanent retinal ischemia increased relative RFC1 protein levels compared to control. C) Retinal ischemia significantly augmented the percentage of mean grey value of RFC1 by 114.5% (n=3). Representative confocal images of control or ischemic retinal microvessels stained by anti-RFC1 antibody (red). Significant immunosignal increase in ischemic microvessels was observed compared to controls. Also, ischemic microvessels demonstrated expected characteristics such as constrictions and protruding pericyte bodies (asterisk). Of note, ischemic pericyte bodies showed denser RFC1 immunosignal (white arrows). D, E) In contrast, retinal ischemia decreased collagen-4 by 42.07% (n=3), Occludin by 50.94% (n=3). F, G) In addition, microvessels treated with LV-RFC1, 10 days before ischemia showed 176% increase in Collagen-4 (n=3) and 60.9% in Occludin (n=3) immunosignal compared to Control-LV delivered ones indicating RFC1 overexpression before ischemia might retrieve loss of collagen-4 and occludin in ischemia. (*$p \leq 0.05$). Nuclei were labelled with Hoechst 33258 (blue) in all images. Data are mean ± S.E.M. Mann-Whitney U; Scale bars: 10 μm.

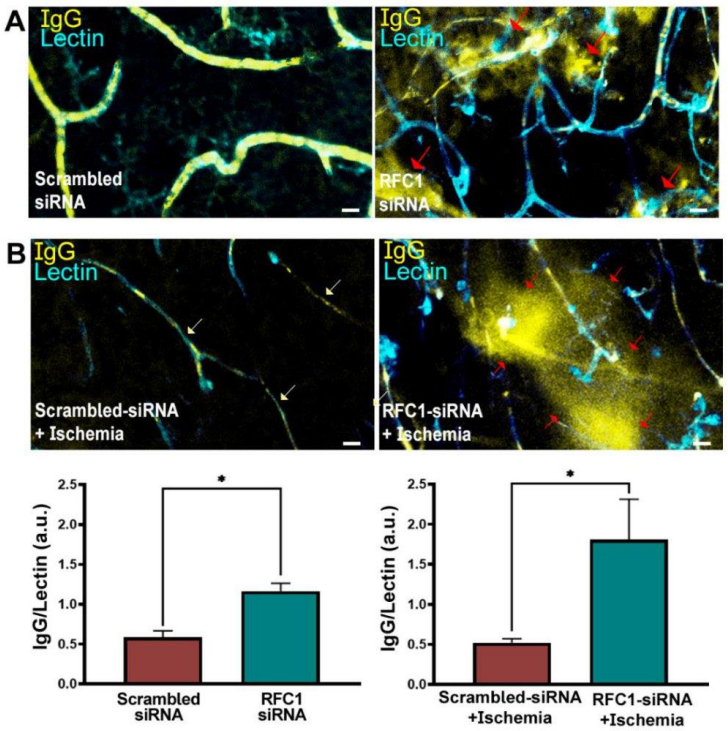

Figure 4.25. siRNA mediated RFC1 knockdown led to inner BRB breakdown and endogenous IgG extravasation. The wholemount retinas were labeled by Lectin (cyan) and incubated with Cy3 labeled goat anti-mouse antibody (yellow) to visualize the

extravasated endogenous mouse IgG. A) RFC1-siRNA mediated knockdown led to significant IgG extravasation (red arrows) in microvessels while Scrambled-siRNA treated retinas showed no extravascular IgG signal ($p = 0.001$; $n = 3$). B) 1 h ischemia led to microvessel constrictions (white arrows) but no IgG extravasation. However, knocking down RFC1 before ischemia provoked inner BRB disruption leading to endogenous IgG extravasation (red arrows) ($p = 0.05$; $n = 3$). Nuclei were labelled with Hoechst 33258 (blue) in all images. Scale bars= 10 μm.

In conclusion, RFC1-siRNA treated mice showed preservation of the number of ganglion cells, total retinal thickness (from the GCL to the RPE), INL thickness and ONL thickness compared to Scrambled-siRNA treated retinas. Thus, it is inferred that RFC1-siRNA treatment does not lead to general toxic effects in the retina at least within 24 h. However advanced techniques are needed to find possible subtle changes.

4.2.5. The Contribution of Folate and Other Folate Receptors in Response to RFC1 Knockdown

Although initial purpose of this thesis was to investigate the presence and the role of RFC1 in the retina, the upregulation of other folate carriers as a compensation mechanism should not be overlooked. To address this concern, FOLRα which binds to folic acid with high affinity rather than biologically active folate form 5-MTHF and carries folic acid from choroidal vessels to the outer 1/3 of the retinal tissue, was immunohistochemically determined in naive and siRNA administrated retinal radial sections. We also performed Western blotting to semi-quantitively asses that if FOLRα levels change in siRNA mediated RFC1 knockdown.

Here, it was determined that FOLRα increased in RPE in response to RFC1-siRNA treatment suggesting that tissue was compensating to preserve folate stored. To investigate the impact of siRNA-mediated RFC1 silencing on the transport of substrates in the retina, the levels of 5-MTHF, which is the primary substrate of RFC1, was measured in whole retinas of RFC1-siRNA, Scrambled-siRNA, and 5-MTHF treated groups.

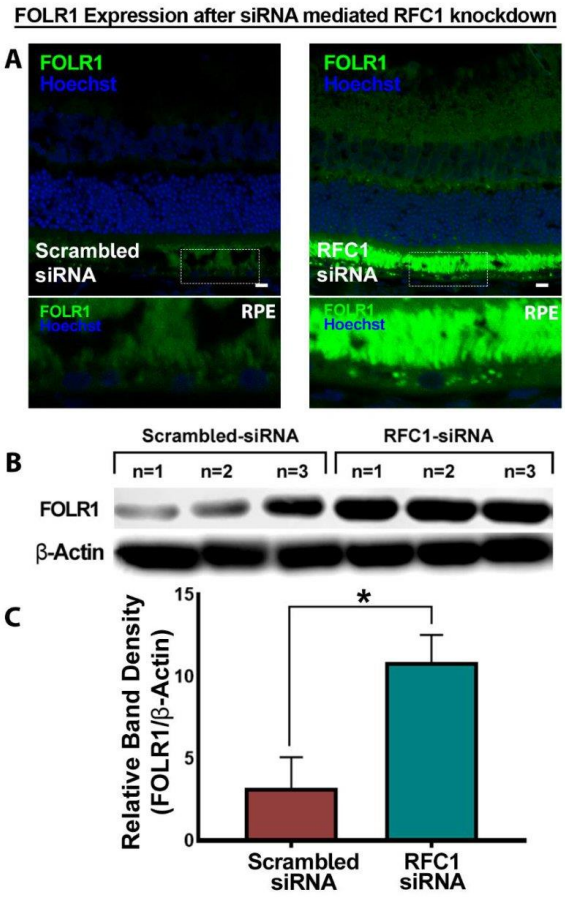

Figure 4.26. The change in FOLR1 expression after siRNA mediated RFC1 knockdown. FOLR1 level changes in response to siRNA mediated RFC1 knockdown. A) Retinal radial sections immunolabeled with anti-FOLR1 antibody. B) Western blotting image of retinas (n=3 mice/group) depicting the increase in FOLR1 protein in RFC1-siRNA treated ones compared to Scrambled-siRNA. β-Actin was used as loading control. 35 µg protein was loaded for each retina Insets shows the FOLR1 staining in RPE. C) The graph illustrates the quantification of the relative band densities of given Western blotting image which expresses FOLR1 band density in proportion to β-Actin, showing a decrease in relative protein levels in RFC1-siRNA treated retinas (*p=0.036). Imaging was performed with 63x oil objective (HC PL APO CS2 63x/1.40 OIL). Scale bar: 10 µm. RPE: retinal pigment epithelium.

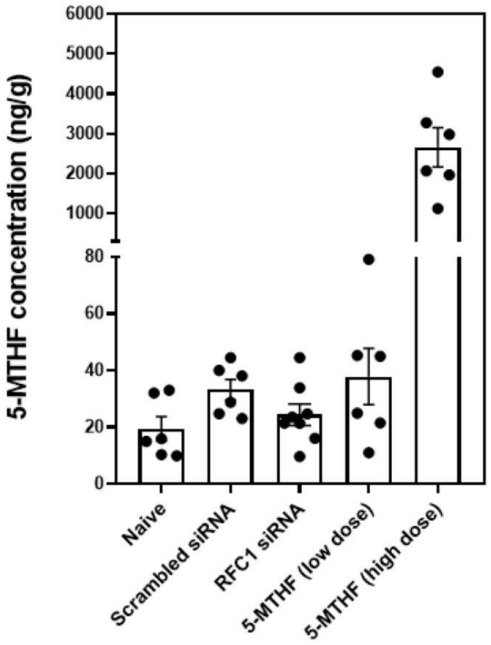

Figure 4.27. Retinal 5-MTHF levels after siRNA mediated RFC1 knockdown. The bar graph represents the 5-MTHF levels in ng/g ±SEM in individual retinas. Retinal 5-MTHF levels tend to be lower in the retinas treated with RFC1-siRNA than Scrambled-siRNA, but not statistically significant (p=0.07; Mann-Whitney U test, Figure). Naive n=6, Scrambled-siRNA n=6, RFC1-siRNA n=8, low dose 5-MTHF n=6, high dose 5-MTHF n=6 retinas.

The analysis of the alteration in the 5-MTHF level in retinas treated with RFC1-siRNA and Scrambled-siRNA did not yield any statistically significant difference. This suggested that the upregulation of FOLRα might have partially but not sufficiently compensate for the 5-MTHF levels for the repair of the inner BRB. However, revealing the relationship between siRNA mediated knockdown of RFC1 and other folate carriers and resulting changes in inner BRB requires extensive additional experiments.

We also examined plasma 5-MTHF levels, a measure of the circulating active form of folate, as it might provide insights into the efficiency of folate metabolism and utilization in the retina as plasma folate levels can be affected by recent dietary folate status. Hence, we measured the plasma 5-MTHF levels of the same animals.

Retinal 5-MTHF (ng/g) was expressed as the proportion to the matched plasma 5-MTHF (ng/ml) levels and expressed as mean ±S.E.M. Although the mean 5-MTHF levels in RFC1-siRNA treated group was lower than Scrambled-siRNA treated group; however, this difference was not statistically significant (p=0.09).

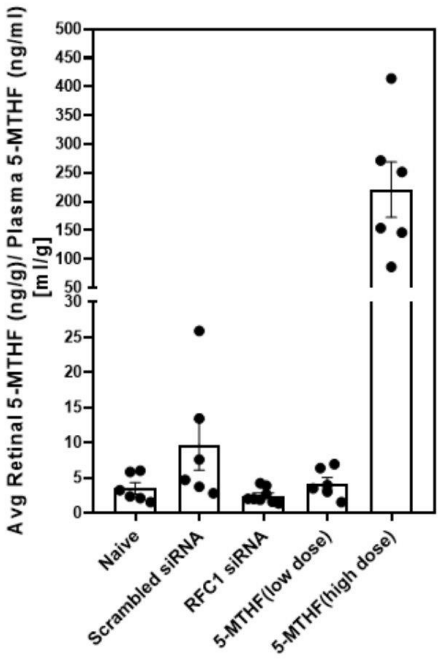

Fig 4.28. Retinal 5-MTHF levels in proportion to plasma. 5-MTHF levels after siRNA mediated RFC1 knockdown. The bar graph represents the average 5-MTHF levels in proportion to plasma 5-MTHF levels in ml/g ±S.E.M. Naïve n=6, Scrambled-siRNA n=6, RFC1-siRNA n=8, low dose 5-MTHF n=6, high dose 5-MTHF n=6.

In conclusion, RFC1 knockdown by intravitreal siRNA in the retina led to a decrease in 5-MTHF levels, albeit were not statistically significant. This result may suggest that siRNA mediated RFC1 knockdown might 1) prevent 5-MTHF transport from inner BRB, hence leading to a slight decrease in retinal 5-MTHF levels, 2) the siRNA mediated RFC1 knockdown leading to inner BRB breakdown can have a significant impact on transport activity by unbalancing microenvironment, disrupting the balance of ions, nutrients and waste products which can indirectly affect 5-MTHF levels. Thus, the results could not indicate nor exclude that the reduction in the 5-

MTHF levels of the retina via RFC1-siRNA could lead to inner BRB breakdown. To address the linkage between RFC1-mediated substrate transport and the inner BRB disruption requires several additional *in vivo* and *in vitro* experiments, which we are curious to find out in our future studies.

5. DISCUSSION

In this thesis, we endeavored to investigate the following aspects: 1) the protein level expression of RFC1 in cerebroretinal pericytes and endothelial cells, 2) the characterization of its potential role in the BBB and inner BRB, and 3) its potential contribution to the pathophysiology of cerebral and retinal ischemia. Here, we discussed how the obtained results align with the current literature and the degree to which main objectives had been accomplished, delineating the findings specific to the brain and retina.

This research was stemmed from the ignorance of a folate transporter named RCF1 in literature in terms of pericytes, the blood brain and retinal barriers and the pathological condition like ischemia although it was proved to be one of the three common genes in the transcripts of mural cells (pericytes and vascular smooth muscle cells). We characterized and proved for the first time that RFC1 was colocalized with known pericytes markers in the brain (PDGFR-β, CD13, and α-SMA). The reason that RFC1 had not been shown in pericytes so far might have several explanations. First, it was emphasized that there was the scarcity of RFC1 antibody; therefore, early studies used anti-serum to determine RFC1 immunohistochemically (26). Thus, lack of confirmed commercial antibodies might have prevented researchers from studying the transporter immunohistochemically. Second, although RFC1 was determined in brain sections in mice, rats, and post-mortem humans, the immunopositivity of RFC1 in the pericytes was unnoticed since pericytes had been largely overlooked by many neuroscientists. Third, most studies evaluating the role of RFC1 in microvessels concentrated on only the endothelial cells, but not the neighboring pericytes (1, 2, 27, 44). Our findings confirmed the results of a recent meta-analysis combining five different mouse brain pericyte transcriptomic studies where the RFC1 gene was one of the only three consistently detected genes in brain pericytes out of the 1180 enriched genes (3).

Next, we investigated the effect of the expression of RFC1 level in acute ischemic stroke. We induced 90 min ischemia followed by 1 h, 24 h, or 48 h recanalization, and detected various RFC1 protein expressions according to brain regions and recanalization time-points. We found that RFC1 was decreased in the core

region at these three time-points. However, RFC1 increased in periinfarct region in 1 h and 24 h validated by immunohistochemistry and Western blotting. Although these results need to be widened and requires detailed examination, they were important because they are the pioneering results evaluating the RFC1 protein specifically in the pathophysiology of ischemia. Besides, according to the transcriptomic studies, RFC1 protein either showed no change or was not even mentioned in the datasets. Only, two studies reported the changes in RFC1 after ischemic stroke. One mentioned that it was upregulated in ischemic microglia in young mice whereas downregulated in old mice, but this difference was not statistically significant. Another study mentioned that ischemic endothelial cells showed no difference in RFC1 expression in the acute (24 h) or subacute (72 h) timeframe but showed upregulation chronically (1 month). However, these studies only considered the changes at the mRNA level, and also the reported changes in the RFC1 level in permanent ischemic stroke models. Interestingly, one study that resembled our stroke model, tMCAo with 60 min occlusion followed by 24 h recanalization, reported no change in the RFC1 level in the isolated microvessels from ischemic hemisphere including both the infarct and periinfarct regions. Nonetheless, this was consistent with our observation that the distribution of RFC1 had changed rather than the expression level of it in the microvessels isolated from the infarct region (see Figure 4.4.) which might be attributed to hypoxia dependent aggregation of protein (123).

The effects of MTX, a drug that functions as a folate analogue, and a non-covalent (competitive) inhibitor of RFC1, on RFC1 was investigated in this thesis. It was observed that the level of RFC1 in the whole brain increased in the first hour following administration of single dose systemic MTX administration. This increase might have been because MTX, a competitive inhibitor of folate transport via RFC1, reduced the intracellular transport of folate through RFC1, thus the cells increased RFC1 levels to meet the folate need. In line with that, it was observed that MTX application increased the RFC1 immunosignal in as soon as 15 minutes in leukemic cell line (L1210/0); however, this upregulation reversed at the end of 24 hour (124). However, to investigate the mechanism of how MTX upregulated RFC1 was beyond the purpose of this thesis hence we used MTX as a pharmacological tool to alter RFC1 levels to intervene ischemic pathophysiology.

Following MTX administration, we induced 90 minutes of ischemia, succeeded by 1 h, 24 h, or 48 h recanalization. Next, we compared the resulting infarct size to those of animals that were not administered MTX but were subjected to same procedures. It was observed that infarct sizes were not different in the 1-h and 24-h recanalization groups between MTX treated and non-treated groups. This result, despite speculatively, might be important for suggesting that the increase in the RFC1 level in the brain 1 h after MTX administration did not provide prominent neuroprotection. However, in the 48-h recanalization group, animals treated with MTX before ischemia had a larger infarct volume than the nontreated ones. It was remarkable that the increase in the infarct size in the 48-h recanalization group coincided with the decrease in RFC1 level that occurred after 48 h with single MTX injection. Despite having this striking simultaneousness, it is difficult to infer that the decrease in total RFC1 level caused by MTX administration was causally associated with an increase in infarct volume. This is because MTX, apart from being a competitive inhibitor of RFC1, changes the transcription of many genes that affect the folate cycle in the cell. Moreover, in one study, the half-life of systemic MTX in mice was found to be 33.8±6.5 minutes (91). Therefore, since it is accepted that the drugs are cleared from the systemic circulation after 4 or 5 half-lives, only the 1-h recanalization group is in the interval where we can observe the role of MTX as a competitive inhibitor. Therefore, the observed difference in infarct size at 48 h recanalization could be attributed to MTX affecting the intracellular pathways and gene transcriptions. However, detection of a larger infarct with a single dose of systemic MTX administration had never been reported in literature before. Therefore, the potential harmful effects of MTX on ischemic stroke should be investigated more closely clinically, considering that it is a widely used drug in rheumatic diseases and as a chemotherapeutic.

The genetic knockout of RFC1 is lethal and no conditional knockout animals could be used in the studies before, so we decided to utilize siRNA technology to manipulate RFC1 levels specifically in the brain of adult mice (125). Two previous in vitro studies using RFC1-siRNA which were performed in primary cultures of human differentiated adipocytes (126), and in rat choroidal epithelial Z310 cells (30), and both did not focus on the microvessels, brain or retina. Hence, our method to knockdown

RFC1 *in vivo* via siRNA could be considered as one of the initial studies and published in the associated paper (80). Since intracerebroventricular administration of RFC1-siRNA was inconclusive, the siRNA was administered intracortically, which resulted in only regional detectable knockdown of RFC1. Furthermore, siRNA mediated RFC1 knockdown led to the disruption of BBB integrity leading to endogenous IgG extravasation, which was replicated in our retinal studies and the potential mechanisms of how ischemia and RFC1 might be associated was discussed in the retinal part of the discussion in detail.

The integrity of BBB is maintained by the expression of tight junction proteins sealing the interfaces of endothelial cells and by lack of pinocytic activity. Autophagy which is a lysosomal degradation pathway that gets activated and participates in the removal of organelles and proteins in the brain is crucial in maintenance of the BBB in health. It is shown that BBB disruption is associated with alleviated autophagy, by redistributing the membranous tight junction proteins, possibly by contributing recycling of those proteins besides autophagy-deficient mice display BBB dysfunction along with a loss of tight junction proteins (123, 127-129). Therefore, autophagy seems to be activated to recycle accumulated cytosolic proteins and to reduce cytotoxicity. Folic acid deficiency leads to autophagy activation in neurons. Furthermore, RFC1, interestingly, shows protein-protein interaction with a lysosomal protein LAMP1, and several other proteins playing role in apoptosis and autophagy pathways (KRAS, HRAS, calnexin, caveolin-1 etc. (130). Therefore, observing the activation of autophagic pathway in the brains with severe barrier impairment due to RFC1 knockdown, raises important questions. Is autophagy a response of the cells to repair the BBB which RFC1 had disrupted by another mechanism? Or could the interaction of RFC1 with autophagy-related proteins play a direct role in the control of the autophagy pathway? These, and several other questions might be crucial to address to explore the interrelationship between BBB impairment, RFC1 and autophagy pathway; however, these will be explored in the future studies.

In the brain part of this thesis, we further investigated the interrelationship with ischemic stroke and RFC1 via MRI, a non-invasive method, also clinically used in human stroke diagnosis and treatment. RFC1-siRNA or Scrambled-siRNA injections were performed intracortically 24 h before the ischemia in the cortical region where it

was aimed to be periinfarct region. After that, we induced 90 min ischemia and 24 h recanalization. The first and most prominent outcome was the increase of the Gd leakage in the brain treated with RFC1-siRNA. However, no neuroprotective effect attributable to RFC1 expression was found since neither the cortical nor hemispheric infarct sizes were not different between groups. However, the main limitation of the MRI studies was the limited number of animals that were able to complete the whole procedure. As our procedure was though, only 2 of the animals injected with RFC1-siRNA were able to complete the entire procedure.

These results should be interpreted in the light of the human clinical study showing that the SNPs of RFC1 gene differed between ischemic stroke and control groups, and some RFC1 genotypes were found to be associated with small arterial occlusions and silent brain infarctions (40). These SNPs were not directly associated with life-time low folate levels or hyperhomocyteinemia in the literature, hence the known risk factors for stroke. Besides, there is no information on how having these SNPs can affect the response of RFC1 to various stress factors and RFC1 modifiers (e.g., NRF-1, HIF1α, and NO, which will be discussed later) or result in dysfunctional or reduced level of RFC1 expression. Our results might shed light on the fact that decrease in the RFC1 function in adults might deteriorate the BBB function, hence worsen ischemic stroke.

The retina part of this thesis was an initial step to investigate the role of ‘once an unnoticed transporter protein’ in the inner BRB. We took a step-by-step approach, defined the presence of the RFC1 protein in the retinal microvessels and established *in vivo* genetic tools to clarify the potential new roles of RFC1 under physiologic conditions, and ischemia. In this thesis, the presence of RFC1 protein in the endothelial cells and pericytes of the inner BRB of mice were shown. It was determined that RFC1 was an essential component for maintaining the inner BRB and had fundamental roles in retinal ischemia.

RFC1 expression at the protein level in endothelial cells and pericytes of retina had never been studied before, despite its consistent detection in transcripts of mural cells (pericytes and vascular smooth muscle cells) of the brain (3). A previous *in vitro* study examined the transport kinetics of folate in rat inner BRB model and identified

RFC1 as the primary responsible transporter for folate by examining RFC1 at the mRNA level (131). Besides, a recent study characterized the localization of folate transporters, hence RFC1 expression at CNS barriers in detail focusing especially on BBB cells including the endothelial cells; however, this study explored neither the retina nor retinal or cerebral pericytes (28). Therefore, this thesis offered a recognition for the roles of RFC1 protein in the CNS (both brain and the retina) and deepens our understanding of other critical functions as well as novel treatment strategies for CNS disorders.

Isolating retinal microvessels with the trypsin digestion method provided an easier and consistent preparation for immunostainings. The results highlighted that, retinal endothelial cells, like their counterparts in the brain, expressed RFC1 protein. As an additional novel finding, the colocalization of RFC1 with the well-defined pericyte markers was detected.

This thesis provided initial insights regarding the functional importance of RFC1 in retinal microvessels. RFC1-siRNA administration to the retina *in vivo* via intravitreal delivery offers some advantages: 1) the retina is the easily reachable, well-known extension of the brain 2) the vitreous cavity is an enclosed space that minimizes the adverse effects of systemic spread and maximizes the effect of applied concentration 3) delivery is fast and feasible (132). The application of RFC1-siRNA deranged the structure of retinal microvessels, led to a significant decrease in the barrier proteins occludin, claudin-5, ZO-1, and collagen-4, which induced the inner BRB disintegration and functional failure of the barrier (Figure 5.1). Although it may be plausible to interpret this striking result with caution, there is a study showing that the tight junction proteins like occludin, claudin-1, and ZO-1 were substantially decreased in the BBB of capillaries isolated from PCFT null mice (133). However, this mouse with deleted PCFT was accepted as a model for hereditary folate malabsorption having led to systemic folate deficiency. Hence, it was not possible to fully exclude the contribution of chronic folate deficiency to these effects. However, in our study, we observed inner BRB changes after acute modifications of the transporter in naive mice, which circumvents the confounding developmental effects of folate deficiency. Moreover, we confirmed that RFC1-siRNA treatment did not lead to any major structural deterioration despite immersive inner BRB breakdown, which

implied the main effect of RFC1 knockdown was primarily observed in the inner BRB. In line with these observations, the experiments with the retinal overexpression of RFC1 via LV had shown an upregulation of occludin, claudin-5 and collagen-4, supporting the role of RFC1 in the expression of inner BRB proteins. As an interesting observation, RFC1 was recently determined as a cGAMP importer in the cGAS-STING pathway that has a role in inflammation, cellular stress, and tumor angiogenesis (25, 26, 134). In mouse tumor models, intratumoral cGAMP treatment led to a decrease in the density of the vessels, a rise in pericyte and collagen-4 coverage, which may indicate that RFC1 may be indirectly involved in remodeling the tumor vasculature in consistence with our observations in inner retinal microvasculature (134).

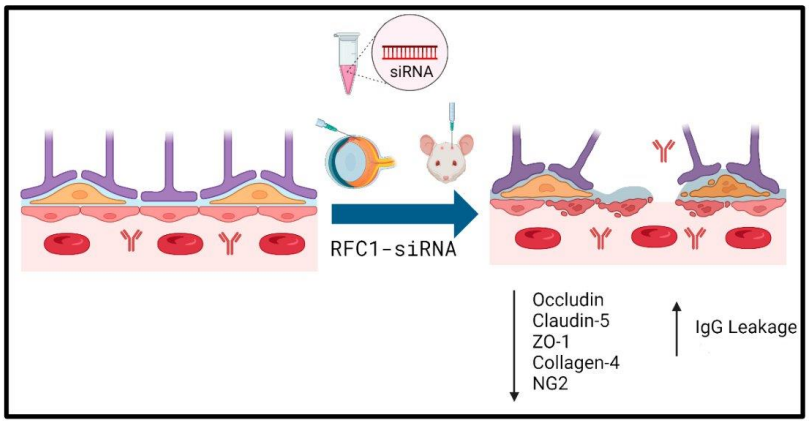

Figure 5.1. Schematic drawing summarizing the findings of RFC1 knockdown in the retina and brain, achieved through intravitreal or intracerebral siRNA delivery. Knocking down RFC1 led to breakdown in inner BRB and BBB. Microvessels with lower RFC1 expression showed structural abnormalities accompanied by defects in the expression of tight junction proteins occludin, claudin-5, ZO-1, and basal membrane protein collagen-4. Finally, extensive IgG leakage strongly suggested functional failure of the inner BRB and BBB. Figure is created with BioRender.com

Based on reports showing that pericytes are eminent for BBB and inner BRB maintenance and contribute to tight junction formation and preservation (135-138), pericyte deficiency in RFC1-siRNA treated retinas was also examined. Although we found no significant decrease in pericyte density and pericyte associated microvascular diameter, we observed immunosignal decrease in pericyte marker NG2 which is

involved in many functions of pericytes including proliferation, motility and importantly, endothelial cell junction assembly by activating integrin signaling (139). For example, the treatment of human microvascular pericytes with NG2-siRNA hindered collagen-4 coverage, ZO-1 expression, and endothelial junction maintenance in endothelial cells. Likewise, tumors from mice whose pericytes do not express NG2 showed similar changes in their endothelial junctions in the same study (84). Although the underlying mechanisms require clarification, NG2 might have been a mediator of the effects observed in tight junction proteins and collagen-4 via RFC1-siRNA. Alternatively, the disintegration of NG2 in RFC1-siRNA treated retinal microvessels might have indicated more comprehensive dysfunction throughout the inner BRB, to which NG2 disruption is only a contributing factor.

Aside from its role in the maintenance of inner BRB under physiologic conditions, the role of RFC1 in acute retinal ischemia was further investigated. Retinal ischemia which is a major underlying condition of blindness worldwide is a severe condition with a poor prognosis generally caused by acute occlusion of retinal arteries. Retinal ischemia was induced by an established method in our laboratory, and an increase in RFC1 protein was observed after 1 h (13, 100). A previous gene profiling study showed RFC1 mRNA upregulation following 1 h ischemia and 24 h recanalization induced by high intraocular pressure retinal ischemia model in rats (66). In contrast, the same study observed no significant change in RFC1 mRNA in 1 h permanent retinal ischemia. Another study showed that 45 min retinal ischemia followed by 48 h recanalization upregulated RFC1 mRNA in rats (65). The possible explanation for these results may be that the retinal ischemia models were different, and the authors only determined mRNA levels, not the protein levels of the samples. The estimation of protein levels from mRNA levels might be unreliable, as post-translational changes could affect the protein levels in early time-points (140). There is only one study performed by kidney ischemia-reperfusion model that determined RFC1 protein levels decreased *in vivo* focusing on the proximal tubules where folate reabsorption occurs, emphasizing its importance in adjusting serum folate levels (141). Several candidate mechanisms offer clues to RFC1 regulation in ischemia, which should be considered only as suggestive with inconclusive evidence for the time being. 1) It has been shown that nitric oxide (NO) has a direct impact on the expression and

function of RFC1 by modifying the thiol groups in the protein resulting in decrease in the activity of RFC1. Production of NO in ischemic-hypoxic state leading to decrease in substrate affinity of active form of folate may result in RFC1 protein level upregulation since the regulation of RFC1 is closely linked to folate balance *in vivo*. For instance, *in vitro* studies of cell lines showed that prolonged culture with reduced folate concentrations below normal levels resulted in increased levels of RFC1 (142-144). Furthermore, in mice that were fed with folate-deficient diet, there was an increase in RFC transcripts and proteins in the small intestine (145). Shortly, ischemia-induced NO production could lead to inhibition of RFC1 activity, ultimately resulting in the upregulation of its protein levels. 2) RFC1 has been defined as one of the 198 hypoxia-related genes in the Molecular Signatures Database (5). In one study, isolated mouse skin endothelial cells exposed to hypoxia had an upregulation in RFC1 in the absence of HIF1α (Hypoxia-inducible factor 1-alpha). However, in another study, cultured endothelial cells from human pulmonary arteries exposed to hypoxia had downregulation of RFC1 mRNA expression (146). Both studies together suggest HIF1α is required for downregulating RFC1 in hypoxia. However, we should regard that both studies were done in cultured cells that had been passaged for more than one time and the literature suggests that RFC1 is upregulated in cultured cells to meet the folate need of proliferating cells (147). Thus, cultured cells used in these studies might have already expressed more RFC1 than naive, and *in vivo* endothelial cells. This could change the regulation of the RFC1 gene in the ischemic state aside from the changes brought by removing cells from their *in vivo* niche. 3) A recent study has identified NRF-1 (Nuclear respiratory factor 1) as the regulator of RFC1 at the blood-brain barrier (148). Additionally, NRF-1 transcriptionally regulates HIF1α by acting as the repressor of the gene. The upregulation of NRF-1 in ganglion cell layers and inner nuclear cell layers in ischemic rats coincided with the layers nourished by inner BRB. Overall, NRF-1 may play a complex role in regulating RFC1 in ischemia. Alternatively, the increase of metabolic needs due to acute phase of ischemia might necessitate the upregulation of RFC1 after 1 h of retinal ischemia for the preservation of the barrier properties. In line with that, further augmentation of RFC1 expression by LV-RFC1 intervention before ischemia salvaged the decreased occludin and collagen-4 levels, otherwise which would be attenuated by ischemia.

Furthermore, prior to inducing ischemia, the knockdown of RFC1 led to impaired barrier functions, as demonstrated by the leakage of endogenous IgG. This finding supports the notion that RFC1 plays a crucial role in safeguarding the integrity of the inner BRB during retinal ischemia. This result can be interpreted in light of a human clinical study that revealed variations in RFC1 gene SNPs between ischemic stroke and control groups. Notably, certain genotypes were found to be associated with small arterial occlusions and silent brain infarctions (40). Since the changes in RFC1 function or structure with these polymorphisms had not been defined, it is possible that our finding of changes in inner BRB via the genetic modifications of RFC1 could carry the potential of being the experimental evidence of the importance of RFC1 in ischemia and small vessel disease. Thus, intriguing questions regarding the therapeutic potential of intervening RFC1 before, during or after ischemia rises.

However, some limitations of our study merit consideration. The genetic manipulations we used were not targeted to cells. In addition, we did not study the underlying pathways of how RFC1 regulates barrier proteins or BRB integrity, and the interplay of folate and other folate transport systems, or efflux systems (Pgp/ABCB1, MRPs/ABCC, BCRP/ABCG2), which warrants further investigations (149).

6. CONCLUSION AND REMARKS

In conclusion, cerebral pericytes, retinal pericytes and endothelial cells express RFC1 protein. RFC1 has a fundamental role in maintaining the integrity of BBB and inner BRB both in health and disease. It has roles in the pathophysiology in cerebral and retinal ischemia. Its level changes with the ischemia in line with its recent definition as a "hypoxia-immune related gene". Furthermore, modifying its levels may serve to reverse the pathologic effects of ischemia on the barrier proteins.

Despite the limitations, this thesis suggests several implications. It proposes a conceptual model of workflow for the other proteins like RFC1 whose presence and roles have not been elucidated so far (Figure 6.1.). Nowadays, the roles of these proteins have been investigated through advanced mathematical models, pathway analyses and the -omics approaches, but the old phrase "seeing is believing" should not be underestimated and *in vivo* studies may provide surprising insights into the role of a protein. The upregulation of RFC1 may be attempted for diseases other than ischemia where the impairment of BRB or BBB is involved in the pathophysiology. Although merely an initial step, these results are encouraging as the presence of RFC1 in BBB and inner BRB may be exploited for targeted drug delivery such as RFC1-targeted nanodrugs, folate conjugated nanodrugs or even clinically widely used RFC1 substrate, methotrexate, can be exploited not only in cancer, but in diseases like ischemia.

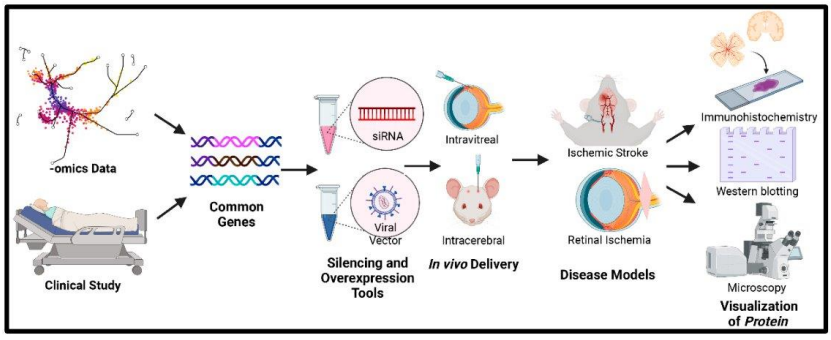

Figure 6.1. Schematic drawing depicts the theoretical representation of the proposed workflow. Uninvestigated genes, which are commonly emphasized in clinical and -omics studies, are silenced using siRNA and overexpressed via viral vector *in vivo* in animals. Disease models that mirror the clinical studies, are chosen to elucidate the

role of the gene in the pathophysiology. Finally, the localization of the protein and the alterations of its levels are investigated using visualization methods such as immunohistochemistry, microscopy, and Western blotting. Figure is created with BioRender.com.

Finally, comprehending the processes of how RFC1 have such an effect on the integrity of BBB and the inner BBB will be a central focus after this thesis. Ongoing research aims to elucidate the properties of RFC1, its intriguing protein-protein interactions, and the roles of it assumes in pathophysiological context.

7. REFERENCES

1. Alam C, Aufreiter S, Georgiou CJ, Hoque MT, Finnell RH, O'Connor DL, et al. Upregulation of reduced folate carrier by vitamin D enhances brain folate uptake in mice lacking folate receptor alpha. Proc Natl Acad Sci U S A. 2019;116(35):17531-40.
2. Alam C, Hoque MT, Finnell RH, Goldman ID, Bendayan R. Regulation of Reduced Folate Carrier (RFC) by Vitamin D Receptor at the Blood-Brain Barrier. Mol Pharmaceut. 2017;14(11):3848-58.
3. He L, Vanlandewijck M, Raschperger E, Andaloussi Mae M, Jung B, Lebouvier T, et al. Analysis of the brain mural cell transcriptome. Sci Rep. 2016;6:35108.
4. Campbell BCV, De Silva DA, Macleod MR, Coutts SB, Schwamm LH, Davis SM, et al. Ischaemic stroke. Nat Rev Dis Primers. 2019;5(1):70.
5. Li W, Yuan P, Liu W, Xiao L, Xu C, Mo Q, et al. Hypoxia-Immune-Related Gene SLC19A1 Serves as a Potential Biomarker for Prognosis in Multiple Myeloma. Front Immunol. 2022;13:843369.
6. Naggar H, Fei YJ, Ganapathy V, Smith SB. Regulation of reduced-folate transporter-1 (RFT-1) by homocysteine and identity of transport systems for homocysteine uptake in retinal pigment epithelial (RPE) cells. Exp Eye Res. 2003;77(6):687-97.
7. Naggar H, Ola MS, Moore P, Huang W, Bridges CC, Ganapathy V, et al. Downregulation of reduced-folate transporter by glucose in cultured RPE cells and in RPE of diabetic mice. Invest Ophthalmol Vis Sci. 2002;43(2):556-63.
8. Smith SB, Huang W, Chancy C, Ganapathy V. Regulation of the reduced-folate transporter by nitric oxide in cultured human retinal pigment epithelial cells. Biochem Biophys Res Commun. 1999;257(2):279-83.
9. Kaur C, Foulds WS, Ling EA. Blood-retinal barrier in hypoxic ischaemic conditions: basic concepts, clinical features and management. Prog Retin Eye Res. 2008;27(6):622-47.
10. London A, Benhar I, Schwartz M. The retina as a window to the brain-from eye research to CNS disorders. Nat Rev Neurol. 2013;9(1):44-53.
11. Yemisci M, Gursoy-Ozdemir Y, Vural A, Can A, Topalkara K, Dalkara T. Pericyte contraction induced by oxidative-nitrative stress impairs capillary reflow despite successful opening of an occluded cerebral artery. Nature Medicine. 2009;15(9):1031-U82.
12. Alarcon-Martinez L, Yilmaz-Ozcan S, Yemisci M, Schallek J, Kilic K, Can A, et al. Capillary pericytes express alpha-smooth muscle actin, which requires prevention of filamentous-actin depolymerization for detection. Elife. 2018;7.
13. Alarcon-Martinez L, Yilmaz-Ozcan S, Yemisci M, Schallek J, Kilic K, Villafranca-Baughman D, et al. Retinal ischemia induces alpha-SMA-mediated capillary pericyte contraction coincident with perivascular glycogen depletion. Acta Neuropathol Commun. 2019;7(1):134.

14. Matherly LH, Hou Z. Structure and function of the reduced folate carrier a paradigm of a major facilitator superfamily mammalian nutrient transporter. Vitam Horm. 2008;79:145-84.

15. Matherly LH, Wilson MR, Hou Z. The major facilitative folate transporters solute carrier 19A1 and solute carrier 46A1: biology and role in antifolate chemotherapy of cancer. Drug Metab Dispos. 2014;42(4):632-49.

16. HUGO Gene Nomenclature Committee, Symbol report for SLC19A1, "*Gene Symbol Reports*", [Internet]; [Access date: 08.08.2023]. Available from: https://www.genenames.org/data/gene-symbol-report/#!/hgnc_id/10937

17. Laboratory TJ. The Jackson Laboratory, Slc19a1 Gene Detail, "*Mouse Genome Database (MGD)*" Bar Harbor, Maine, [Internet]; [Access date: 08.08.2023]. Available from: http://www.informatics.jax.org/marker/MGI:103182

18. Williams FM, Flintoff WF. Isolation of a human cDNA that complements a mutant hamster cell defective in methotrexate uptake. J Biol Chem. 1995;270(7):2987-92.

19. Goldman ID, Lichtenstein NS, Oliverio VT. Carrier-mediated transport of the folic acid analogue, methotrexate, in the L1210 leukemia cell. J Biol Chem. 1968;243(19):5007-17.

20. Dixon KH, Lanpher BC, Chiu J, Kelley K, Cowan KH. A novel cDNA restores reduced folate carrier activity and methotrexate sensitivity to transport deficient cells. J Biol Chem. 1994;269(1):17-20.

21. Menezo Y, Elder K, Clement A, Clement P. Folic Acid, Folinic Acid, 5 Methyl TetraHydroFolate Supplementation for Mutations That Affect Epigenesis through the Folate and One-Carbon Cycles. Biomolecules. 2022;12(2).

22. Bohanec Grabar P, Leandro-Garcia LJ, Inglada-Perez L, Logar D, Rodriguez-Antona C, Dolzan V. Genetic variation in the SLC19A1 gene and methotrexate toxicity in rheumatoid arthritis patients. Pharmacogenomics. 2012;13(14):1583-94.

23. Zhang Q, Zhang X, Zhu Y, Sun P, Zhang L, Ma J, et al. Recognition of cyclic dinucleotides and folates by human SLC19A1. Nature. 2022.

24. Dang Y, Zhou D, Du X, Zhao H, Lee CH, Yang J, et al. Molecular mechanism of substrate recognition by folate transporter SLC19A1. Cell Discov. 2022;8(1):141.

25. Luteijn RD, Zaver SA, Gowen BG, Wyman SK, Garelis NE, Onia L, et al. SLC19A1 transports immunoreactive cyclic dinucleotides. Nature. 2019;573(7774):434-8.

26. Ritchie C, Cordova AF, Hess GT, Bassik MC, Li L. SLC19A1 Is an Importer of the Immunotransmitter cGAMP. Mol Cell. 2019;75(2):372-81 e5.

27. Hinken M, Halwachs S, Kneuer C, Honscha W. Subcellular localization and distribution of the reduced folate carrier in normal rat tissues. Eur J Histochem. 2011;55(1):e3.

28. Sangha V, Hoque MT, Henderson JT, Bendayan R. Novel localization of folate transport systems in the murine central nervous system. Fluids Barriers CNS. 2022;19(1):92.

29. Spector R, Lorenzo AV. Folate transport in the central nervous system. Am J Physiol. 1975;229(3):777-82.

30. Grapp M, Wrede A, Schweizer M, Huwel S, Galla HJ, Snaidero N, et al. Choroid plexus transcytosis and exosome shuttling deliver folate into brain parenchyma. Nat Commun. 2013;4:2123.

31. Erlacher M, Grunert SC, Cseh A, Steinfeld R, Salzer U, Lausch E, et al. Reversible pancytopenia and immunodeficiency in a patient with hereditary folate malabsorption. Pediatr Blood Cancer. 2015;62(6):1091-4.

32. Desai A, Sequeira JM, Quadros EV. The metabolic basis for developmental disorders due to defective folate transport. Biochimie. 2016;126:31-42.

33. Gelineau-van Waes J, Heller S, Bauer LK, Wilberding J, Maddox JR, Aleman F, et al. Embryonic development in the reduced folate carrier knockout mouse is modulated by maternal folate supplementation. Birth Defects Res A Clin Mol Teratol. 2008;82(7):494-507.

34. Relton CL, Wilding CS, Pearce MS, Laffling AJ, Jonas PA, Lynch SA, et al. Gene-gene interaction in folate-related genes and risk of neural tube defects in a UK population. J Med Genet. 2004;41(4):256-60.

35. De Marco P, Calevo MG, Moroni A, Merello E, Raso A, Finnell RH, et al. Reduced folate carrier polymorphism (80A-->G) and neural tube defects. Eur J Hum Genet. 2003;11(3):245-52.

36. Almekkawi AK, AlJardali MW, Daadaa HM, Lane AL, Worner AR, Karim MA, et al. Folate Pathway Gene Single Nucleotide Polymorphisms and Neural Tube Defects: A Systematic Review and Meta-Analysis. J Pers Med. 2022;12(10).

37. Liu J, Mo W, Zhang Z, Yu H, Yang A, Qu F, et al. Single Nucleotide Polymorphisms in SLC19A1 and SLC25A9 Are Associated with Childhood Autism Spectrum Disorder in the Chinese Han Population. J Mol Neurosci. 2017;62(2):262-7.

38. O'Brien NL, Quadri G, Lightley I, Sharp SI, Guerrini I, Smith I, et al. SLC19A1 Genetic Variation Leads to Altered Thiamine Diphosphate Transport: Implications for the Risk of Developing Wernicke-Korsakoff's Syndrome. Alcohol Alcohol. 2022;57(5):581-8.

39. Okada M, Suzuki S, Togashi K, Sugai A, Yamamoto M, Kitanaka C. Targeting Folate Metabolism Is Selectively Cytotoxic to Glioma Stem Cells and Effectively Cooperates with Differentiation Therapy to Eliminate Tumor-Initiating Cells in Glioma Xenografts. Int J Mol Sci. 2021;22(21).

40. Cho Y, Kim JO, Lee JH, Park HM, Jeon YJ, Oh SH, et al. Association of reduced folate carrier-1 (RFC-1) polymorphisms with ischemic stroke and silent brain infarction. PLoS One. 2015;10(2):e0115295.

41. Sweeney MD, Zhao Z, Montagne A, Nelson AR, Zlokovic BV. Blood-Brain Barrier: From Physiology to Disease and Back. Physiol Rev. 2019;99(1):21-78.

42. Wang YH, Zhao RB, Russell RG, Goldman ID. Localization of the murine reduced folate carrier as assessed by immunohistochemical analysis. Bba-Biomembranes. 2001;1513(1):49-54.

43. Zhao R, Aluri S, Goldman ID. The proton-coupled folate transporter (PCFT-SLC46A1) and the syndrome of systemic and cerebral folate deficiency of infancy: Hereditary folate malabsorption. Mol Aspects Med. 2017;53:57-72.

44. Geier EG, Chen EC, Webb A, Papp AC, Yee SW, Sadee W, et al. Profiling solute carrier transporters in the human blood-brain barrier. Clin Pharmacol Ther. 2013;94(6):636-9.

45. Bridges CC, El-Sherbeny A, Ola MS, Ganapathy V, Smith SB. Transcellular transfer of folate across the retinal pigment epithelium. Curr Eye Res. 2002;24(2):129-38.

46. Lukowski SW, Lo CY, Sharov AA, Nguyen Q, Fang L, Hung SS, et al. A single-cell transcriptome atlas of the adult human retina. EMBO J. 2019;38(18):e100811.

47. Feigin VL, Krishnamurthi RV, Parmar P, Norrving B, Mensah GA, Bennett DA, et al. Update on the Global Burden of Ischemic and Hemorrhagic Stroke in 1990-2013: The GBD 2013 Study. Neuroepidemiology. 2015;45(3):161-76.

48. Gorelick PB. The global burden of stroke: persistent and disabling. Lancet Neurol. 2019;18(5):417-8.

49. Peppiatt CM, Howarth C, Mobbs P, Attwell D. Bidirectional control of CNS capillary diameter by pericytes. Nature. 2006;443(7112):700-4.

50. O'Farrell FM, Mastitskaya S, Hammond-Haley M, Freitas F, Wah WR, Attwell D. Capillary pericytes mediate coronary no-reflow after myocardial ischaemia. Elife. 2017;6.

51. Gurler G, Soylu KO, Yemisci M. Importance of Pericytes in the Pathophysiology of Cerebral Ischemia. Noro Psikiyatr Ars. 2022;59(Suppl 1):S29-S35.

52. Taskiran-Sag A, Yemisci M, Gursoy-Ozdemir Y, Erdener SE, Karatas H, Yuce D, et al. Improving Microcirculatory Reperfusion Reduces Parenchymal Oxygen Radical Formation and Provides Neuroprotection. Stroke. 2018;49(5):1267-75.

53. Gaudin A, Yemisci M, Eroglu H, Lepetre-Mouelhi S, Turkoglu OF, Donmez-Demir B, et al. Squalenoyl adenosine nanoparticles provide neuroprotection after stroke and spinal cord injury. Nat Nanotechnol. 2014;9(12):1054-62.

54. Dalkara T, Alarcon-Martinez L.,Yemisci M. Role of Pericytes in Neurovascular Unit and Stroke. In: (eds.) JCea, editor. Non-Neuronal Mechanisms of Brain Damage and Repair After Stroke. Switzerland: Springer International Publishing; 2016.

55. Dalkara T, Alarcon-Martinez L, Yemisci M. Pericytes in Ischemic Stroke. Adv Exp Med Biol. 2019;1147:189-213.

56. Gursoy-Ozdemir Y, Yemisci M, Dalkara T. Microvascular protection is essential for successful neuroprotection in stroke. J Neurochem. 2012;123 Suppl 2:2-11.

57. Nortley R, Korte N, Izquierdo P, Hirunpattarasilp C, Mishra A, Jaunmuktane Z, et al. Amyloid beta oligomers constrict human capillaries in Alzheimer's disease via signaling to pericytes. Science. 2019;365(6450).

58. Kisler K, Nelson AR, Montagne A, Zlokovic BV. Cerebral blood flow regulation and neurovascular dysfunction in Alzheimer disease. Nat Rev Neurosci. 2017;18(7):419-34.

59. Osborne NN, Casson RJ, Wood JP, Chidlow G, Graham M, Melena J. Retinal ischemia: mechanisms of damage and potential therapeutic strategies. Prog Retin Eye Res. 2004;23(1):91-147.

60. D'Onofrio PM, Koeberle PD. What can we learn about stroke from retinal ischemia models? Acta Pharmacol Sin. 2013;34(1):91-103.

61. Devlin AM, Clarke R, Birks J, Evans JG, Halsted CH. Interactions among polymorphisms in folate-metabolizing genes and serum total homocysteine concentrations in a healthy elderly population. Am J Clin Nutr. 2006;83(3):708-13.

62. Vesela K, Pavlikova M, Janosikova B, Andel M, Zvarova J, Hyanek J, et al. Genetic determinants of folate status in Central Bohemia. Physiol Res. 2005;54(3):295-303.

63. Chango A, Emery-Fillon N, de Courcy GP, Lambert D, Pfister M, Rosenblatt DS, et al. A polymorphism (80G->A) in the reduced folate carrier gene and its associations with folate status and homocysteinemia. Mol Genet Metab. 2000;70(4):310-5.

64. Vihinen M. When a Synonymous Variant Is Nonsynonymous. Genes (Basel). 2022;13(8).

65. Abcouwer SF, Lin CM, Wolpert EB, Shanmugam S, Schaefer EW, Freeman WM, et al. Effects of ischemic preconditioning and bevacizumab on apoptosis and vascular permeability following retinal ischemia-reperfusion injury. Invest Ophthalmol Vis Sci. 2010;51(11):5920-33.

66. Andreeva K, Zhang M, Fan W, Li X, Chen Y, Rebolledo-Mendez JD, et al. Time-dependent Gene Profiling Indicates the Presence of Different Phases for Ischemia/Reperfusion Injury in Retina. Ophthalmol Eye Dis. 2014;6:43-54.

67. Kestner RI, Mayser F, Vutukuri R, Hansen L, Gunther S, Brunkhorst R, et al. Gene Expression Dynamics at the Neurovascular Unit During Early Regeneration After Cerebral Ischemia/Reperfusion Injury in Mice. Front Neurosci. 2020;14:280.

68. Rakers C, Schleif M, Blank N, Matuskova H, Ulas T, Handler K, et al. Stroke target identification guided by astrocyte transcriptome analysis. Glia. 2019;67(4):619-33.

69. Kidani N, Hishikawa T, Hiramatsu M, Nishihiro S, Kin K, Takahashi Y, et al. Cerebellar Blood Flow and Gene Expression in Crossed Cerebellar Diaschisis after Transient Middle Cerebral Artery Occlusion in Rats. Int J Mol Sci. 2020;21(11).

70. Jiang L, Mu H, Xu F, Xie D, Su W, Xu J, et al. Transcriptomic and functional studies reveal undermined chemotactic and angiostimulatory properties of aged microglia during stroke recovery. J Cereb Blood Flow Metab. 2020;40(1_suppl):S81-S97.

71. Munji RN, Soung AL, Weiner GA, Sohet F, Semple BD, Trivedi A, et al. Profiling the mouse brain endothelial transcriptome in health and disease models reveals a core blood-brain barrier dysfunction module. Nat Neurosci. 2019;22(11):1892-902.

72. Zheng F, Zhou YT, Zeng YF, Liu T, Yang ZY, Tang T, et al. Proteomics Analysis of Brain Tissue in a Rat Model of Ischemic Stroke in the Acute Phase. Front Mol Neurosci. 2020;13:27.

73. Teppo J, Vaikkinen A, Stratoulias V, Matlik K, Anttila JE, Smolander OP, et al. Molecular profile of the rat peri-infarct region four days after stroke: Study with MANF. Exp Neurol. 2020;329:113288.

74. Gu RF, Fang T, Nelson A, Gyoneva S, Gao B, Hedde J, et al. Proteomic Characterization of the Dynamics of Ischemic Stroke in Mice. J Proteome Res. 2021;20(7):3689-700.

75. Wang Y, Guo W, Xie S, Liu Y, Xu D, Chen G, et al. Multi-omics analysis of brain tissue metabolome and proteome reveals the protective effect of gross saponins of Tribulus terrestris L. fruit against ischemic stroke in rat. J Ethnopharmacol. 2021;278:114280.

76. Dongsheng H, Zhuo Z, Jiamin L, Hailan M, Lijuan H, Fan C, et al. Proteomic Analysis of the Peri-Infarct Area after Human Umbilical Cord Mesenchymal Stem Cell Transplantation in Experimental Stroke. Aging Dis. 2016;7(5):623-34.

77. Ramiro L, Garcia-Berrocoso T, Brianso F, Goicoechea L, Simats A, Llombart V, et al. Integrative Multi-omics Analysis to Characterize Human Brain Ischemia. Mol Neurobiol. 2021;58(8):4107-21.

78. Ramos-Cejudo J, Gutierrez-Fernandez M, Rodriguez-Frutos B, Exposito Alcaide M, Sanchez-Cabo F, Dopazo A, et al. Spatial and temporal gene expression differences in core and periinfarct areas in experimental stroke: a microarray analysis. PLoS One. 2012;7(12):e52121.

79. Choi IA, Yun JH, Kim JH, Kim HY, Choi DH, Lee J. Sequential Transcriptome Changes in the Penumbra after Ischemic Stroke. Int J Mol Sci. 2019;20(24).

80. Gurler G, Belder N, Beker MC, Sever-Bahcekapili M, Uruk G, Kilic E, et al. Reduced folate carrier 1 is present in retinal microvessels and crucial for the inner blood retinal barrier integrity. Fluids Barriers CNS. 2023;20(1):47.

81. Discovery H. Accell™ siRNA References 8100 Cambridge Research Park, Waterbeach, Cambridge, CB25 9TL, United Kingdom2021 [Access date: 01.09]. Available from: https://horizondiscovery.com/-/media/Files/Horizon/resources/Reading-lists/accell-sirna-ref-reading.pdf

82. Taniguchi T, Endo KI, Tanioka H, Sasaoka M, Tashiro K, Kinoshita S, et al. Novel use of a chemically modified siRNA for robust and sustainable in vivo gene silencing in the retina. Sci Rep. 2020;10(1):22343.

83. Calkins DJ, Yu-Wai-Man P, Newman NJ, Taiel M, Singh P, Chalmey C, et al. Biodistribution of intravitreal (lenadogene) nolparvovec gene therapy in nonhuman primates. Mol Ther Methods Clin Dev. 2021;23:307-18.

84. You WK, Yotsumoto F, Sakimura K, Adams RH, Stallcup WB. NG2 proteoglycan promotes tumor vascularization via integrin-dependent effects on pericyte function. Angiogenesis. 2014;17(1):61-76.

85. Zudaire E, Gambardella L, Kurcz C, Vermeren S. A computational tool for quantitative analysis of vascular networks. PLoS One. 2011;6(11):e27385.

86. Feng D, Nagy JA, Pyne K, Dvorak HF, Dvorak AM. Ultrastructural localization of platelet endothelial cell adhesion molecule (PECAM-1, CD31) in vascular endothelium. J Histochem Cytochem. 2004;52(1):87-101.

87. Kureli G, Yilmaz-Ozcan S, Erdener SE, Donmez-Demir B, Yemisci M, Karatas H, et al. F-actin polymerization contributes to pericyte contractility in retinal capillaries. Exp Neurol. 2020;332:113392.

88. Uruk G, Yilmaz-Ozcan., S., Cakir-Aktas, C., Taskiran-Sag, A., Donmez-Demir, B., Duran, J., Guinovart, J.J., Karatas-Kurşun, H., Dalkara, T., Yemisci, M. . Disrupted Cerebral Peri-Microvascular Glycogen Promotes Capillary Constrictions and Aggravates Ischemia in Mice. bioRxiv. 2022.

89. Faul F, Erdfelder E, Lang AG, Buchner A. G*Power 3: a flexible statistical power analysis program for the social, behavioral, and biomedical sciences. Behav Res Methods. 2007;39(2):175-91.

90. Bieber M, Gronewold J, Scharf AC, Schuhmann MK, Langhauser F, Hopp S, et al. Validity and Reliability of Neurological Scores in Mice Exposed to Middle Cerebral Artery Occlusion. Stroke. 2019;50(10):2875-82.

91. Lobo ED, Balthasar JP. Pharmacokinetic-pharmacodynamic modeling of methotrexate-induced toxicity in mice. J Pharm Sci. 2003;92(8):1654-64.

92. Gregorios JB, Gregorios AB, Mora J, Marcillo A, Fojaco RM, Green B. Morphologic alterations in rat brain following systemic and intraventricular methotrexate injection: light and electron microscopic studies. J Neuropathol Exp Neurol. 1989;48(1):33-47.

93. Ohdo S, Inoue K, Yukawa E, Higuchi S, Nakano S, Ogawa N. Chronotoxicity of methotrexate in mice and its relation to circadian rhythm of DNA synthesis and pharmacokinetics. Jpn J Pharmacol. 1997;75(3):283-90.

94. Boulay AC, Saubamea B, Decleves X, Cohen-Salmon M. Purification of Mouse Brain Vessels. J Vis Exp. 2015(105):e53208.

95. Chauveau F, Cho TH, Perez M, Guichardant M, Riou A, Aguettaz P, et al. Brain-targeting form of docosahexaenoic acid for experimental stroke treatment: MRI evaluation and anti-oxidant impact. Curr Neurovasc Res. 2011;8(2):95-102.

96. Durand A, Chauveau F, Cho TH, Kallus C, Wagner M, Boutitie F, et al. Effects of a TAFI-inhibitor combined with a suboptimal dose of rtPA in a murine thromboembolic model of stroke. Cerebrovasc Dis. 2014;38(4):268-75.

97. Durand A, Chauveau F, Cho TH, Bolbos R, Langlois JB, Hermitte L, et al. Spontaneous reperfusion after in situ thromboembolic stroke in mice. PLoS One. 2012;7(11):e50083.

98. Riou A, Chauveau F, Cho TH, Marinescu M, Nataf S, Nighoghossian N, et al. MRI assessment of the intra-carotid route for macrophage delivery after transient cerebral ischemia. NMR Biomed. 2013;26(2):115-23.

99. Marinescu M, Chauveau F, Durand A, Riou A, Cho TH, Dencausse A, et al. Monitoring therapeutic effects in experimental stroke by serial USPIO-enhanced MRI. Eur Radiol. 2013;23(1):37-47.

100. Karatas H, Erdener SE, Gursoy-Ozdemir Y, Gurer G, Soylemezoglu F, Dunn AK, et al. Thrombotic distal middle cerebral artery occlusion produced by topical FeCl(3) application: a novel model suitable for intravital microscopy and thrombolysis studies. J Cereb Blood Flow Metab. 2011;31(6):1452-60.

101. Chou JC, Rollins SD, Fawzi AA. Trypsin digest protocol to analyze the retinal vasculature of a mouse model. J Vis Exp. 2013(76):e50489.

102. Beker M, Caglayan AB, Beker MC, Altunay S, Karacay R, Dalay A, et al. Lentivirally administered glial cell line-derived neurotrophic factor promotes post-ischemic neurological recovery, brain remodeling and contralesional pyramidal tract plasticity by regulating axonal growth inhibitors and guidance proteins. Exp Neurol. 2020;331:113364.

103. Brandli A, Stone J. Using the Electroretinogram to Assess Function in the Rodent Retina and the Protective Effects of Remote Limb Ischemic Preconditioning. J Vis Exp. 2015(100):e52658.

104. Verbeek MM, Blom AM, Wevers RA, Lagerwerf AJ, van de Geer J, Willemsen MA. Technical and biochemical factors affecting cerebrospinal fluid 5-MTHF, biopterin and neopterin concentrations. Mol Genet Metab. 2008;95(3):127-32.

105. Nandania J, Kokkonen M, Euro L, Velagapudi V. Simultaneous measurement of folate cycle intermediates in different biological matrices using liquid chromatography-tandem mass spectrometry. J Chromatogr B Analyt Technol Biomed Life Sci. 2018;1092:168-78.

106. Trippett TM, Garcia S, Manova K, Mody R, Cohen-Gould L, Flintoff W, et al. Localization of a human reduced folate carrier protein in the mitochondrial as well as the cell membrane of leukemia cells. Cancer Res. 2001;61(5):1941-7.

107. The Human Protein Atlas, Cerebral Cortex - Antibody staining, "*The open access resource for human proteins.*", [Internet]; [Access date: 08.08.2023]. Available from: https://v23.proteinatlas.org/ENSG00000173638-SLC19A1/tissue/cerebral+cortex

108. Uhlen M, Fagerberg L, Hallstrom BM, Lindskog C, Oksvold P, Mardinoglu A, et al. Proteomics. Tissue-based map of the human proteome. Science. 2015;347(6220):1260419.

109. Unal-Cevik I, Kilinc M, Gursoy-Ozdemir Y, Gurer G, Dalkara T. Loss of NeuN immunoreactivity after cerebral ischemia does not indicate neuronal cell loss: a cautionary note. Brain Res. 2004;1015(1-2):169-74.

110. Ma D, Huang H, Moscow JA. Down-regulation of reduced folate carrier gene (RFC1) expression after exposure to methotrexate in ZR-75-1 breast cancer cells. Biochem Biophys Res Commun. 2000;279(3):891-7.

111. Swanson RA, Morton MT, Tsao-Wu G, Savalos RA, Davidson C, Sharp FR. A semiautomated method for measuring brain infarct volume. J Cereb Blood Flow Metab. 1990;10(2):290-3.

112. Kim KA, Shin D, Kim JH, Shin YJ, Rajanikant GK, Majid A, et al. Role of Autophagy in Endothelial Damage and Blood-Brain Barrier Disruption in Ischemic Stroke. Stroke. 2018;49(6):1571-9.

113. Tanida I, Ueno T, Kominami E. LC3 and Autophagy. Methods Mol Biol. 2008;445:77-88.

114. Chancy CD, Kekuda R, Huang W, Prasad PD, Kuhnel JM, Sirotnak FM, et al. Expression and differential polarization of the reduced-folate transporter-1 and the folate receptor alpha in mammalian retinal pigment epithelium. J Biol Chem. 2000;275(27):20676-84.

115. Hou Z, Cherian C, Drews J, Wu J, Matherly LH. Identification of the minimal functional unit of the homo-oligomeric human reduced folate carrier. J Biol Chem. 2010;285(7):4732-40.

116. Drori S, Sprecher H, Shemer G, Jansen G, Goldman ID, Assaraf YG. Characterization of a human alternatively spliced truncated reduced folate carrier increasing folate accumulation in parental leukemia cells. Eur J Biochem. 2000;267(3):690-702.

117. Hou Z, Matherly LH. Oligomeric structure of the human reduced folate carrier: identification of homo-oligomers and dominant-negative effects on carrier expression and function. J Biol Chem. 2009;284(5):3285-93.

118. Wei Y, Gong J, Xu Z, Thimmulappa RK, Mitchell KL, Welsbie DS, et al. Nrf2 in ischemic neurons promotes retinal vascular regeneration through regulation of semaphorin 6A. Proc Natl Acad Sci U S A. 2015;112(50):E6927-36.

119. Auricchio A, Kobinger G, Anand V, Hildinger M, O'Connor E, Maguire AM, et al. Exchange of surface proteins impacts on viral vector cellular specificity and transduction characteristics: the retina as a model. Hum Mol Genet. 2001;10(26):3075-81.

120. Wang X, Liu Y, Sun Y, Liu W, Jin X. Blood brain barrier breakdown was found in non-infarcted area after 2-h MCAO. J Neurol Sci. 2016;363:63-8.

121. Chen B, Friedman B, Cheng Q, Tsai P, Schim E, Kleinfeld D, et al. Severe blood-brain barrier disruption and surrounding tissue injury. Stroke. 2009;40(12):e666-74.

122. Jin X, Liu J, Yang Y, Liu KJ, Yang Y, Liu W. Spatiotemporal evolution of blood brain barrier damage and tissue infarction within the first 3h after ischemia onset. Neurobiol Dis. 2012;48(3):309-16.

123. Yang Z, Lin P, Chen B, Zhang X, Xiao W, Wu S, et al. Autophagy alleviates hypoxia-induced blood-brain barrier injury via regulation of CLDN5 (claudin 5). Autophagy. 2021;17(10):3048-67.

124. Liu S, Gao C, Zhang R, Zhao X, Cui L, Li W, et al. Germline Genetic Variations in Methotrexate Candidate Genes Are Associated with Pharmacokinetics and Outcome in Pediatric Acute Lymphoblastic Leukemia in China. Blood. 2016;128(22).

125. Zhao R, Russell RG, Wang Y, Liu L, Gao F, Kneitz B, et al. Rescue of embryonic lethality in reduced folate carrier-deficient mice by maternal folic acid supplementation reveals early neonatal failure of hematopoietic organs. J Biol Chem. 2001;276(13):10224-8.

126. Petrus P, Bialesova L, Checa A, Kerr A, Naz S, Backdahl J, et al. Adipocyte Expression of SLC19A1 Links DNA Hypermethylation to Adipose Tissue Inflammation and Insulin Resistance. J Clin Endocrinol Metab. 2018;103(2):710-21.

127. Yang Z, Huang C, Wu Y, Chen B, Zhang W, Zhang J. Autophagy Protects the Blood-Brain Barrier Through Regulating the Dynamic of Claudin-5 in Short-Term Starvation. Front Physiol. 2019;10:2.

128. Kim KA, Kim D, Kim JH, Shin YJ, Kim ES, Akram M, et al. Autophagy-mediated occludin degradation contributes to blood-brain barrier disruption during ischemia in bEnd.3 brain endothelial cells and rat ischemic stroke models. Fluids Barriers CNS. 2020;17(1):21.

129. Bhattacharya A, Wei Q, Shin JN, Abdel Fattah E, Bonilla DL, Xiang Q, et al. Autophagy Is Required for Neutrophil-Mediated Inflammation. Cell Rep. 2015;12(11):1731-9.

130. The Biological General Repository for Interaction Datasets (BioGRID), Slc19a1,"*Database of Protein, Genetic and Chemical Interactions*" [Access date: 08.08.2023]. Available from: https://thebiogrid.org/112461/summary/homo-sapiens/slc19a1.html

131. Hosoya K, Fujita K, Tachikawa M. Involvement of reduced folate carrier 1 in the inner blood-retinal barrier transport of methyltetrahydrofolate. Drug Metab Pharmacokinet. 2008;23(4):285-92.

132. Meyer CH, Krohne TU, Charbel Issa P, Liu Z, Holz FG. Routes for Drug Delivery to the Eye and Retina: Intravitreal Injections. Dev Ophthalmol. 2016;55:63-70.

133. Wang X, Cabrera RM, Li Y, Miller DS, Finnell RH. Functional regulation of P-glycoprotein at the blood-brain barrier in proton-coupled folate transporter (PCFT) mutant mice. FASEB J. 2013;27(3):1167-75.

134. Yang H, Lee WS, Kong SJ, Kim CG, Kim JH, Chang SK, et al. STING activation reprograms tumor vasculatures and synergizes with VEGFR2 blockade. J Clin Invest. 2019;129(10):4350-64.

135. Al Ahmad A, Gassmann M, Ogunshola OO. Maintaining blood-brain barrier integrity: pericytes perform better than astrocytes during prolonged oxygen deprivation. J Cell Physiol. 2009;218(3):612-22.

136. Yang T, Guo L, Fang Y, Liang M, Zheng Y, Pan M, et al. Pericytes of Indirect Contact Coculture Decrease Integrity of Inner Blood-Retina Barrier Model In Vitro by Upgrading MMP-2/9 Activity. Dis Markers. 2021;2021:7124835.

137. Daneman R, Zhou L, Kebede AA, Barres BA. Pericytes are required for blood-brain barrier integrity during embryogenesis. Nature. 2010;468(7323):562-6.

138. Bell RD, Winkler EA, Sagare AP, Singh I, LaRue B, Deane R, et al. Pericytes control key neurovascular functions and neuronal phenotype in the adult brain and during brain aging. Neuron. 2010;68(3):409-27.

139. Stallcup WB. The NG2 Proteoglycan in Pericyte Biology. Adv Exp Med Biol. 2018;1109:5-19.

140. Fortelny N, Overall CM, Pavlidis P, Freue GVC. Can we predict protein from mRNA levels? Nature. 2017;547(7664):E19-E20.

141. Yang C, Wijerathne CUB, Tu GW, Woo CWH, Siow YL, Madduma Hewage S, et al. Ischemia-Reperfusion Injury Reduces Kidney Folate Transporter Expression and Plasma Folate Levels. Front Immunol. 2021;12:678914.

142. Sirotnak FM, Moccio DM, Yang CH. A novel class of genetic variants of the L1210 cell up-regulated for folate analogue transport inward. Isolation, characterization, and degree of metabolic instability of the system. J Biol Chem. 1984;259(21):13139-44.

143. Matherly LH, Czajkowski CA, Angeles SM. Identification of a highly glycosylated methotrexate membrane carrier in K562 human erythroleukemia cells up-regulated for tetrahydrofolate cofactor and methotrexate transport. Cancer Res. 1991;51(13):3420-6.

144. Jansen G, Westerhof GR, Jarmuszewski MJ, Kathmann I, Rijksen G, Schornagel JH. Methotrexate transport in variant human CCRF-CEM leukemia cells with elevated levels of the reduced folate carrier. Selective effect on carrier-mediated transport of physiological concentrations of reduced folates. J Biol Chem. 1990;265(30):18272-7.

145. Liu M, Ge Y, Cabelof DC, Aboukameel A, Heydari AR, Mohammad R, et al. Structure and regulation of the murine reduced folate carrier gene: identification of four noncoding exons and promoters and regulation by dietary folates. J Biol Chem. 2005;280(7):5588-97.

146. Manalo DJ, Rowan A, Lavoie T, Natarajan L, Kelly BD, Ye SQ, et al. Transcriptional regulation of vascular endothelial cell responses to hypoxia by HIF-1. Blood. 2005;105(2):659-69.

147. Bozard BR, Ganapathy PS, Duplantier J, Mysona B, Ha Y, Roon P, et al. Molecular and biochemical characterization of folate transport proteins in retinal Muller cells. Invest Ophthalmol Vis Sci. 2010;51(6):3226-35.

148. Alam C, Hoque MT, Sangha V, Bendayan R. Nuclear respiratory factor 1 (NRF-1) upregulates the expression and function of reduced folate carrier (RFC) at the blood-brain barrier. FASEB J. 2020;34(8):10516-30.

149. Assaraf YG. The role of multidrug resistance efflux transporters in antifolate resistance and folate homeostasis. Drug Resist Updat. 2006;9(4-5):227-46.

8. APPENDICES

APPENDIX-1: Ethical Approval for Thesis Studies

T.C.
HACETTEPE ÜNİVERSİTESİ
Hayvan Deneyleri Yerel Etik Kurulu

Sayı : 52338575 – [illegible]

HAYVAN DENEYLERİ ETİK KURUL KARARI

TOPLANTI TARİHİ	:	24.12.2019 (SALI)
TOPLANTI SAYISI	:	2019/13
DOSYA KAYIT NUMARASI	:	2019/76
KARAR NUMARASI	:	2019/13– 06
ONAY BİTİŞ TARİHİ		24.12.2024
ARAŞTIRMA YÜRÜTÜCÜSÜ	:	Prof. Dr. Müge Yemişçi ÖZKAN
HAYVAN DENEYLERİNDE GÖREVLİ ARAŞTIRMACILAR	:	Gökçe GÜRLER, Dr. Buket Nebiye DEMİR, Dr. Canan Çakır AKTAŞ, Dr. Nevin BELDER.
DİĞER YARDIMCI ARAŞTIRMACILAR	:	
ONAYLANAN HAYVAN TÜRÜ ve SAYISI	:	***273 Adet Swiss Albino Fare (8-12 Hafta)***

Üniversitemiz Nörolojik Bilimler ve Psikiyatri Enstitüsü öğretim üyelerinden Prof. Dr. Müge Yemişçi ÖZKAN'ın araştırma yürütücüsü olduğu 2019/76 kayıt numaralı ***"İndirgenmiş Folat Taşıyıcısı 1'in Beyin ve Retina Mikrodolaşımındaki Rolünün İncelenmesi"*** isimli çalışma Hayvan Deneyleri Yerel Etik Kurulu Yönergesi'ne göre uygun bulunarak oy birliği ile onaylanmasına karar verilmiştir.

Araştırma yürütücüsü en geç, onay bitiş tarihinden sonraki 1 ay içerisinde proje sonuç raporunu Kurulumuza teslim etmekle yükümlüdür.

Prof. Dr. Sema ÇALIŞ
Etik Kurul Başkanı

Hacettepe Üniversitesi Hayvan Deneyleri Yerel Etik Kurulu 06100 Sıhhiye-Ankara
Telefon: 0 (312) 305 1090-1082 • Faks: 0 (312) 310 0580
www.etikkurul.hacettepe.edu.tr/index_hdk.php
Ayrıntılı Bilgi için:

T.C.
HACETTEPE ÜNİVERSİTESİ
Hayvan Deneyleri Yerel Etik Kurulu

Sayı : 52338575-51

HAYVAN DENEYLERİ ETİK KURUL KARARI

TOPLANTI TARİHİ	:	30.03.2021 (SALI)
TOPLANTI SAYISI	:	2021/03
DOSYA KAYIT NUMARASI	:	2020/58 (ONAY TARİHİ: 25.11.2020)
KARAR NUMARASI	:	2021/03- 19
ONAY BİTİŞ TARİHİ		25.11.2025
ARAŞTIRMA YÜRÜTÜCÜSÜ	:	Prof. Dr. Müge Yemişçi ÖZKAN
HAYVAN DENEYLERİNDE GÖREVLİ ARAŞTIRMACILAR	:	Gökçe GÜLER (Doktora Tezi), Prof. Dr. Müge Yemişçi ÖZKAN, Prof. Dr. Hülya Karataş KURŞUN, Nevin BELDER, Buket Nebiye DEMİR, Canan Çakır AKTAŞ, Melike Sever BAHÇEKAPILI
DİĞER YARDIMCI ARAŞTIRMACILAR	:	
ONAYLANAN HAYVAN TÜRÜ ve SAYISI	:	***184 Adet Swiss Albino Fare (8-12 Hafta)***

Kurulumuzun 25.11.2020 tarihli toplantısında 2020/58 dosya kayıt numarası ile onaylanmış olan Üniversitemiz Nörolojik Bilimler ve Psikiyatri Enstitüsü öğretim üyelerinden Prof. Dr. Müge Yemişçi ÖZKAN'ın araştırma yürütücüsü olduğu ***"SLC19A1 İfadesinin İskemik İnme ve Retinal İskemideki Rolünün Araştırılması"*** başlıklı .proje için verilen 25.03.2021 tarihli araştırmacı revizyonu, proje revizyonu ve başlık değişikliği dilekçesi Kurulumuzun 30.03.2021 tarihli toplantısında görüşülmüş ve **uygun bulunmuştur.** Proje ekibine Üniversitemiz Nörolojik Bilimler ve Psikiyatri Enstitüsü öğretim elemanları Dr. Buket Nebiye DEMİR, Dr. Canan Çakır AKTAŞ ve Dr. Melike Sever BAHÇEKAPILI hayvan deneylerinde görevli araştırmacılar olarak dahil edilmiştir. Araştırmanın başlığı ***"İndirgenmiş Folat Taşıyıcısı 1'in Rolünün İskemik İnme ve Retinal İskemi Modellerinde Araştırılması"*** olarak değiştirilmiş ve kayıtlarımıza eklenmiştir.

Araştırma yürütücüsü en geç, onay bitiş tarihinden sonraki 1 ay içerisinde proje sonuç raporunu Kurulumuza teslim etmekle yükümlüdür.

Prof. Dr. Sema ÇALIŞ
Etik Kurul Başkanı

Hacettepe Üniversitesi Hayvan Deneyleri Yerel Etik Kurulu 06100 Sıhhiye-Ankara
Telefon: 0 (312) 305 1090-1082 • Faks: 0 (312) 310 0580
www.etikkurul.hacettepe.edu.tr/index_hdk.php

Ayrıntılı Bilgi için:

APPENDIX-2: Thesis Originality Report

turnitin

Dijital Makbuz

Bu makbuz ödevinizin Turnitin'e ulaştığını bildirmektedir. Gönderiminize dair bilgiler şöyledir:

Gönderinizin ilk sayfası aşağıda gönderilmektedir.

Gönderen:	Gokce Gurler
Ödev başlığı:	tez
Gönderi Başlığı:	tez
Dosya adı:	birlestirilmis.docx
Dosya boyutu:	11.12M
Sayfa sayısı:	80
Kelime sayısı:	25,780
Karakter sayısı:	147,924
Gönderim Tarihi:	08-Ağu-2023 05:09ÖS (UTC+0300)
Gönderim Numarası:	2143105995

ABSTRACT

Turnitin Orijinallik Raporu

İşleme konu: 08-Ağu-2023 17:10 +03
NUMARA: 2143105995
Kelime Sayısı: 25780
Gönderildi: 1

tez Gokce Gurler tarafından

Benzerlik Endeksi	Kaynağa göre Benzerlik
%14	Internet Sources: %10 Yayınlar: %12 Öğrenci Ödevleri: %2

< 1% match (09-May-2023 tarihli internet)
https://vdoc.pub/documents/folic-acid-and-folates-2r5ga1jhbs5g

< 1% match (Dilaver Kaya, Yasemin Gürsoy-Özdemir, Muge Yemisci, Neşe Tuncer, Sevinç Aktan, Turgay Dalkara. "VEGF Protects Brain against Focal Ischemia without Increasing Blood–Brain Permeability When Administered Intracerebroventricularly", Journal of Cerebral Blood Flow & Metabolism, 2005)
Dilaver Kaya, Yasemin Gürsoy-Özdemir, Muge Yemisci, Neşe Tuncer, Sevinç Aktan, Turgay Dalkara. "VEGF Protects Brain against Focal Ischemia without Increasing Blood–Brain Permeability When Administered Intracerebroventricularly", Journal of Cerebral Blood Flow & Metabolism, 2005

< 1% match (30-Oca-2023 tarihli internet)
https://www.researchgate.net/profile/Bobbi-Fleiss/publication/319453095_Brain_Edema_in_Developing_Brain_Diseases/links/59d21fc74585150177f60799/Brain-Edema-in-Developing-Brain-Diseases.pdf

< 1% match (29-Oca-2023 tarihli internet)
https://www.researchgate.net/publication/23409934_Astrocytes_are_More_Resistant_to_Focal_Cerebral_Ischemia_Than_Neurons_and_Die_by_

< 1% match (07-Şub-2023 tarihli internet)
https://www.researchgate.net/publication/330030450_Analyzing_the_impact_of_glaucoma_on_the_macular_architecture_using_spectral-domain_optical_coherence_tomography

< 1% match (30-Oca-2023 tarihli internet)
https://www.researchgate.net/publication/302779197_Expression_of_CYP_4A_o-hydroxylase_and_formation_of_20-hydroxyeicosatetraenoic_acid_20-HETE_in_cultured_rat_brain_astrocytes

< 1% match (11-Ağu-2022 tarihli internet)
https://www.researchgate.net/publication/362232284_Hypoxia-Immune-Related_Gene_SLC19A1_Serves_as_a_Potential_Biomarker_for_Prognosis_in_Multiple_Myeloma

< 1% match (31-Oca-2023 tarihli internet)
https://www.researchgate.net/publication/260916711_Endothelin_Receptor-A_Antagonist_Attenuates_Retinal_Vascular_and_Neuroretinal_Pathology_in_Diabetic_Mice

< 1% match (Gulce Kureli, Sinem Yilmaz-Ozcan, Sefik Evren Erdener, Buket Donmez-Demir, Muge Yemisci, Hulya Karatas, Turgay Dalkara. "F-actin polymerization contributes to pericyte contractility in retinal capillaries", Experimental Neurology, 2020)
Gulce Kureli, Sinem Yilmaz-Ozcan, Sefik Evren Erdener, Buket Donmez-Demir, Muge Yemisci, Hulya Karatas, Turgay Dalkara. "F-actin polymerization contributes to pericyte contractility in retinal capillaries", Experimental Neurology, 2020

< 1% match (11-Tem-2022 tarihli internet)
https://tel.archives-ouvertes.fr/tel-03510239/document

< 1% match (26-Şub-2022 tarihli internet)
https://tel.archives-ouvertes.fr/tel-03469012/file/sygal_fusion_28372-le_gal-rozenn.pdf

< 1% match (28-Oca-2022 tarihli internet)
http://hub.hku.hk/bitstream/10722/304447/1/content.pdf

< 1% match (20-Nis-2019 tarihli internet)
https://ankursinha.in/planet-neuroscience/

< 1% match (15-Mar-2023 tarihli internet)
https://www.mdpi.com/2218-273X/13/3/534/xml

< 1% match (12-Ağu-2022 tarihli internet)
https://www.mdpi.com/2072-6694/13/12/3056/htm

< 1% match (12-Eki-2022 tarihli internet)
https://www.mdpi.com/2075-4418/10/11/969/htm

< 1% match (10-Mar-2023 tarihli internet)
https://www.mdpi.com/2073-4409/11/19/3108

< 1% match (Camille Alam, Md. Tozammel Hoque, Richard H. Finnell, I. David Goldman, Reina Bendayan. "Regulation of Reduced Folate Carrier (RFC) by Vitamin D Receptor at the Blood-Brain Barrier", Molecular Pharmaceutics, 2017)
Camille Alam, Md. Tozammel Hoque, Richard H. Finnell, I. David Goldman, Reina Bendayan. "Regulation of Reduced Folate Carrier (RFC) by Vitamin D Receptor at the Blood-Brain Barrier", Molecular Pharmaceutics, 2017

< 1% match (06-Mar-2014 tarihli öğrenci ödevleri)

9. CURRICULUM VITAE